A FINITE ELEMENT STUDY OF STRESSES IN STEPPED SPLINED SHAFTS, AND PARTIALLY SPLINED SHAFTS UNDER BENDING, TORSION, AND COMBINED LOADINGS

by

Donald Alexander Baker

Thesis submitted to the Faculty of the

Virginia Polytechnic Institute and State University

in partial fulfillment of the requirements for the degree of

MASTER OF SCIENCE

in

MECHANICAL ENGINEERING

APPROVED:

_____

Dr. Reginald G. Mitchiner, Chairperson

_____ _____

Dr. Charles E. Knight **Dr. Robert L. West**

May 4, 1999
Blacksburg, Virginia

Keywords: Spline, Shaft, FEM, Solid, Modeling

A FINITE ELEMENT STUDY OF STRESSES IN STEPPED SPLINED SHAFTS, AND PARTIALLY SPLINED SHAFTS UNDER BENDING, TORSION, AND COMBINED LOADINGS

by

Donald Alexander Baker

Dr. Reginald G. Mitchiner, Chairman

Mechanical Engineering

(ABSTRACT)

The maximum von Mises stress is calculated for solid finite element models of splined shafts with straight-sided teeth. One spline shaft is stepped with larger diameter section containing spline teeth and the smaller diameter section circular and cylindrical with no spline teeth. A second shaft is not stepped, but contains incomplete spline teeth.

Finite element analyses are performed for the cases of a stepped shaft of three different step size ratios (d/D). The second set of models consists of a solid cylindrical shaft with incomplete spline teeth. The incomplete regions of the spline teeth are modeled in three radii (R). Bending, torsion, and combined loads are applied to each model, including several combinations of bending and torsion between pure bending and pure torsion. Finite element stress results are converged to within 2% for verification.

The stresses in the stepped splined shafts are up to 50% greater than nominal stresses in the non-splined section and up to 88% greater than nominal stresses splined section. Stresses in the partially splined shaft showed little or no correlation between the hob

radius and the magnitude of the peak von Mises stress, but show a strong correlation between the peak stress and the proportion of bending to torsion. The peak von Mises stress occurs when the applied load consists of greater proportions of torsion as opposed to bending. Stresses in the partially splined shaft are up to 42% greater than the well-developed nominal stress in the non-splined section of the shaft, and up to 7% greater than the nominal stresses in the splined section.

Acknowledgements

The completion of this thesis would not have been possible without the help several people. First, I would like to thank my Lord and Savior Jesus Christ.

My gratitude, love, and respect go out to my caring and understanding wife, Talaya Nicole Baker. The countless sacrifices that she has made for me to be able to accomplish this task are too numerous to list. Also, my gratitude goes out to my mother Beverly, and my father James, for their many years of love and support.

I also thank Dr. Reginald G. Mitchiner, chairman of my advisory committee. His guidance of my research and contribution to my education has been invaluable. I credit him with fostering my development both as a scholar and engineering professional during my time at Virginia Tech. My thanks also go out to Dr. R.L. West, and Dr. C. E. Knight, who also sit on my advisory committee, for their advice, guidance, and support.

Finally, I would like to thank all of the good friends I have made during my studies at Virginia Tech.

Table of Contents

List of Tables

List of Figures

I. INTRODUCTION

Splined connections are widely used as a coupling mechanism in rotating machinery. Splined shafts transmit torque from one rotating member to another. The application of the splined connection for the transmission of torque alone is well documented in the literature. However, the design of a splined connection under combined bending and torsional loads (such as those induced by shaft misalignment) is not as well understood. In these cases, design techniques such as tapering or crowning of the spline teeth are used to accommodate such misalignment. When crowned splines are used, the load bearing capacity of the corresponding straight tooth spline is reduced. Thus, a larger diameter shaft must be employed to offset the loss of load carrying capacity. There is a dearth of literature on how to design a splined shaft connection if either of these methods is not utilized.

The splined shaft modeled in this study is used in continuous underground mining machines that extract coal from the earth. The shaft transmits torque from a helical gear reducer to a planetary gear reducer on the cutter turret. The shaft design incorporates a groove that narrows the shaft cross-section and purposely weakens the shaft. This design feature causes the shaft to fail in rupture before the reduction gearing assemblies suffer any damage. In this way the shaft, which is relatively inexpensive, acts as a mechanical fuse for the more expensive gear reducer components. Thus, to insure proper failure it is necessary that all stresses be well understood throughout the shaft.

The purpose of this research is to investigate finite element models of both stepped splined shafts, and splined shafts with incomplete teeth (called partially splined shafts hereafter), with various step ratios and hob radii when subjected to combinations of bending and torsion loads. According to Volfson [1], the effect of axial forces on the shaft is usually not significant and can be omitted. Typically, studies of splined shafts focus only on torsional loads, with induced bending loads due to shaft misalignment not being considered. With the exception of crowning of the spline teeth, standard practice has been to totally avoid bending stresses induced by axial misalignment in a given application. Stresses caused by bending forces cannot be ignored, since their values often are as great as 25% of those caused by torque [1]. Using a combination of finite element analysis and analytical modeling, the intent of this research is to characterize and quantify the combined effects of static torsion and static bending loads upon the stresses in stepped splined shafts and partially splined shafts (shafts containing incomplete spline teeth).

Finite element analysis is a numerical method in which a particular body is subdivided into discrete partitions (called elements) that are bound by nodes. Each element is connected to adjacent elements by the nodes. The finite element method requires that the fundamental differential equations governing the overall problem be reduced to a system of algebraic equations from which a general solution is obtained. Boundary conditions and environmental factors are applied to the subdivided model. The equations governing the individual elements are then combined and solved to obtain the solution for the overall problem. Algor version 3.18 WIN by Algor, Inc. was the computer software package used to perform the finite element analysis in this study.

Splines have an advantage over shaft key and slot systems. Shafts with external keys are subject to very high stress concentrations at the key root, thus decreasing the fatigue life of the shaft. Shafts with slots cut into them to accept keys are also substantially weakened. Splines allow bending and torsion loads to be distributed over several teeth; each of which acts like a key that is attached to the shaft. This arrangement affords splined connections much greater strength than keyed connections.

A spline connection consists of two parts: an internal spline and an external spline. A sketch of both the internal and external spline is shown in Figure 1. The internal spline makes up the outer part of the connection. Grooves are machined into the inner diameter of the shaft, parallel to the shaft axis. The internal spline is also known as the "female" part of the connection. The external spline makes up the inner part of the connection. It has similar grooves cut into the outer surface of a shaft, parallel to the shaft axis. The external spline is also known as the "male" part of the connection. The splines of interest in this research are external, straight-sided splines with flat roots. Since no mating member is considered in its analysis, such splines are referred to as "open".

External splines are typically manufactured using a technique called hobbing. A rotating tool called a hob is used to cut grooves into a solid shaft. The teeth of the hob are shaped according to the desired involute or flat-sided profile demanded by the particular design. The hob arrangement is illustrated in Figure 2.

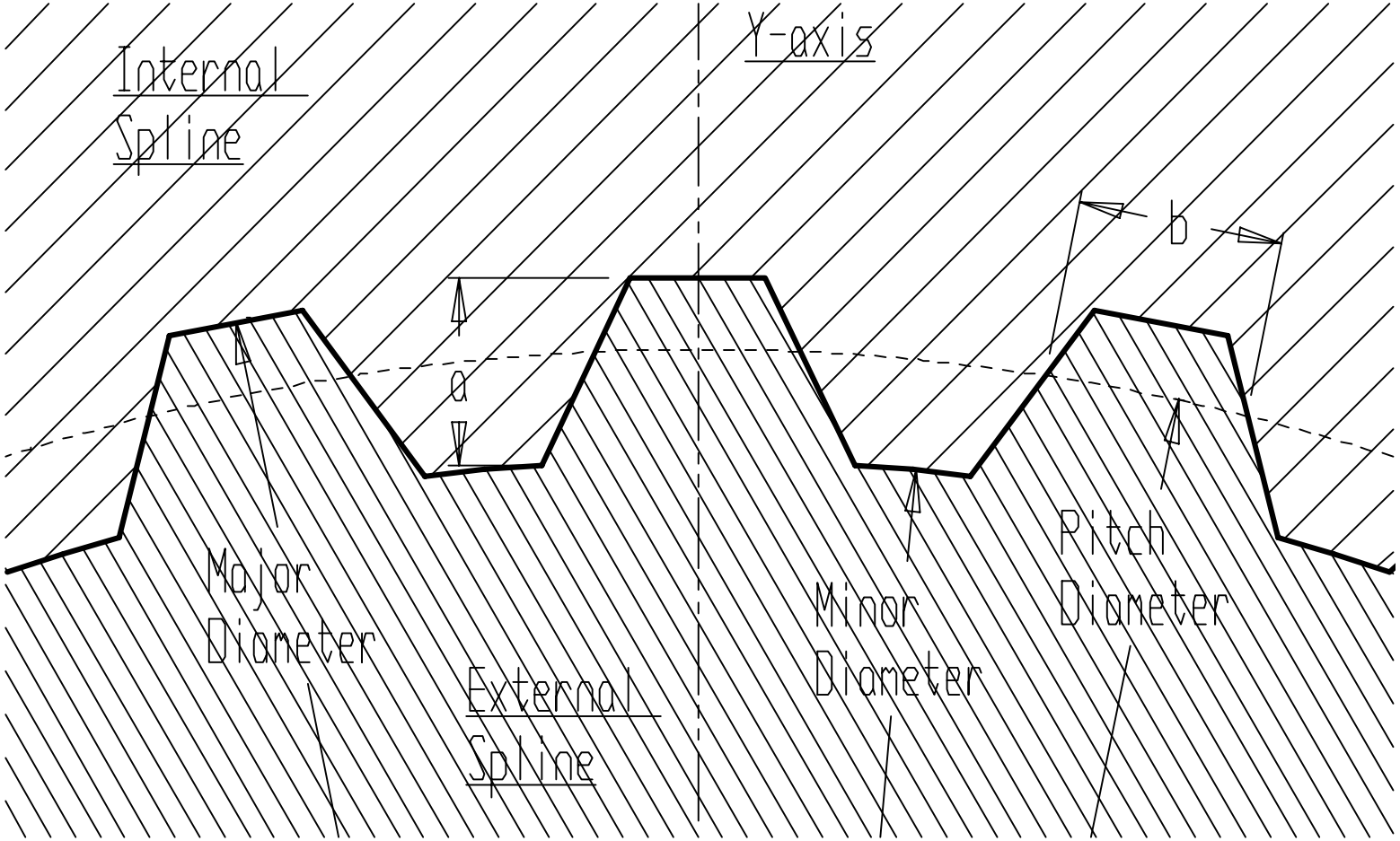

Figure 1. Illustration of an internal and external spline pair.

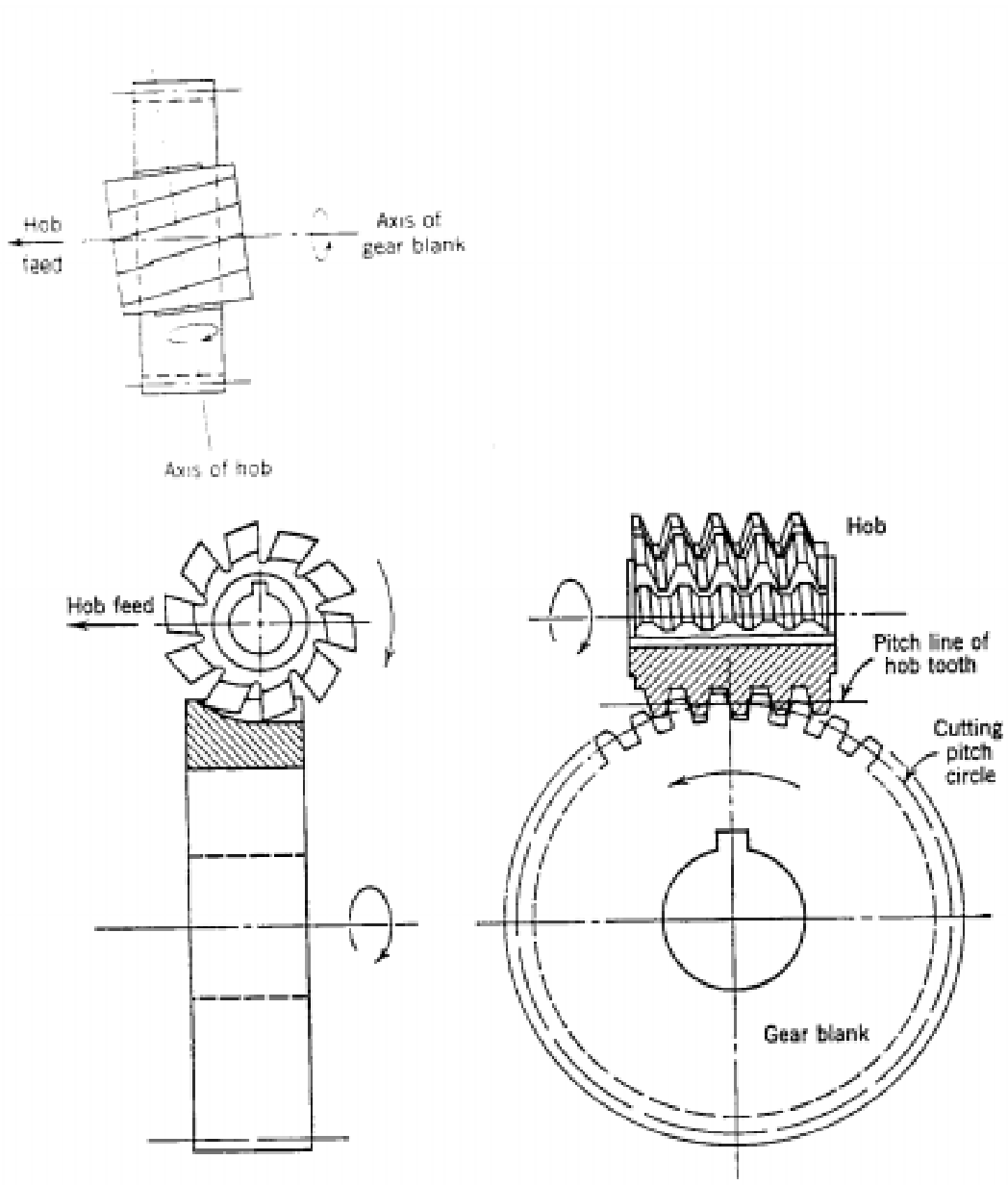

Figure 2. Diagram of a hob tool generating splines on a shaft [3].

Typically, an engineer consults ANSI B92.1 1970 [2] for guidance in designing a spline coupling. According to this standard, two key parameters are used to define the spline: the pitch and the number of teeth. Splines and gears are similar in that many of the same techniques are used to manufacture them. They also share very similar terminology. However, where gears have only one number to describe the pitch, splines have two. For instance, in a spline with a pitch number of 12/24, the numerator is known as the diametral pitch (P) and controls the pitch diameter. The denominator, which is always double the numerator, is known as the stub pitch (P_s). The stub pitch controls the tooth depth or thickness. The pitch number along with the number of teeth (N) defines the diameter of the pitch circle (D) according to the following formula:

$$D = \frac{N}{P} \tag{1.1}$$

The other parameters needed to construct the spline such as the pressure angle (ϕ), base diameter ($D \cdot cos\phi$), circular pitch (p), minor diameter (D_i), and major diameter (D_o), are all defined similarly for gears.

The diameter of the pitch circle is defined as:

$$D_p = \frac{Np}{\pi} \tag{1.2}$$

The thickness (on the pitch circle) of a spline tooth is found using Equation (1.3):

$$t_p = \frac{\pi}{N}\frac{D_p}{2} \tag{1.3}$$

The fit type is not particularly relevant here since mating between internal and external spline teeth is not considered in this analysis. The stresses in a splined shaft can

be calculated using the stress formulae given in the ANSI B92.1 1970 standards. However, those equations do not consider the effects of a step or partial splines on the stresses in a splined shaft.

The first splined shaft considered is the stepped splined shaft, shown in Figure 3 and Figure 4. Normally, an engineer consults a reference such as *Peterson's Stress Concentration Factors* [3] for the appropriate stress concentration factor, depending on the fillet radius. However, such references do not provide the necessary factors for combinations of design features such as a stepped shaft, with splines. The effect of the splines on the transmission of stresses across the shaft step is of key interest. The stepped shaft consists of a straight section that is smooth and cylindrical in shape, with some diameter d. It also consists of a splined section, which has major and minor diameters (D_i and D_o), respectively. Several models were constructed with various ratios of d/D_o (0.50, 0.750, and 0.8865), to study the effects of this ratio on the variation of stresses along the shaft.

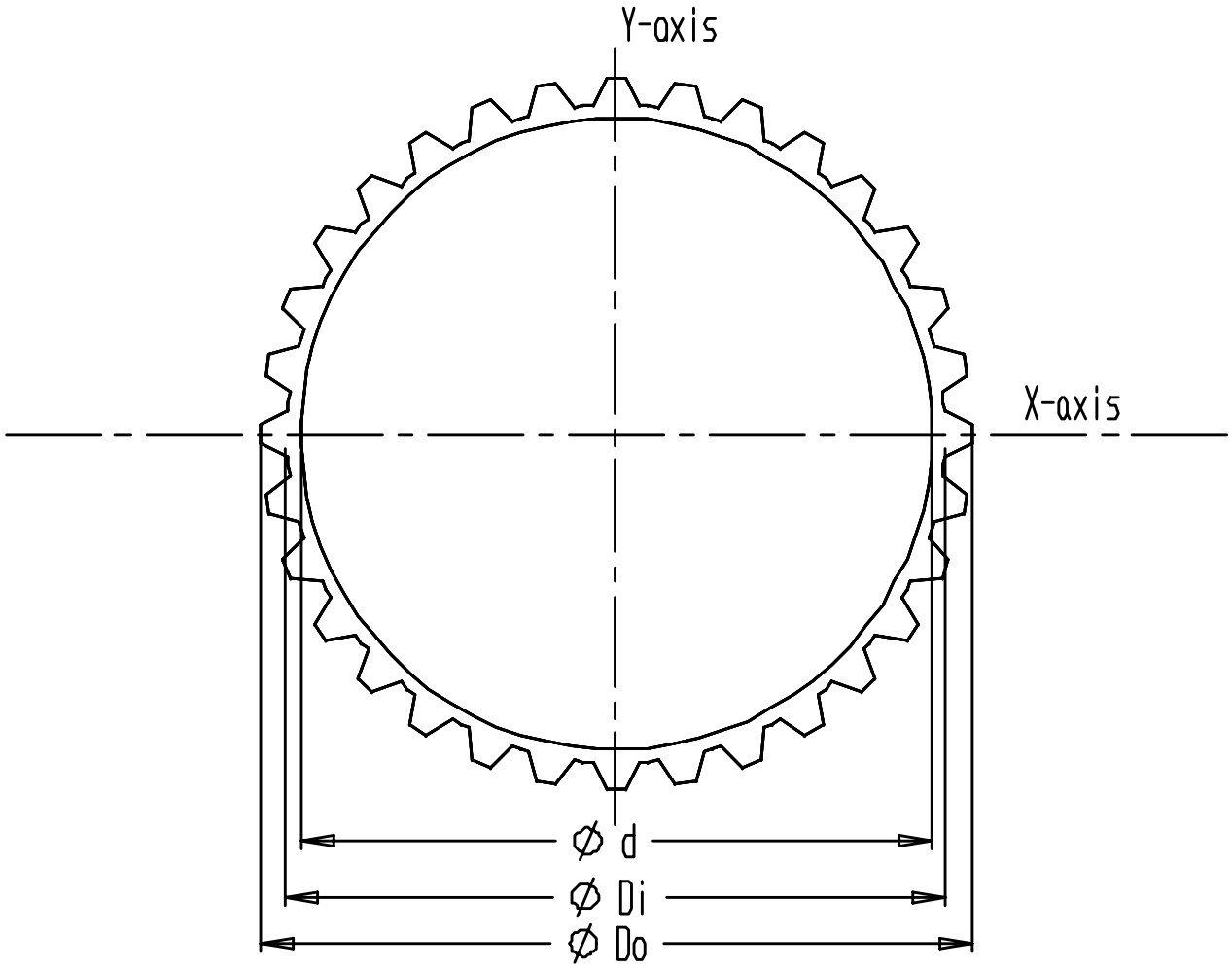

Figure 3. Schematic view of a stepped shaft: Front view

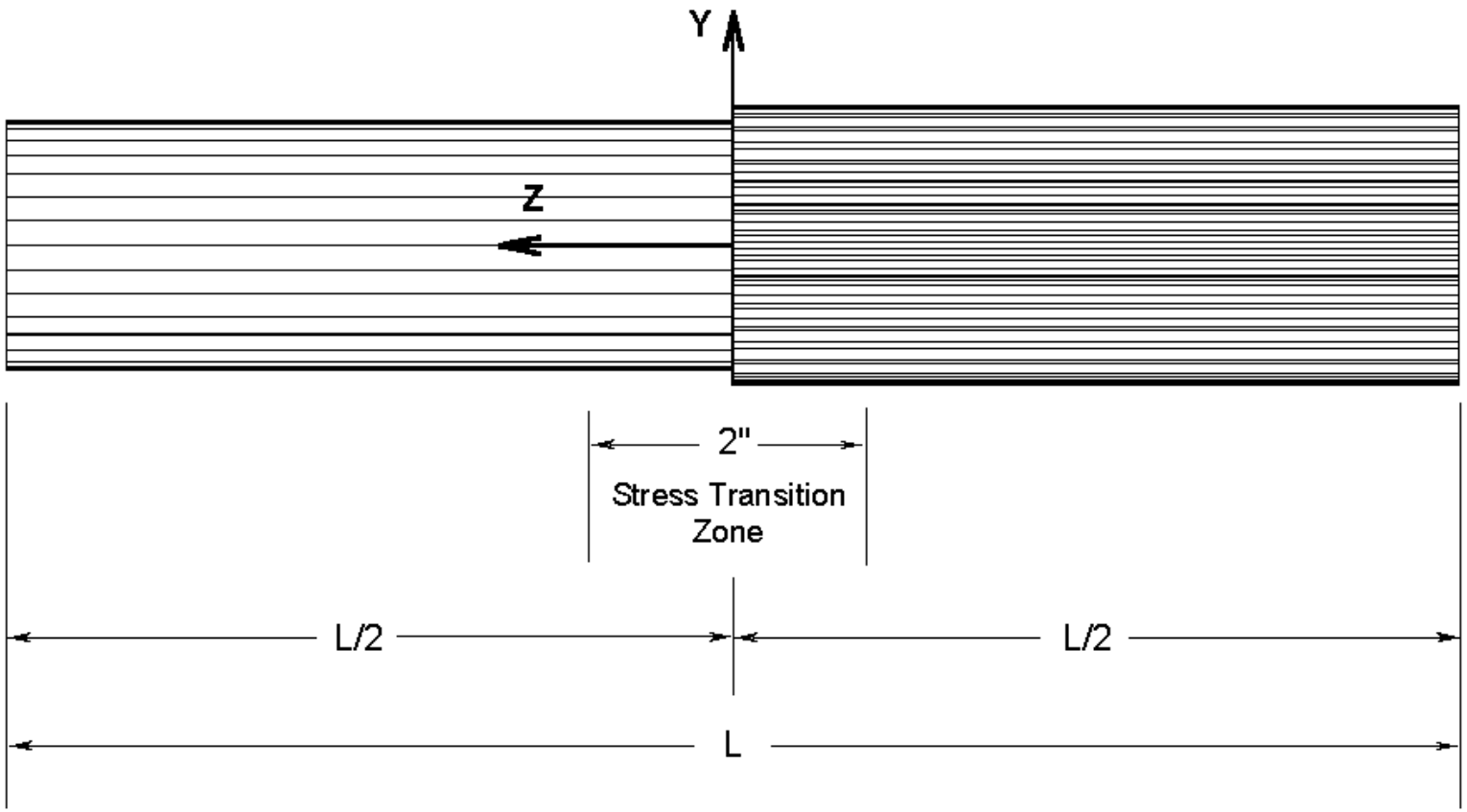

Figure 4. Schematic view of a stepped shaft: Plan view.

The second type of structure studied in this thesis was the partially splined shaft, shown in Figure 5 and Figure 6. The partially splined shaft consists of a straight, smooth, circular section of some diameter (D_o) and a splined section, also with major diameter (D_o). In the partially splined shaft, the major diameter of the shaft does not step down to a smaller sized shaft. Instead, the hobbing tool stops cutting the shaft at some intermediate position, resulting in incomplete splines that extend only partially along the length of the shaft.

Several partially splined models were constructed using several hob radii, (R=1.00"(0.0254m), R=1.50"(0.0381m), and R=2.0"(0.0508m)) to create the incomplete spline teeth. This was done to examine the effects of the incomplete tooth shape on the variation of stress in the zone of transition between the straight and partially splined sections of the shafts.

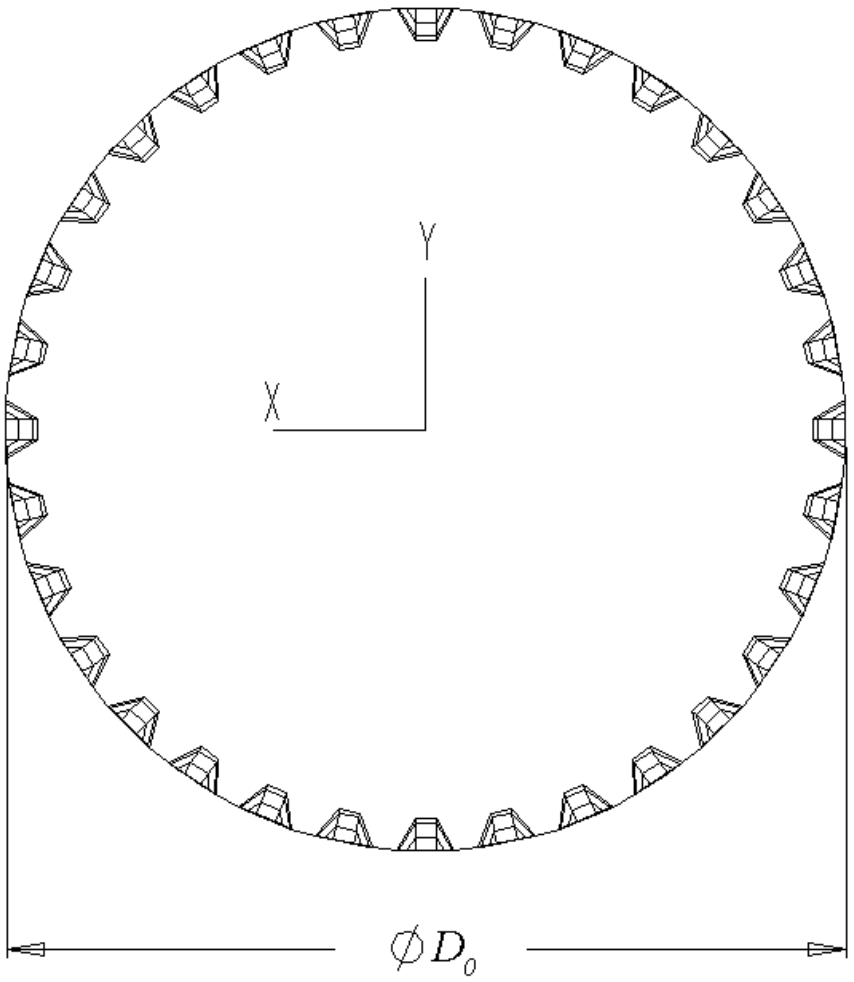

Figure 5. Schematic view of a partially splined shaft: Front view

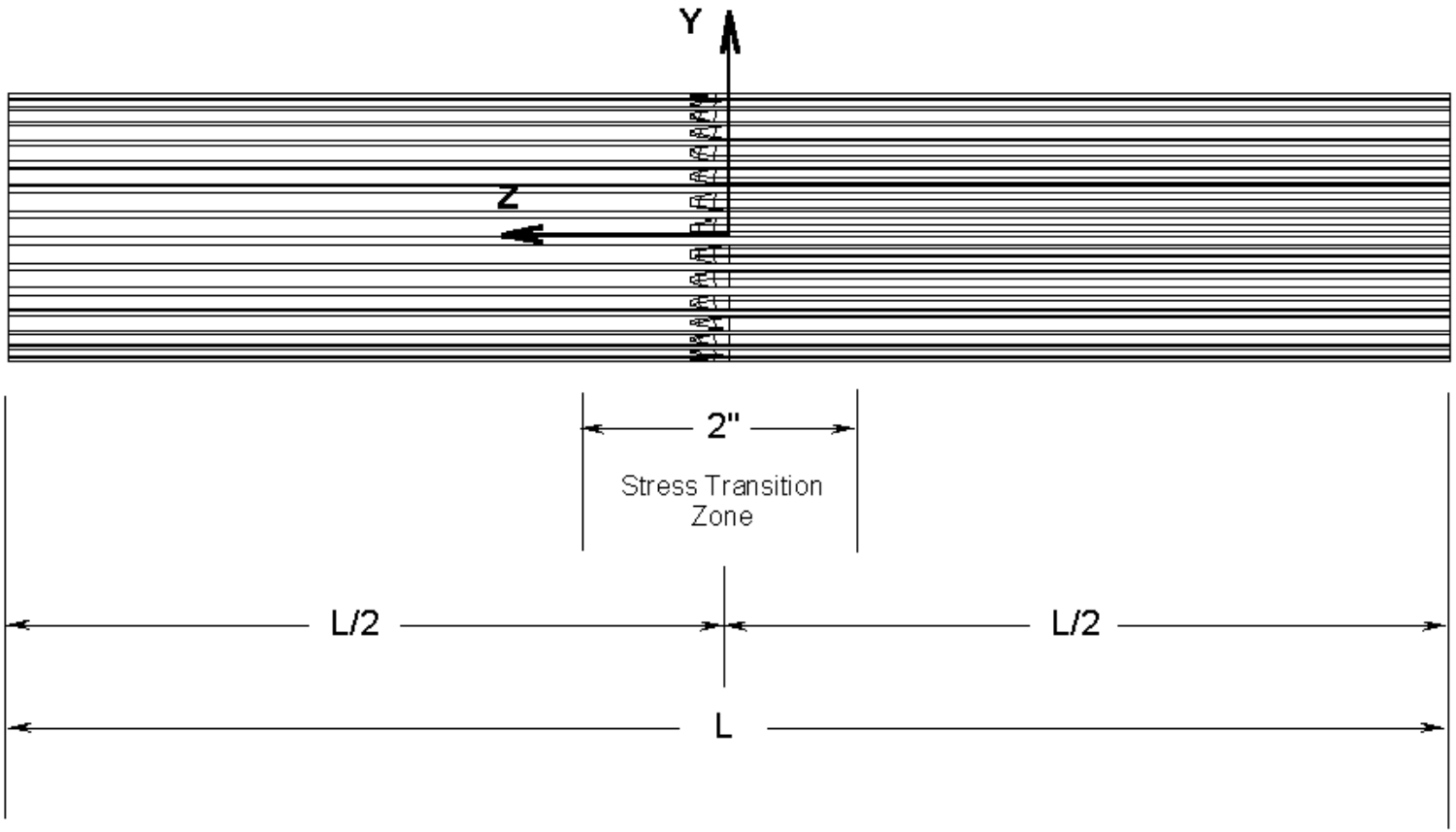

Figure 6. Schematic view of a partially splined shaft: Plan View

Forensic specimens of failed shafts from the Fairchild mining vehicles indicate that failure occurs at a recurring location on the stepped shaft. As shown in Figure 7, the Fairchild specimens tend to fail about Z=0.0"(0.0m) to Z=0.25"(0.00636m) from the shaft step, in the non-splined portion of the shaft. Conventional wisdom concerning stress concentrations for stepped, round shafts without splines indicates that the peak stresses will occur at the root of the fillet or at the step. Shaft failures should occur wherever peak stresses occur. It will later be shown through finite element modeling of the shafts, that the locations of the predicted peak stresses coincide with locations of failure in the Fairchild specimens. It will further be shown that the manner in which the shafts are loaded will have an effect on the peak stress in the shaft. Table 1 shows the dimensions used to generate the splined shaft models.

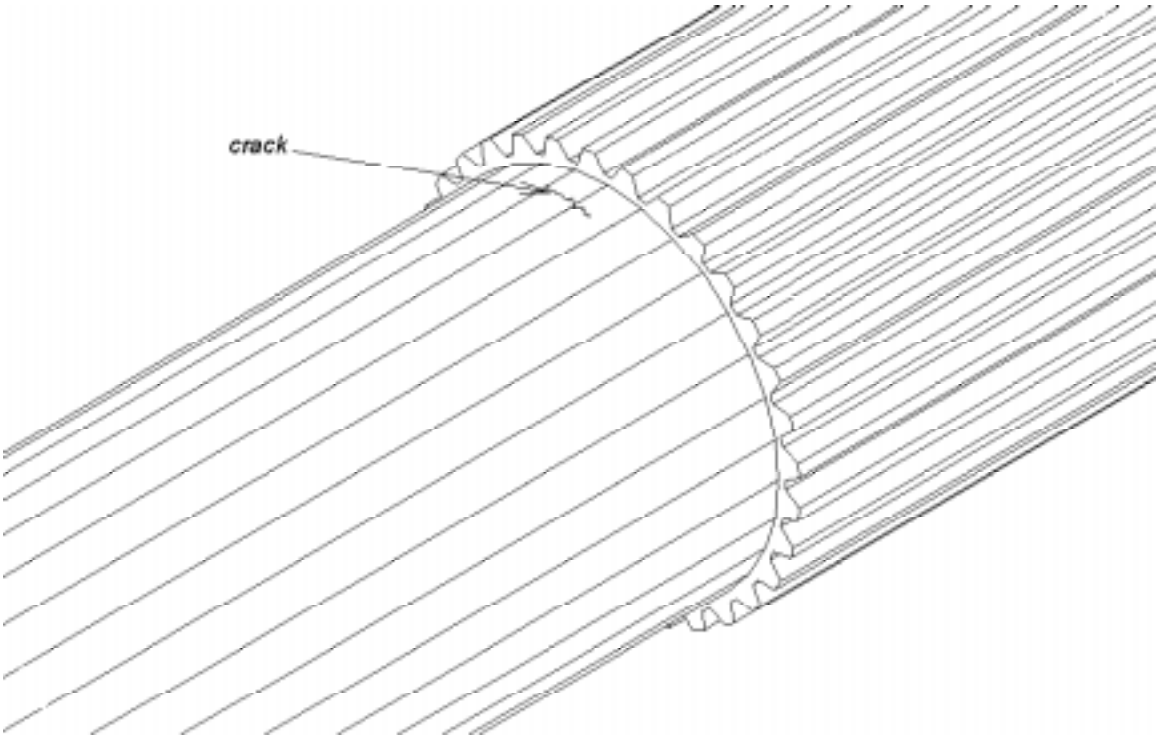

Figure 7. A sketch of a Fairchild shaft specimen showing the location of cracks which eventually led to failure of the shaft. (Specimen provided by R. Plumley of Fairchild International, Inc. of Glen Lyn, VA to R.G. Mitchiner of Virginia Polytechnic Institute and State University).

Table 1. Splined Shaft Specifications

Number of Spline Teeth	*(N)*	32	
Pitch Number		12/24	
Diametral Pitch		12	
Stub Pitch		24	
Pressure Angle	ϕ	30°	
Base Diameter	D_b	2.3094"	(0.0586m)
Pitch Diameter	D_p	2.6667"	(0.0677m)
Major Diameter	(D_o)	2.7500"	(0.6985m)
Minor Diameter	(D_i)	2.5390"	(0.0645m)
Non-Splined Section Diameter	*(d)*	2.4375"	(0.0619m)
Tooth Thickness (at pitch diameter)	*(t)*	0.1309"	(0.0033m)
Tooth Height $(D_o - D_i)$	*(a)*	0.2110"	(0.0054m)
Stepped Shaft			
$d/D_o=0.500$	d =	1.3750"	(0.0349m)
$d/D_o=0.750$	d =	2.0625"	(0.0524m)
$d/D_o=0.886$	d =	2.4375"	(0.0619m)
Partially Splined Shaft			
	$d = Do$	2.7500"	(0.0699m)
	R=	1.0000"	(0.0254m)
	R=	1.5000"	(0.0381m)
	R=	2.0000"	(0.0508m)

Splined shafts have a different cross-sectional profile than prismatic, circular shafts. Despite this difference, one can still make some reasonable, qualitative predictions about the stress variation patterns in the splined shaft under bending and torsion loads. For instance, Figure 8 shows an example of the stress contours that would result on a cross-section of a splined shaft under pure torsion. Notice that the pattern resembles what one might find in a circular shaft under pure torsion, until one examines the region immediately near the roots of the spine teeth. Each contour line drawn on Figure 8 represents the stress value that varies radially outward from the center of the shaft cross-section. The teeth represent a perturbing feature that upsets the normal pattern that would exist were the teeth not present. The normal pattern would be a family of concentric circles that vary outward from the central axis of the cross-section.

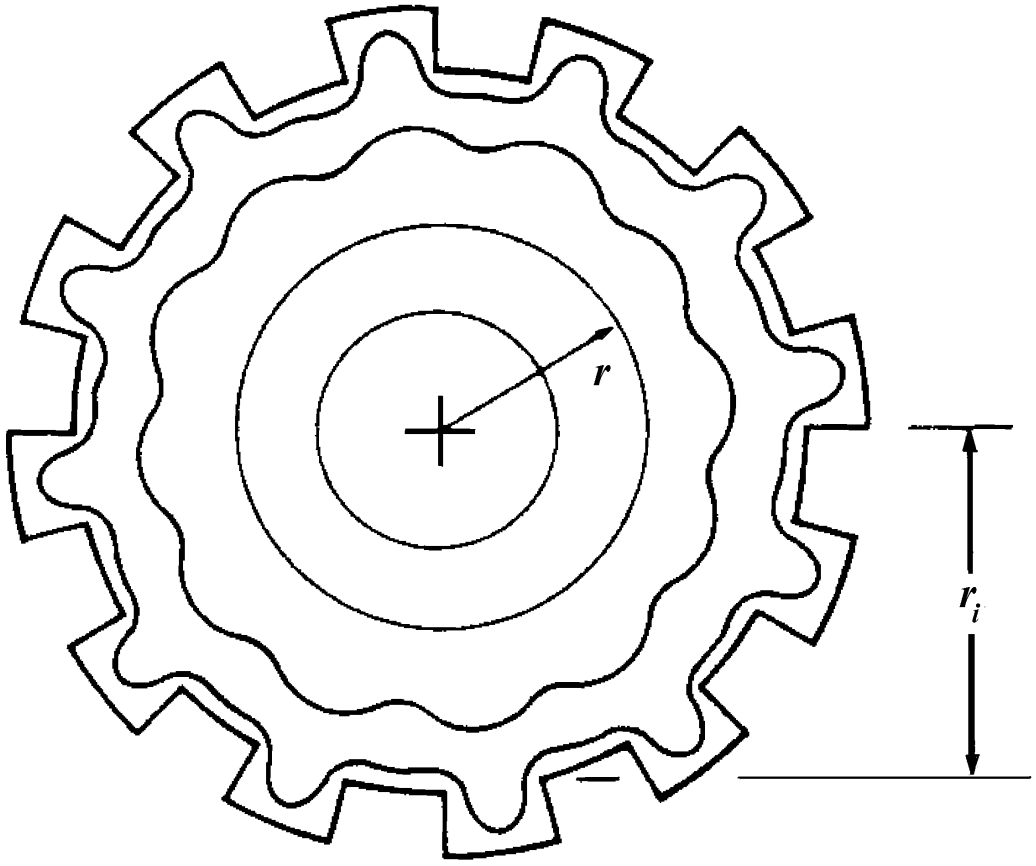

Figure 8. Example of stress contours in a splined shaft under pure torsion. (Adapted from [5])

Under pure bending loads, the expected stress variation pattern is different. Since the teeth in a splined shaft run parallel to its axis, one would expect the teeth to have a minimal effect upon the stress variation throughout the cross-section of the shaft. Figure 9 illustrates what the stress variation will look like in the splined shaft under pure bending. When bending and torsion loads are combined, the resulting stress contour will be some combination of what is shown in Figure 8 and Figure 9. For the stepped shaft, the stress contour on the cross-section in vicinity of the step is not easily predictable. Likewise, near the incomplete teeth of partially splined shaft, there is no way to readily characterize the pattern of stress variation. By using finite element analysis, it will be possible to characterize the stresses resulting from combinations of bending and torsion loads for each type of structure.

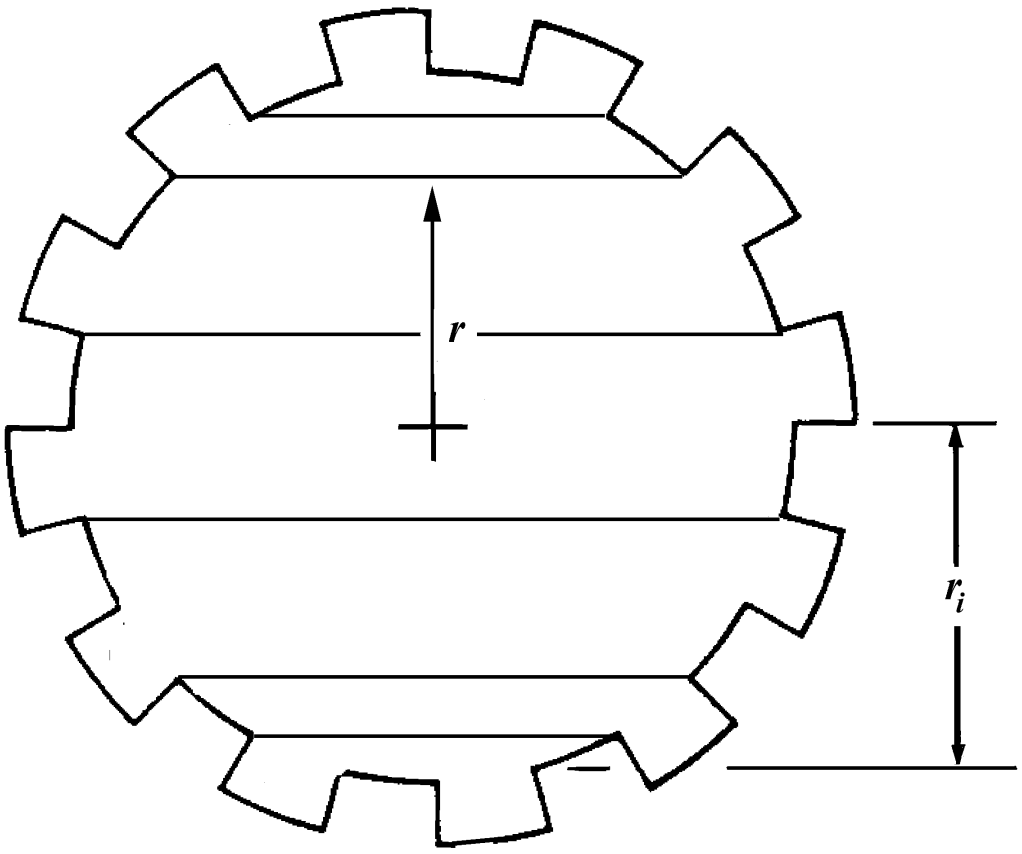

Figure 9. Example of stress contours in a splined shaft under pure bending (Adapted from [5]).

II. LITERATURE REVIEW

Stress results for the types of structures considered in this research have not previously been obtained in literature by the time of this writing. In fact, few examples can be found in literature in which three-dimensional models are used to analyze splines at all. Most studies of splines are performed using two-dimensional modeling.

The analytical models used to predict the stresses in the non-splined sections of the models were straightforward. To calculate the axial stress due to bending in a solid bar of circular cross-section, the beam flexure formula is used [4]:

$$\sigma = \frac{My}{I} \tag{2.1}$$

Where σ is the axial stress normal to the plane of the cross section, M is the moment applied to the bar cross-section, y is the distance from neutral surface to the top outer surface of the bar, and I is the cross-section moment of inertia. Recall that for circular cross-sections:

$$I = \frac{\pi r^4}{4} \tag{2.2}$$

Similarly, the shear stress due to torsional loads in a bar with a circular cross-section can be calculated from the following formula [4]:

$$\tau = \frac{Tr}{J} \tag{2.3}$$

Where τ is the shear stress in the plane of the cross-section due to torsion, T is the applied torque, r is the radial distance from the neutral surface to the outer surface of the bar, and J is the polar moment of inertia of the bar. For a prismatic bar with a circular cross-section, J is defined as:

$$J = \frac{\pi r^2}{4} \tag{2.4}$$

Depending on the ratio of bending to torsion, the von Mises stress is calculated by combining Equations (2.1) and (2.3). The von Mises stress is an equivalent, or effective stress that represents the overall magnitude of stress at a point, regardless of the orientation at which the stress is considered. The von Mises is defined by Equation (2.5)[5]:

$$\sigma' = \frac{1}{\sqrt{2}}\left[(\sigma_x - \sigma_y)^2 + (\sigma_y - \sigma_z)^2 + (\sigma_z - \sigma_x)^2 + 6(\tau_{xy}^2 + \tau_{yz}^2 + \tau_{zx}^2)\right]^{1/2} \tag{2.5}$$

Equation (2.5) describes the general, three-dimensional state of stress at a point in the shaft. It is assumed that the material under consideration exhibits linear elastic mechanical behavior is isotropic, and homogenous. It is further assumed that the loads placed on the shaft will result in deflections that are small enough not to significantly alter its geometry. Only shear stress due to torsion is considered. Any shear effects introduced by transverse loads are ignored. The shear stress is assumed to vary only radially from the axis of the shaft, provided that the stress is considered in a cross-section normal to the axis of shaft. Thus, Equation (2.5) reduces to:

$$\sigma' = \sqrt{\sigma_z^2 + 3\tau_{xz}^2} \tag{2.6}$$

Where σ' now represents the von Mises stress magnitude, σ_z axial stress developed in the shaft cross-section due to bending, and τ_{xz} is the shear stress on the shaft due to applied torque. Note that in this form, the combined stress magnitude resembles that of the conic section known as the ellipse. This provides some clue as to what the stress distribution in a shaft will look like under combined bending and torsion loads.

Similarly, Algor uses Equation (2.7) to calculate the von Mises stress [6]:

$$\sigma_e = \sqrt{0.5[(\sigma_x - \sigma_y)^2 + (\sigma_y - \sigma_z)^2 + (\sigma_z - \sigma_x)^2] + 3(\tau^2_{xy} + \tau^2_{yz} + \tau^2_{zx})} \qquad (2.7)$$

The Design Guide to Involute Splines by Cedoz and Chaplin [7], provides general information about the design of spline connections. The work is based closely upon the actual ANSI B92.1 1970 standard for splines. Cedoz and Chaplin [7] give the following equation for calculating shear stress at the root of the spline teeth:

$$S_s = \frac{2T}{DN_e L_g t} \qquad (2.10)$$

In Equation (2.10), S_s is the shear stress at the tooth root, T is the torque applied to the splined shaft, D is the pitch diameter, N_e is the number of teeth actually in contact, L_g is the length of the tooth engagement, and t is the tooth thickness on the pitch circle. It was found that Equation (2.10) does not compare well with the shear stresses obtained from the modeling in this research since it depends upon actual engagement of teeth between the internal and external splines. Such a scenario is not relevant, since only open splines with no mating members are considered in this research. Cedoz and Chaplin [7] also

suggest the following equation for calculating the nominal shear stress developed under the root of a spline tooth when subjected only to pure torsion.

$$S_t = \frac{32TD_{re}}{\pi\left(D_{re}^4 - D_{in}^4\right)} \tag{2.11}$$

Where S_t is the torsional shear stress, D_{in} is the shaft inside diameter, and D_{re} is the minor diameter of the splined shaft. This form of the equation is not particularly useful for this research since it applies to external splines with teeth on the inner diameter of an annular shaft.

Machinery's Handbook [8] addressed some of the same material on spline design as Cedoz and Chaplin [7]. Machinery's Handbook [8] also included an equation for calculating the shear stress at the root of external spline teeth on a solid shaft. That equation is written below as Equation (2.12).

$$S_s = \frac{16TK_a}{\pi D_{re}{}^3 K_f} \tag{2.12}$$

Where T is the transmitted torque and D_{re} is the minor diameter of the external spline. The parameters K_a and K_f are the load application factor and fatigue factor, respectively. Both K_a and K_f are set to unity in order for Equation (2.12) to be applicable to this work. Equation (2.12) then reduces to the following:

$$S_s = \frac{16T}{\pi D_{re}{}^3} \tag{2.13}$$

The final form of the Equation (2.13) differs from Equation (2.10) because it gives results for a solid shaft rather than a hollow shaft.

Hayashi and Hayashi [9] developed formulas for estimating the torsional stiffness of "small" involute spline shaft couplings. Several splined couplings were fabricated and tested. The torsional stresses obtained from these tests compared with theoretical stresses that they formulated. The formulas they developed for torsional stress were very similar to the formulas developed for the same stress in Machinery's Handbook, providing support for their use here. Peterson's Stress Concentration Factors [3] cited a three-dimensional photoelastic study of splines by Yoshitake [3] of a particular eight-tooth spline. The study varied the tooth fillet radius in three tests. For each test, a torsional stress concentration factor was generated for an external open spline or, a spline with no mating member. The following formula for torsional stress at the root of the splines is given in Peterson's [3]:

$$\tau_{\max} = \frac{16T}{\pi D_o^{\,3}} K_{ts} \tag{2.14}$$

Where T is the applied torque, d is the major diameter of the spline, and K_{ts} is the torsional stress concentration factor. The curve shown in Figure 10 is useful only for eight-tooth splines with stress relieving fillets between the teeth. However, the splined shaft models considered in this research are thirty-two tooth splines, with no fillets at the tooth roots. The K_{ts} values in Figure 10 would not be useful for obtaining the proper K_t value to correctly predict the torsional stress in the splined shaft models here. Therefore, the Yoshitake [3] curve was not used to predict the stresses in the splined shafts.

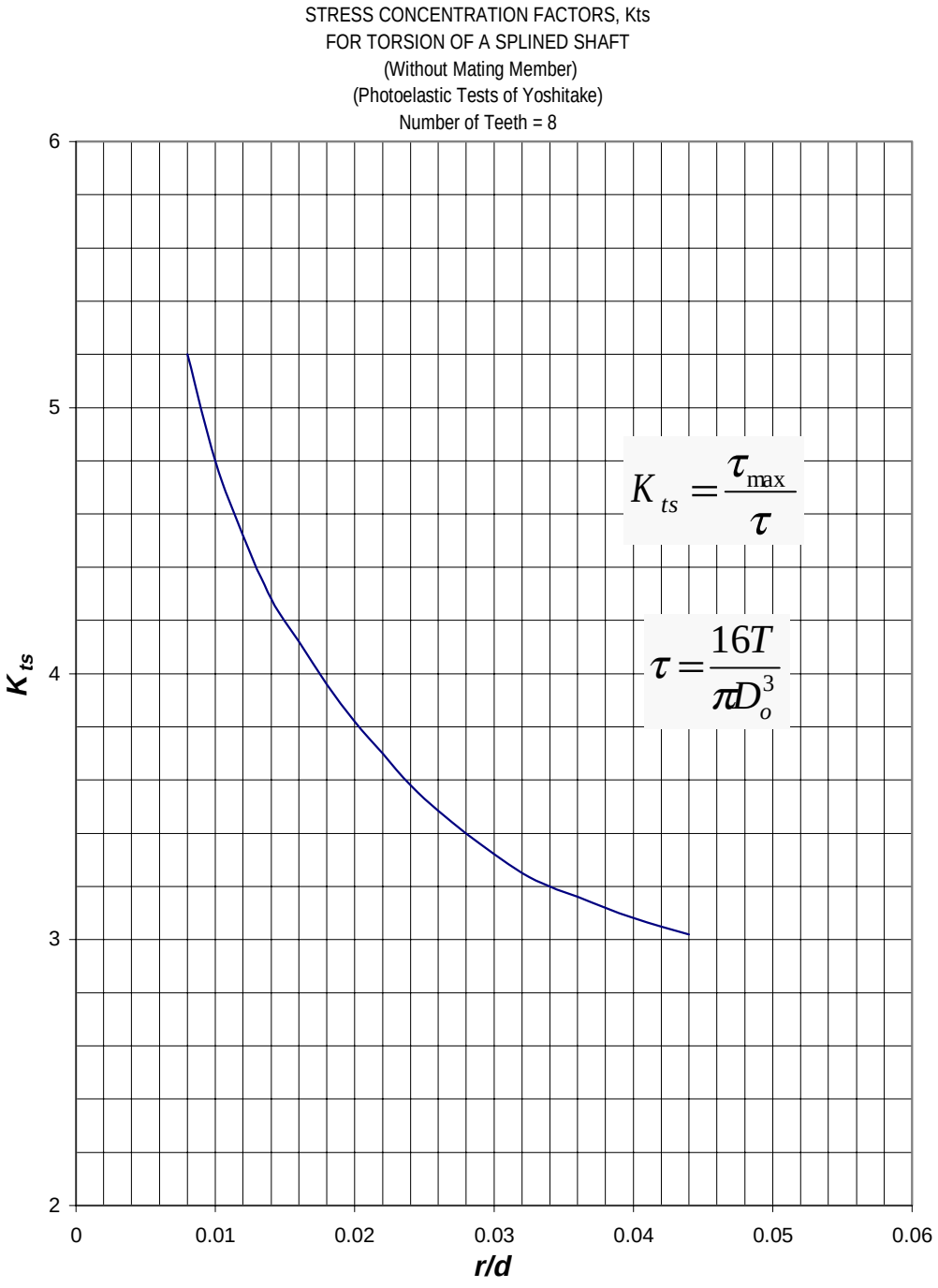

Figure 10. Stress concentration factor K_{ts} for torsion of an 8-tooth splined shaft (adapted from [3]).

The equations used to construct the analytical models for the splined sections of the shafts were similar in form to those used for the non-splined sections. However, the source of the values for *I* and *J* were different for the splined sections. Numerical values for *I* and *J* were determined using Cadkey 97, the drafting software used to generate the solid models used in this research. The computer-generated values for *I* and *J* were then substituted into Equations (2.15) and (2.16), respectively. The computer-generated values were used to insure that the torsional stiffness properties of the splined sections were accurately captured when calculating the nominal bending and torsional stresses, i.e. Equations (2.17) and (2.18). The von Mises stresses obtained using the latter method did not compare well with those generated through finite element analysis, deviating as much as 30%. However, the deviation increased as the magnitude of torsional load on the shaft increased relative to the bending load increased. This indicates that the analytical model used underestimates the torsional stiffness of the splines.

An alternative method for determining the torsional stiffness of the splined shaft section was developed based upon the results of Iwao and Teru Hayashi [9]. This method involves determining the stiffness of the splined section of the shaft both calculating the stiffness of the individual teeth and the shaft without the teeth. The two stiffness values are then combined using linear superposition.

Consider a round, circular cross section shaft under pure torsion. The angular deflection experienced at one end of the shaft, relative to the other is:

$$\phi = \frac{TL}{JG} \tag{2.15}$$

The angular strain then, is defined by the following:

$$\gamma = \frac{r\phi}{L} \tag{2.16}$$

The torsional shear stress experienced by the shaft is then:

$$\tau_{xy} = G\frac{T}{k_r}\frac{D_i}{2} \tag{2.17}$$

Where k_r=JG may be thought of a torsional rigidity constant, analogous to the EI constant commonly used in beam flexure analysis. Also, let

$$k_r = k_{t,r} + k_{r,r} \tag{2.18}$$

Where $k_{t,r}$ is the torsional stiffness of all 32 spline teeth, and $k_{r,r}$ is the torsional stiffness of the circular shaft without the teeth. To find $k_{t,r,}$ the following equation is used:

$$k_{t,r} = \frac{8ab^3 + 32a^3b}{3}G \tag{2.19}$$

Where a is the spline tooth height, b is the spline tooth width, and G is the modulus of rigidity of the shaft material. To find $k_{r,r}$ the following equation is used:

$$k_{r,r} = \frac{\pi D_i^4}{32}G \tag{2.20}$$

Note that $k_{r,r}$ is calculated using D_i the minor diameter of the splined shaft. Combining Equations (2.17), and (2.18):

$$k_r = \left[\frac{8ab^3 + 32a^3b}{3} + \frac{\pi D_i^4}{32}\right]G \tag{2.21}$$

Finally, combining Equations (2.19) and (2.20):

$$\tau_{xy} = \frac{TD_i}{2}\left[\frac{8ab^3 + 32a^3b}{3} + \frac{\pi D_i^4}{32}\right]^{-1} \tag{2.22}$$

where a is the tooth height from the spline root, b is the linear width of the tooth on the pitch circle, and D_i is again the minor diameter. Equation (2.22) [9] is an alternative method for determining the torsional shear stress on a splined shaft. Equation (2.22) uses linear superposition to combine the torsional stiffness of the spline teeth and the torsional stiffness of the body of the shaft without the teeth. This analytical method overestimates the spline stiffness more than the method of using the computer generated stiffness. Therefore, the computer-generated moments of inertia were used to calculate the torsional stiffness in the splined sections of all the models. The analytical model used here was expected to contain some error when calculating torsional stresses in the splined shaft since it adapts a solution developed for bars with purely circular cross-sections. In addition, the analytical model does not take into account the stress concentrations developed at the tooth roots, which become significant under torsional loads.

III. MODELING

3.1 Initial Modeling Efforts

The first efforts to model splined shafts in this investigation were using the Structural Dynamics Research Corporation (SDRC) Integrated Dynamics and Engineering Analysis Software version 5.4 (IDEAS). Though not carried to completion, attempts were made at the early stages of the research to model the inner, external spline and the outer, internal spline parts of the connection. Primitives, or parts with very simple geometries compared to the spline, were used initially to test different approaches.

First, an attempt was made to model contact stresses and gaps between mating teeth. Using IDEAS, a square bar was modeled as the internal shaft and a solid block with a square hole was modeled as the external mating member, as shown in Figure 11a. The bar cross-section was slightly smaller that of the hole in the block, as shown in Figure 11b. This was done to create an initial gap as might be found in mating spline teeth with a side-fit. Both the bar and the block were each was restrained at one end. A torque was applied to the end of the bar opposite from restrained end. Gap elements were used to span the gap between the bar and the block.

The resulting displacements did not behave as predicted. Even after consulting the software's SDRC for customer support, it was not possible to get consistent, meaningful results using the gap element strategy. Therefore, it was decided to drop the modeling of the external member and to proceed by modeling the open spline only.

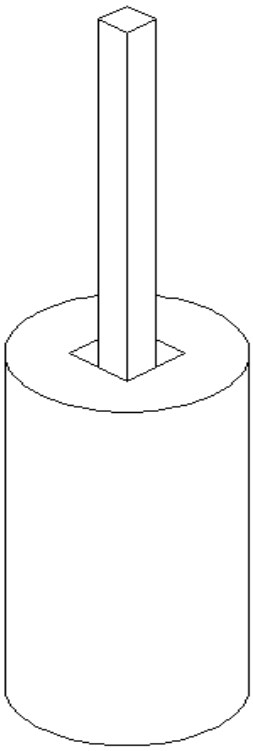

(a)

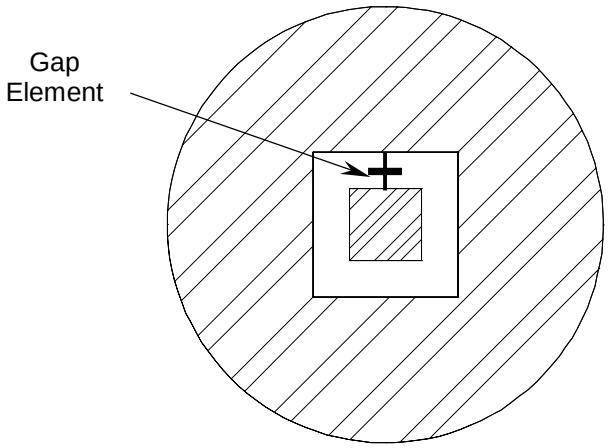

(b)

Figure 11. Primitive shaped used to test the feasibility of using gap elements to model the contact stresses between the external splines and the mating internal spline.

The modeling of open, external splines in IDEAS turned out to be problematic as well. The wire frame pattern of the spline (or spline profile) was generated in IDEAS Master Modeling application. Design parameters from the Fairchild drawing were used as the basis for generating the spline. The final tooth profile was generated using instructions found in Shigley and Mischke [10]. To reduce the required computer resources, all arcs used in the construction of the tooth profile were eliminated, and replaced by chords which spanned the endpoints of those arcs. This made it unnecessary for the computational resources to be spent on generating spline approximations for the circular arcs. The difference in the resulting stresses was negligible.

This spline profile was then extruded along the Z-axis of the shaft with ENDCAPS on option selected to form a solid. A circle was then drawn on the end of the solid splined shaft. The diameter of the circle is smaller that the minor diameter of the spline section. This circle was extruded in the opposite direction on the global Z-axis with ENDCAPS ON, to form a solid cylinder. Then, an attempt was made to join the cylinder and the spline section to form the desired stepped, splined shaft, using IDEAS's Boolean JOIN function. Unfortunately, this Boolean joining process proved ineffective in IDEAS. The IDEAS software was then abandoned for a more robust analysis tool.

A computer-aided drafting (CAD) tool called Cadkey97 Release 1.02 by Baystate Technologies, Inc., was used to generate wireframe models of the spline shaft structures, in lieu of IDEAS. Cadkey97 also included a tool called CK SOLIDS, which converts the wireframe geometry from Cadkey97 into a closed surface. This surface was then exported to Algor in a file format called Initial Graphics Exchange Standard (IGES). In

this work, all IGES format models were saved in the sub-format called Trimmed Surface. This sub-format ensured that all surfaces that composed the model share only two edges. One final attempt was made to use IDEAS by importing to it the IGES format files of the spline models. The idea was that the geometry could be successfully generated using some other CAD software, thereby bypassing the problems with IDEAS Master Modeling package. IDEAS can import such files, and imported the spline model IGES files without incident. IDEAS seemed unable to create a finite element model from the IGES surface files. Thus, IDEAS was not used in any aspect of the subsequent modeling for this research.

To perform the finite element modeling for this work, a modeling software package called Algor, version 3.18 WIN was used. Algor's CAD tools were insufficient for creating the necessary geometry for the splined shafts. Therefore, all of the splined shaft geometry was created using Cadkey97. The advantage to using the combination of Cadkey97 and Algor is that both could be run from any suitably equipped desktop computer and eliminated the need for a dedicated, high-end workstation. Due to the numerically intensive nature of the three dimensional solid modeling performed for this research, large amounts of memory and processing capability were required. The final finite element results from Algor were generated on a workstation with a Pentium II 400 MHz central processing unit with 256 MB of RAM, and 12.8 GB of fixed storage.

3.2 Wireframe Modeling

Cadkey97 was used to create the involute spline tooth profile, the wireframe geometry of the splined shaft structures, and the solid models of the same. The final 32-tooth spline pattern was generated by first drawing the pitch, major, minor, and base circles. By determining the line of action of force indicated by the pressure angle (30 degrees for this work); and indicating the important points of intersection of the tooth width on the pitch circle with tangent points on the base circle, the tooth profile was generated. The beginning of the spline profile construction is illustrated in Figure 12.

Once the base dimensions of the spline cross section were determined, the tooth geometry was developed. First, the tooth centerline was located at some angle relative to the vertical centerline of the spline. The tooth width was then determined by measuring the angle π/N relative to the centerline of the tooth, on the pitch circle. The "boundary" of the single tooth was determined by locating the centerlines of the adjacent teeth along the pitch circle; each π/N radians away from either side of the center tooth. To generate the sides of the tooth, the line of action of force on the tooth had to be determined. This was accomplished by locating the line that is tangent to the base circle and intersects the pitch circle at the tooth edge. This line, called the pressure line, is shown labeled along with the other spline elements in Figure 13.

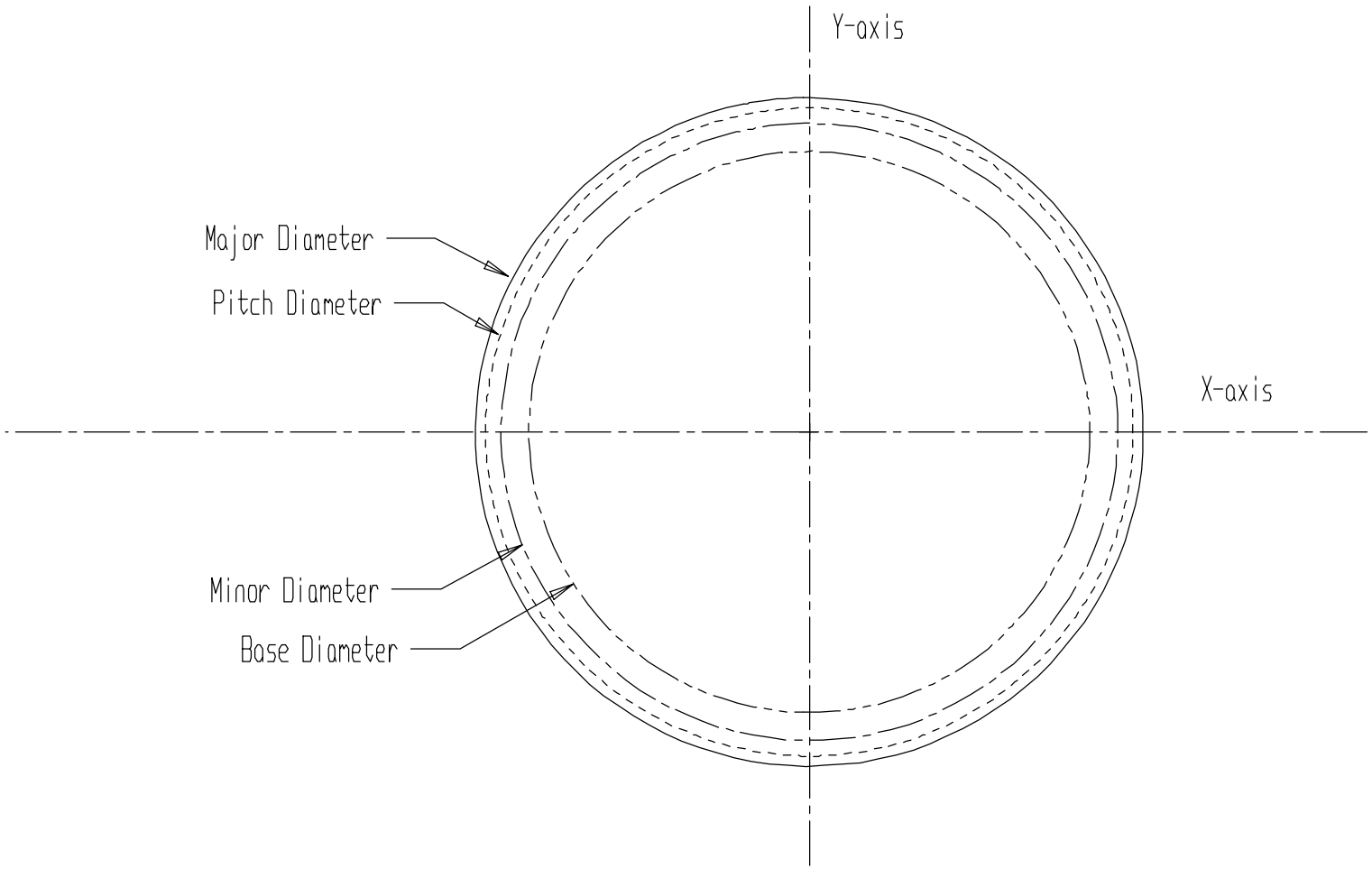

Figure 12. Curves used to construct the fundamental spline profile

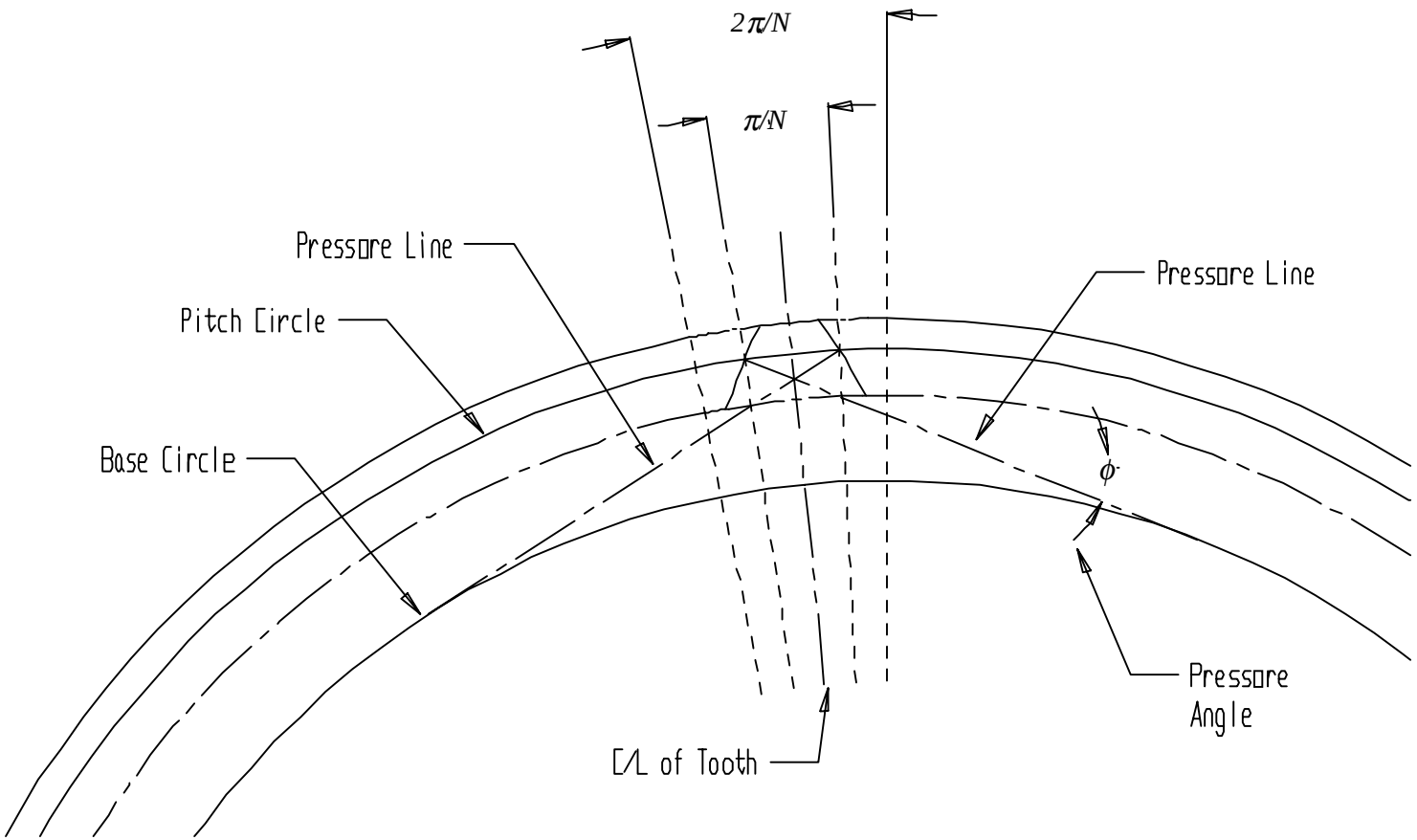

Figure 13. An illustration of the process used to construct the spline profile.

Once the pressure line was constructed, the tooth profile was generated by drawing circles with the centers at the points where the pressure lines and the base circle are tangent. These circles also intersect the width of the tooth on the pitch circle, as shown in Figure 14. Once the necessary geometric boundaries of the single tooth were established, the remaining, unneeded portions of the various curves and lines were trimmed back leaving only the tooth profile, also shown in Figure 14.

Once the single tooth profile was generated, a slight modification was necessary. Cadkey 97 uses spline algorithms to represent curves, including circular arcs. A geometric spline is a mathematical method of numerically discretizing and generalizing geometric data so that can be easily handled by a digital computer or output device. To reduce the required number of parameters and computer resources to process the desired shaped, all the arcs were removed and replaced with equivalent linear chords that spanned the same endpoints as the arcs. In Figure 15, the differences between the curved tooth geometry and the straight-sided tooth are illustrated.

With its geometry now composed of all straight-line entities, the remainder of the geometry generation for the spline was straightforward. The single tooth profile was replicated radially about the center of the spline 32 times, reflecting the desired number of spline teeth. It was then necessary to connect each of the individual teeth with straight-line segments as shown in Figure 16. The solid geometry was generated using the completed 32-tooth shown in Figure 17.

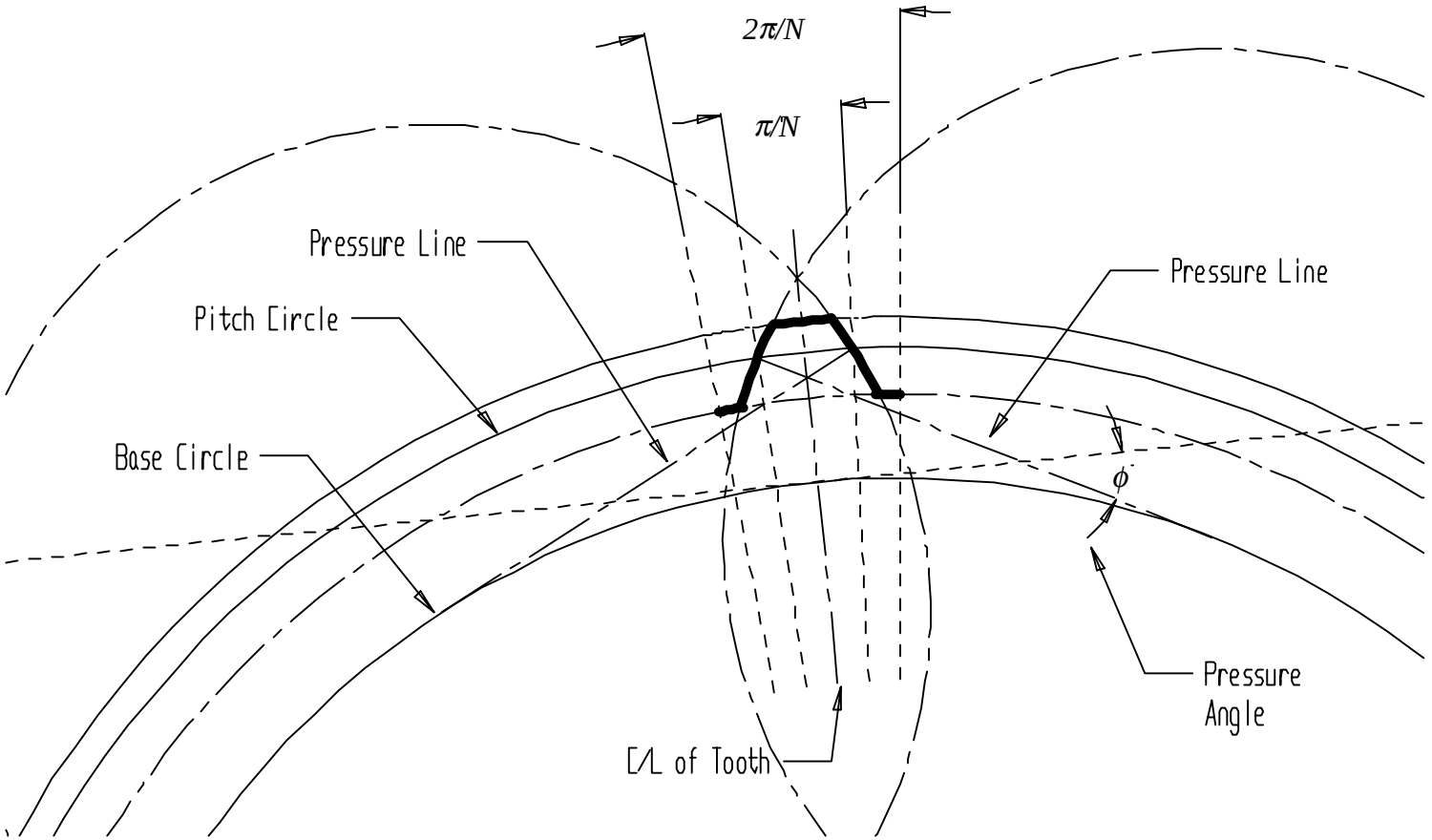

Figure 14. Bold lines show the outline of the tooth.

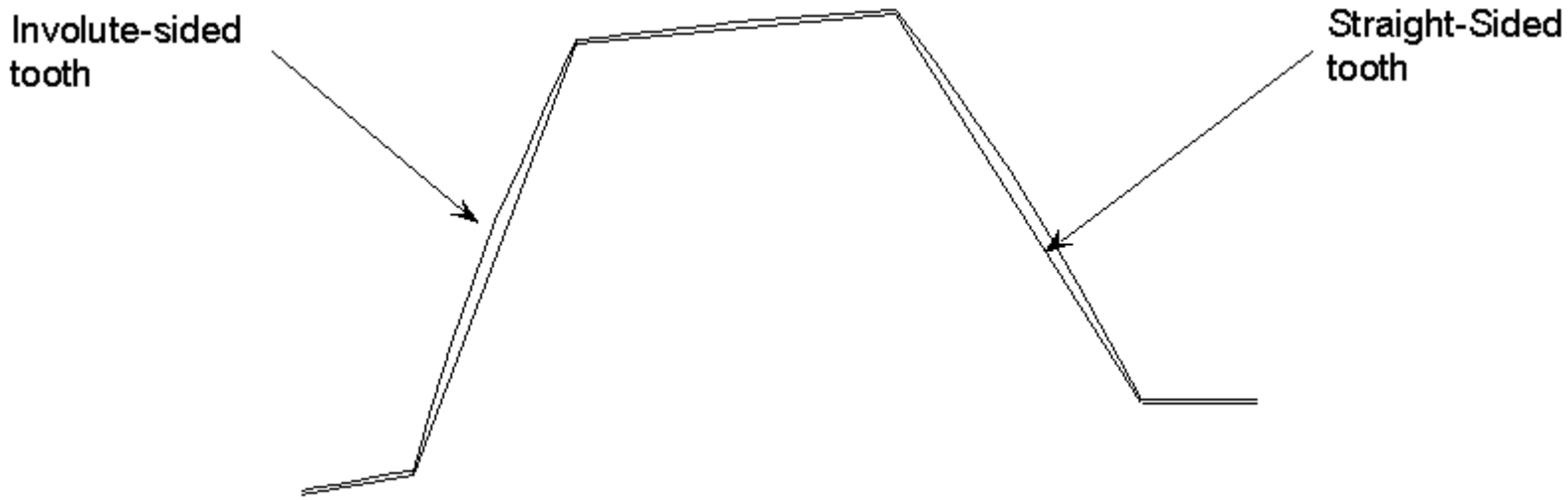

Figure 15. Spline teeth with both the involute and straight sided tooth profiles

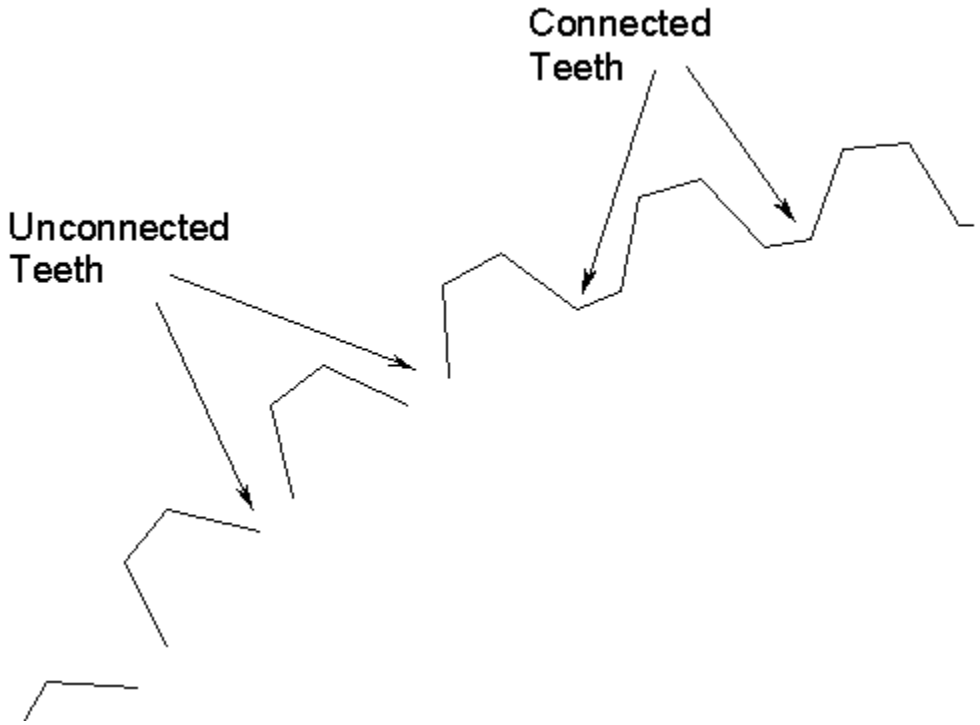

Figure 16. Construction of the spline profile, with some teeth connected and others that have yet to be connected.

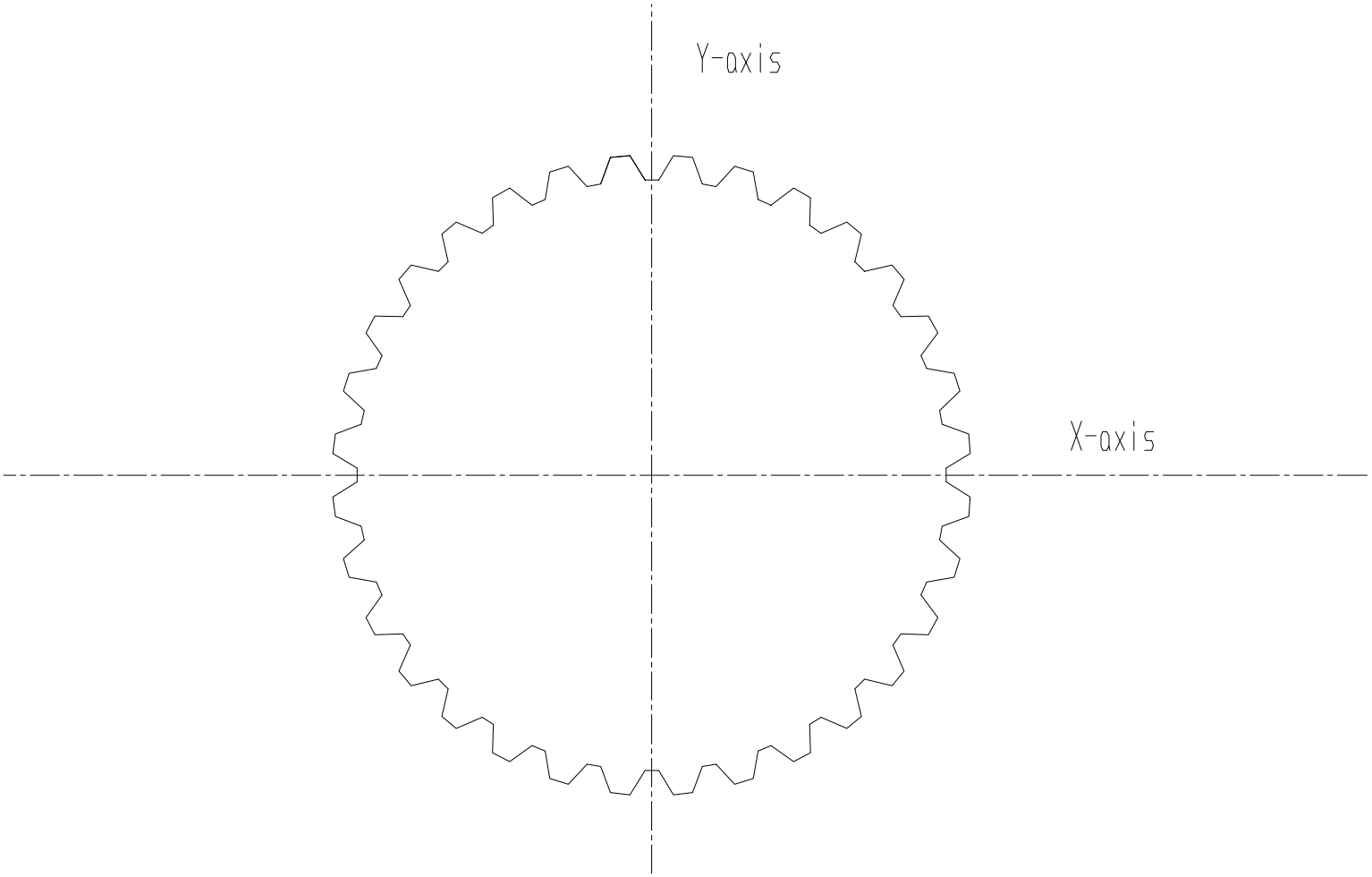

Figure 17. Completed spline cross-section profile.

3.3 Solid Geometry Generation

Before the actual IGES format spline structures could be built in Algor, a few intermediate steps had to be completed in Cadkey97. There were two basic 32 tooth splined structures being studied in this research. The first is a stepped shaft with a splined half and a smooth, round half. It is now necessary to outline the process of constructing the stepped member. A circle representing the cross section of the smooth, round half of the stepped shaft was placed concentrically within the newly created 32 tooth spline profile, as seen below in Figure 18.

Each cross-section profile was then projected equal distances away, in a direction normal to the original in-plane locations, but in opposite directions. The proper optimum length to which each cross-section was projected was based on trial-and-error. Several lengths were experimented with, in order to determine which minimum section length would result in well-developed nominal stresses away from the zone of transition. The completed wireframe is shown in Figure 19.

This wireframe geometry established in Cadkey97 was then converted to solid form. The planes were defined between the bounding curves of the wireframe, establishing an enclosed volume upon which a solid could be based. This was accomplished by opening the solid modeling module called CK SOLIDS, included with Cadkey97. It was during this process that the advantage of using only linear geometric entities to create the spline profile was fully realized. The completed solid geometry model of the stepped splined shaft is shown in Figure 20.

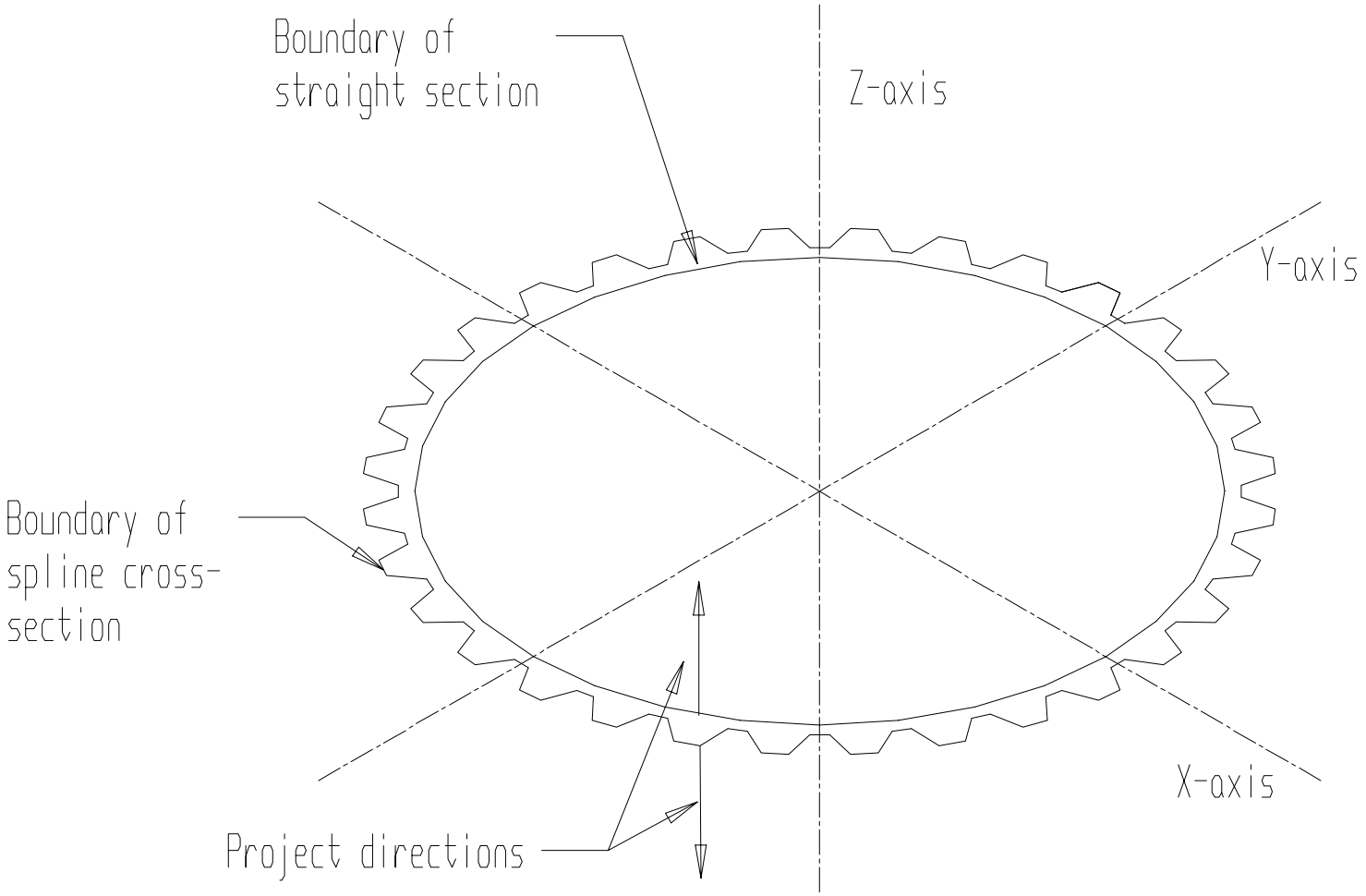

Figure 18. Spline profile with cross-section of straight section shown.

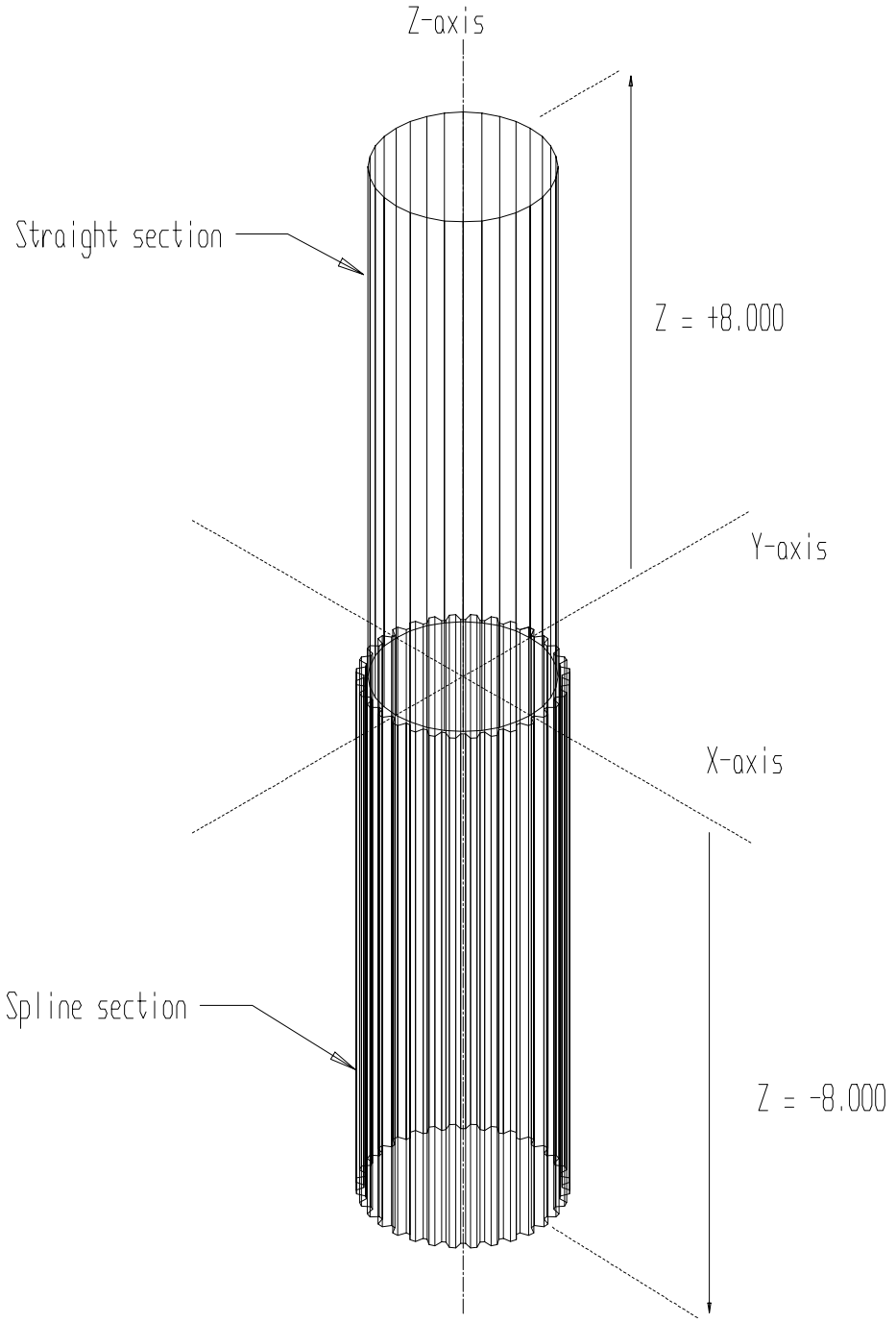

Figure 19. The spline profile curve and the straight section curve are projected in opposite directions to form the stepped splined shaft model.

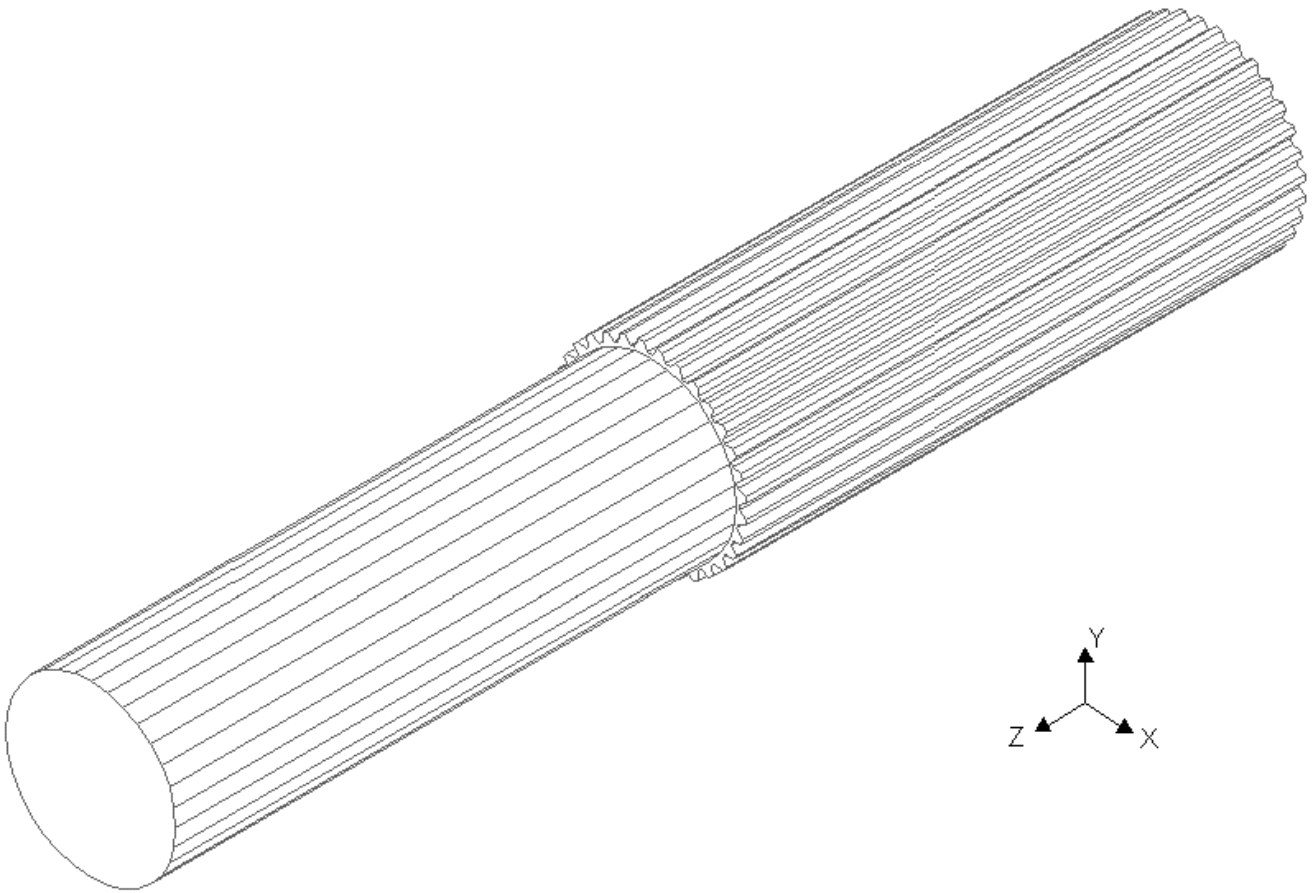

Figure 20. Isometric rendering of stepped, splined shaft

Once this solidifying process was completed, the finished model was then exported from CK SOLIDS as a trimmed surface IGES file. This made it possible for other external programs such as Algor to use the geometric model as input data to build a finite element model.

The second type of structure studied in this research was the non-stepped spline shaft. The interesting feature of the non-stepped structure is that it contains splines that only run partially up the length of the shaft. The splines terminate near the mid-plane of the shaft, resulting in incomplete splines. The size of these incomplete splines was varied to observe the effect on the stresses in the shaft. It is now necessary to discuss the procedure by which these structures were generated.

First, the same spline profile already generated from the construction of the stepped shaft was used to begin construction of the partially splined shaft. A line was created that extends from the root of a spline tooth to that distance corresponding to the desired hob radius. In the case shown in Figure 21, the distance is 1"(0.0254m). Similar hob tool cross-sections were developed with radii of 1.5"(0.0381m) and 2.0"(0.0508m). The hob cross-section was then rotated 90 degrees in preparation for the volume sweep that would create the solid hob as shown in Figure 22. The hob tool will be used to create the incomplete teeth in the partially splined shaft.

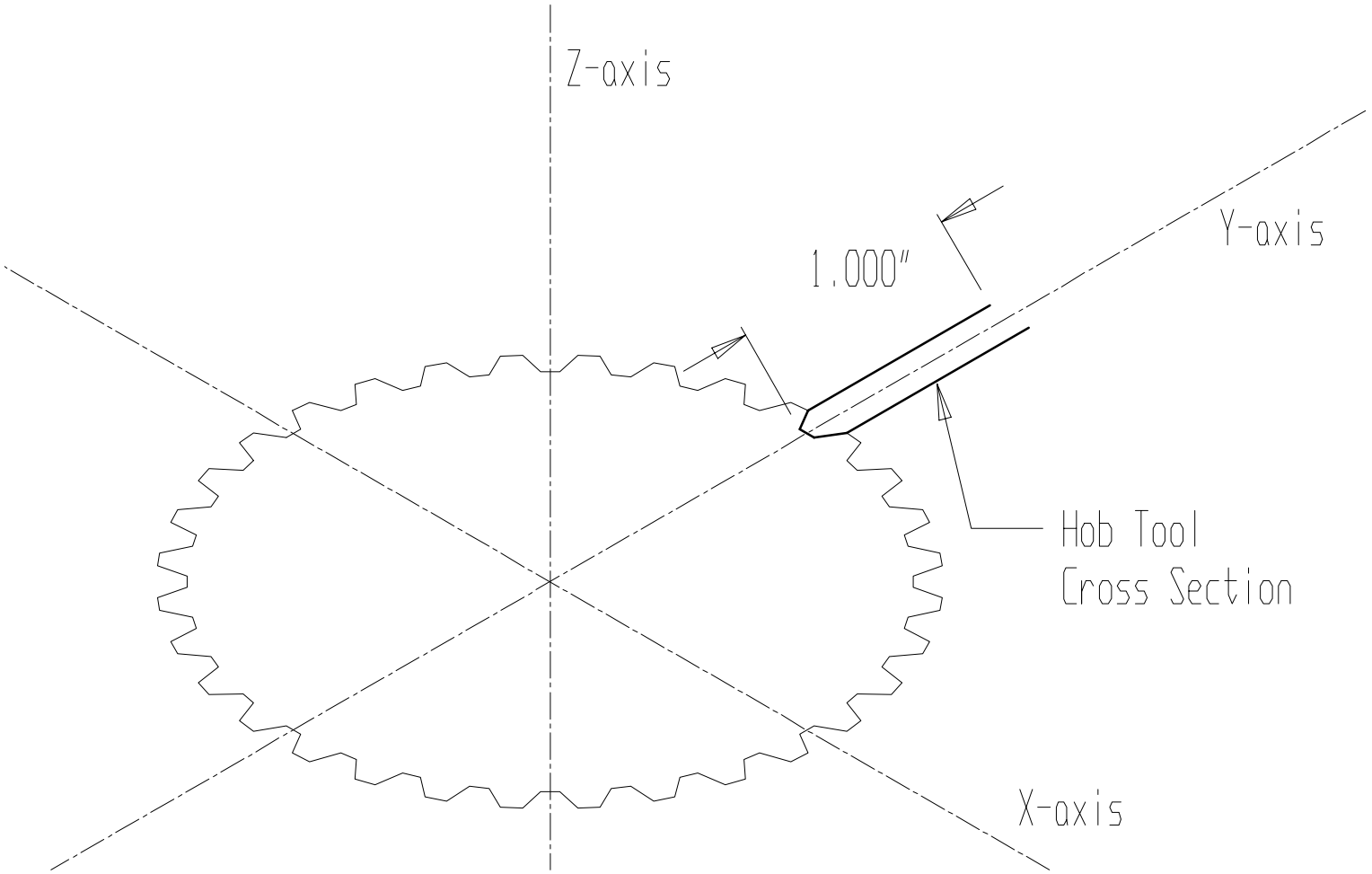

Figure 21. Spline profile with hob tool cross-section (1.00"(0.0254m) radius hob shown)

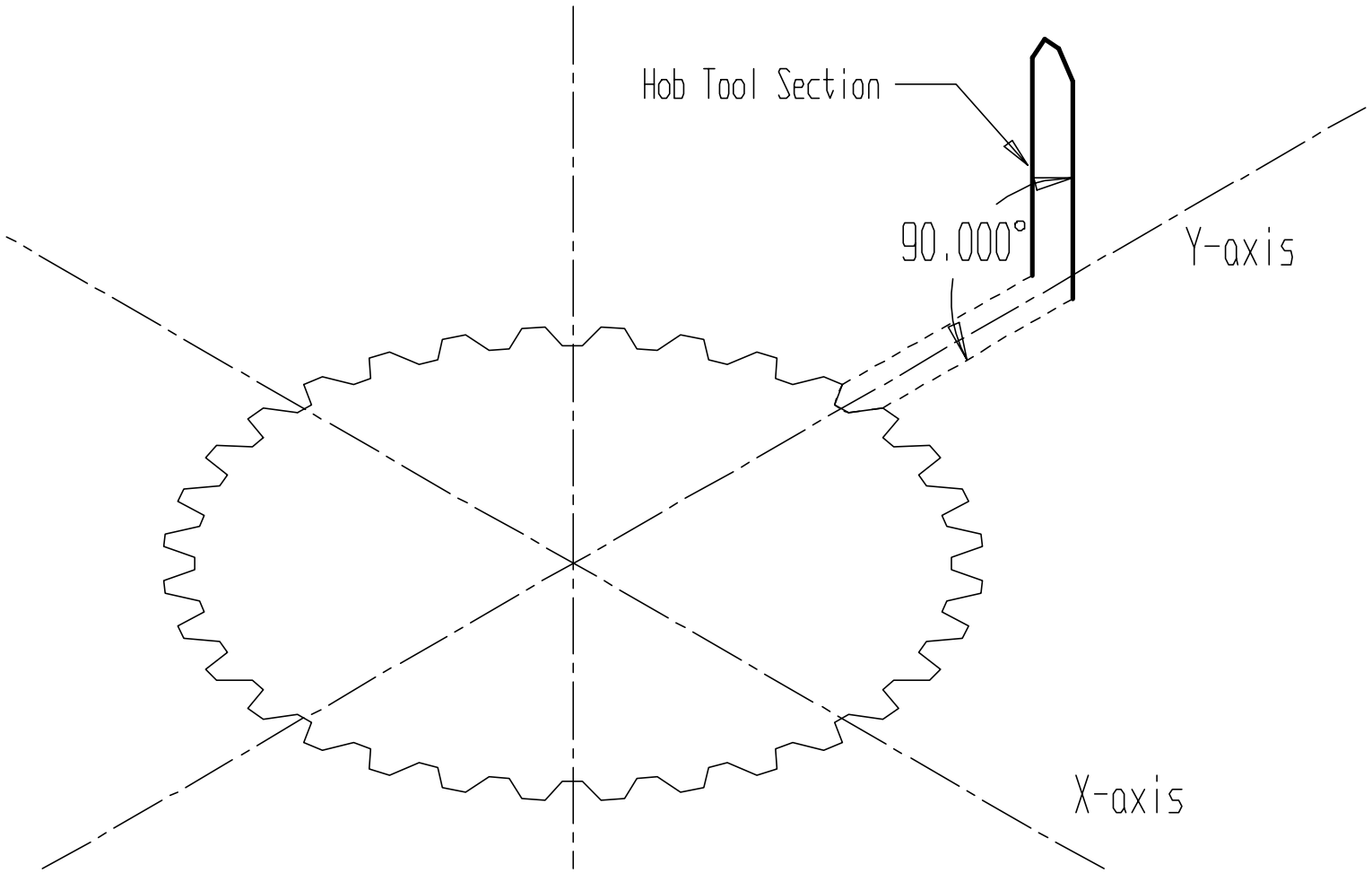

Figure 22. Hob tool cross-section shown after 90°rotation.

From this position, the rotate-copy/join command in Cadkey 97 was used to sweep the hob cross-section through a 180° path about the x-axis, as shown in Figure 23. This generated a wireframe model of the hob that was converted to a solid using the Solidify command in CK Solids. The solid hob model is shown in Figure 24. CK Solids is a solid modeling engine included with Cadkey 97. Note that only a single half-hob is shown in Figure 23 and Figure 24 to maintain clarity. However, a total of 32 hob-tools were placed between the splines to create the incomplete tooth shape.

The sweep angle need not be 360 degrees to accomplish the desired effect. The solid hob was stored in drawing layer (Layer 2) separate from the spline shaft geometry for clarity when constructing the remainder of the geometry. Only the original spine profile remained in the active drawing layer (Layer 1). At this point, the remainder of the solid geometry was generated. First, the curve used to generate the straight, non-splined section of the shaft was generated. This was accomplished by constructing the boundary of the straight section. Rather than using a circular arc, a 32-sided polygon was used to represent the boundary. This eliminated the difficulties that the Cadkey 97 software had in making a transition from the cylindrical shape of the non-splined section to the straight edges of the spline. Each vertex on the outer edge of the spline teeth was connected, ensured that points on the surface of the spline lie exactly on the surface of the straight section of the shaft. Figure 25 shows the resulting geometry.

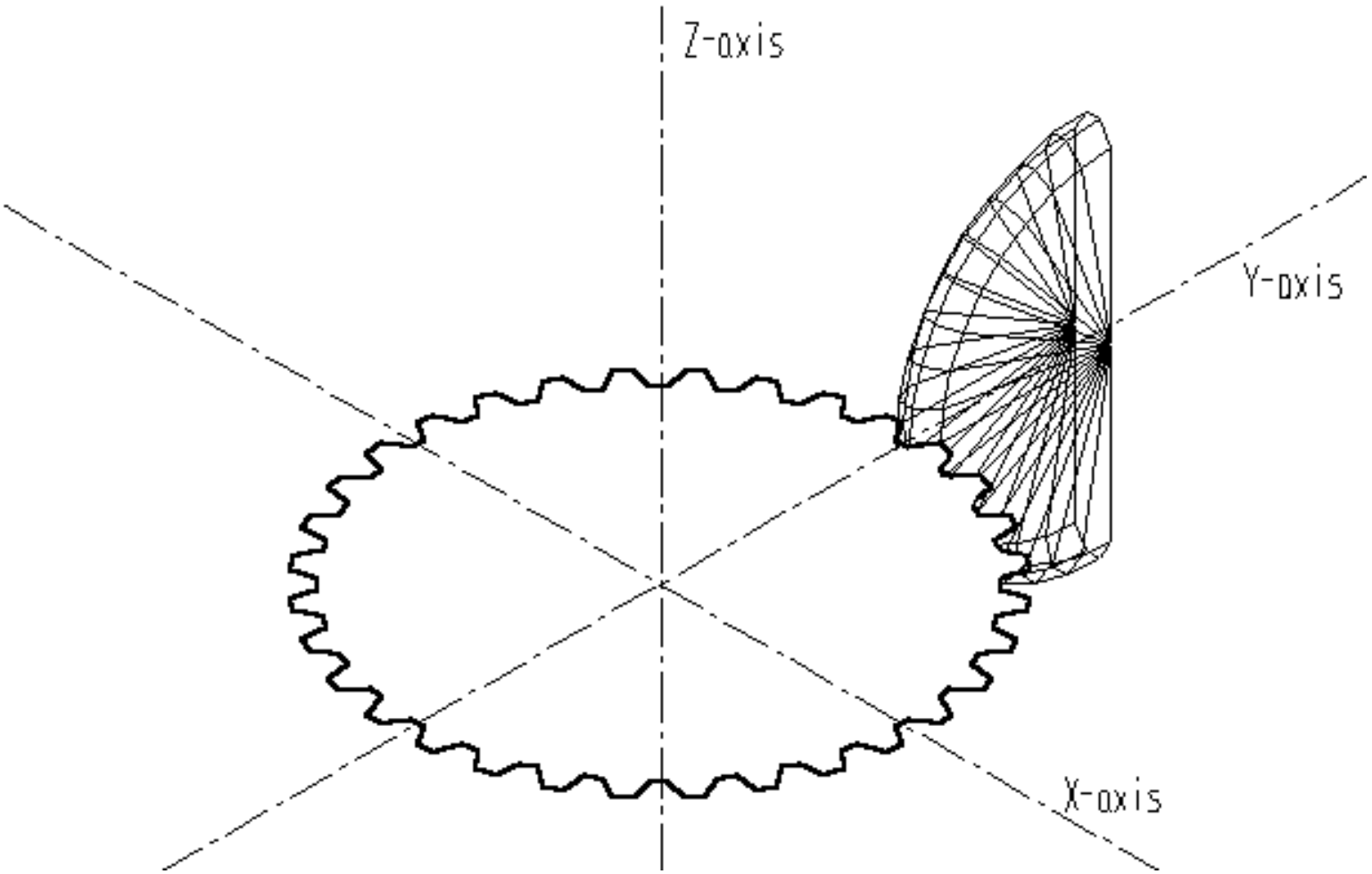

Figure 23. Spline profile with wireframe of half hob-tool shown. Only a single hob is shown for clarity.

Figure 24. Spline profile with solid rendering of half hob tool shown.

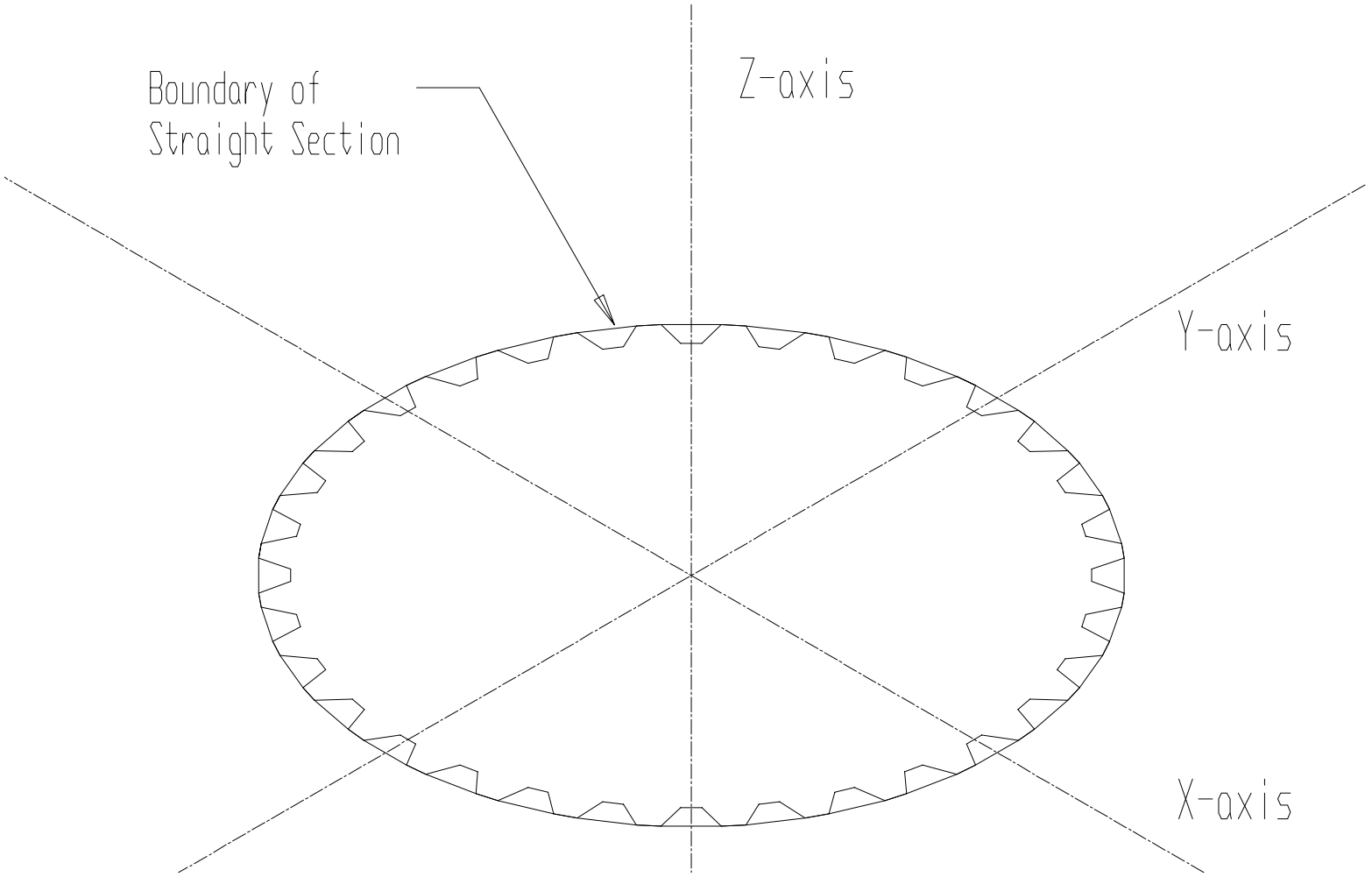

Figure 25. Sketch of partially-spline profile. The boundary of the straight section will be projected to create the non-splined section of the shaft. The spline profile will be projected to create the splined section of the shaft.

Constructing the remainder of the shaft was simply a matter of extruding each curve 8"(0.2032m) in the plus (+) Z and minus (-) Z directions. The resulting wireframe geometry is shown in Figure 26. This wireframe geometry was then itself converted to solid form in CK Solids, the same as the hob part. This solidified form of the intermediate model is shown in Figure 27. Note how the splines simply butt against the straight section in a dead end. This was modified once the hob part was brought into the active layer and the model was ready to be completed.

In Figure 29 the solid shaft is shown, ready to be cut by the hob part. To finish the geometry, the hob part was copied between each tooth. Figure 30 shows the shaft with the hob part copied onto the space between each spline tooth. The Boolean DIFFERENCE operation was the performed on the hob parts and the shaft. The hob part copies were subtracted from the shaft. The final solid geometry model of the partially splined shaft is shown in Figure 31. Figure 32 is a detailed view of the incomplete spline teeth in the partially splined shaft.

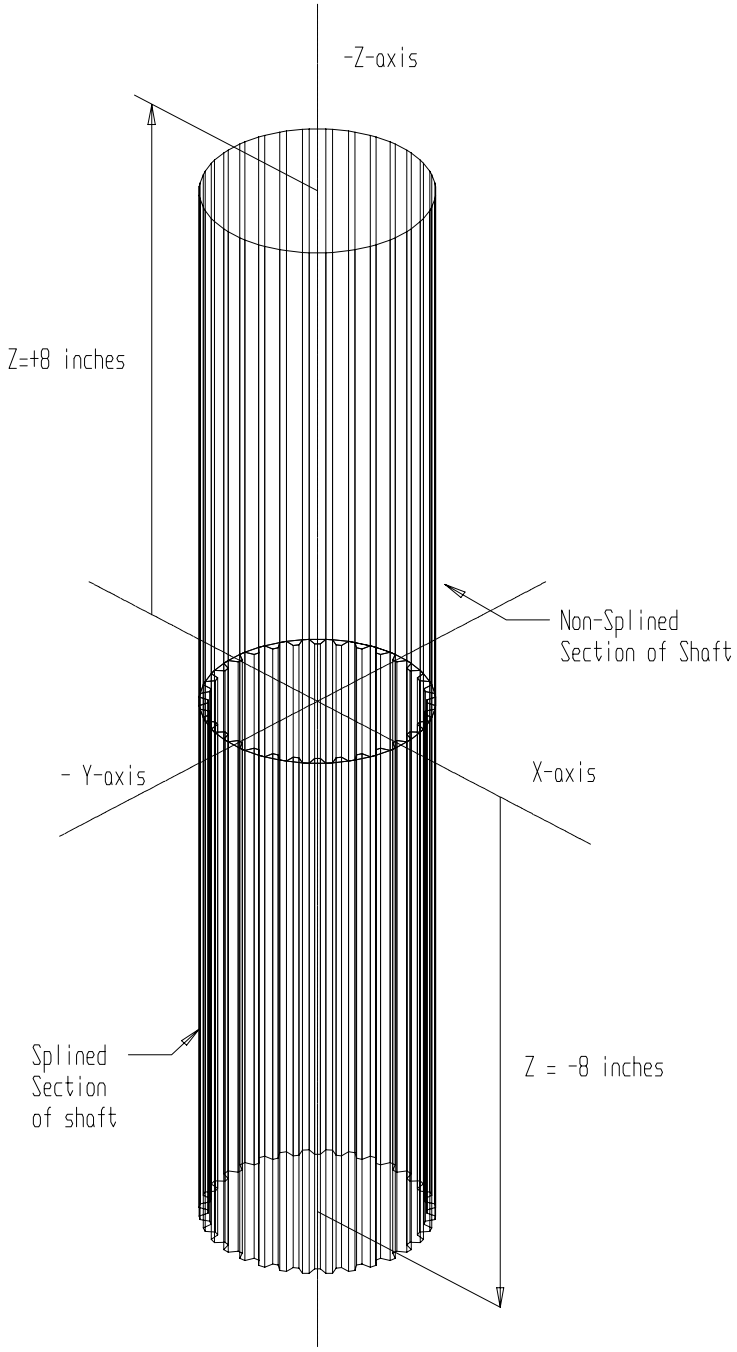

Figure 26. The wireframe geometry of the partially splined shaft after projection of both curves; both the splined and non-splined sections are shown here in their entirety.

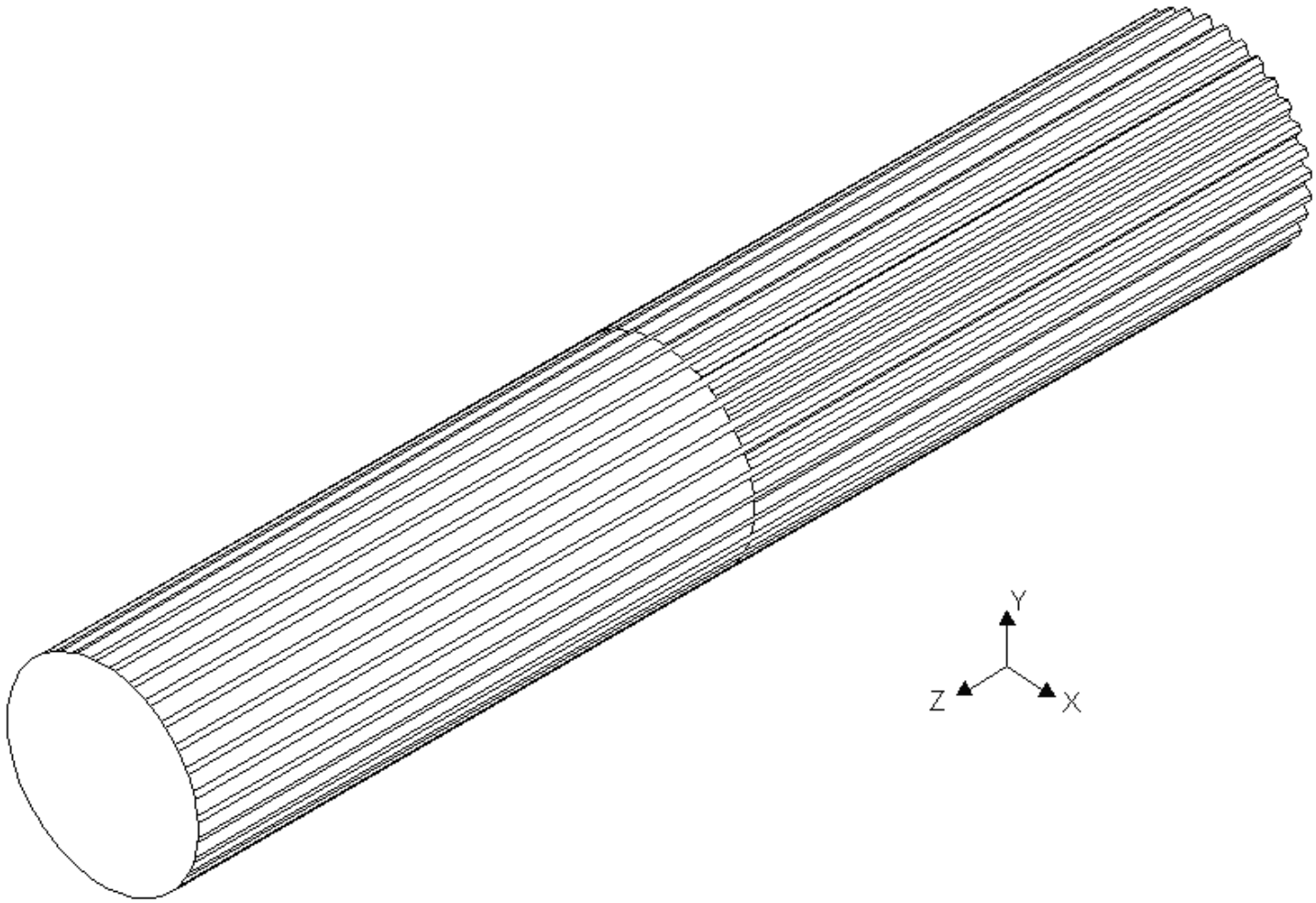

Figure 27. Solid rendering of partially splined shaft before the incomplete tooth shape is applied. The splines now directly abutt the, non-splined section.

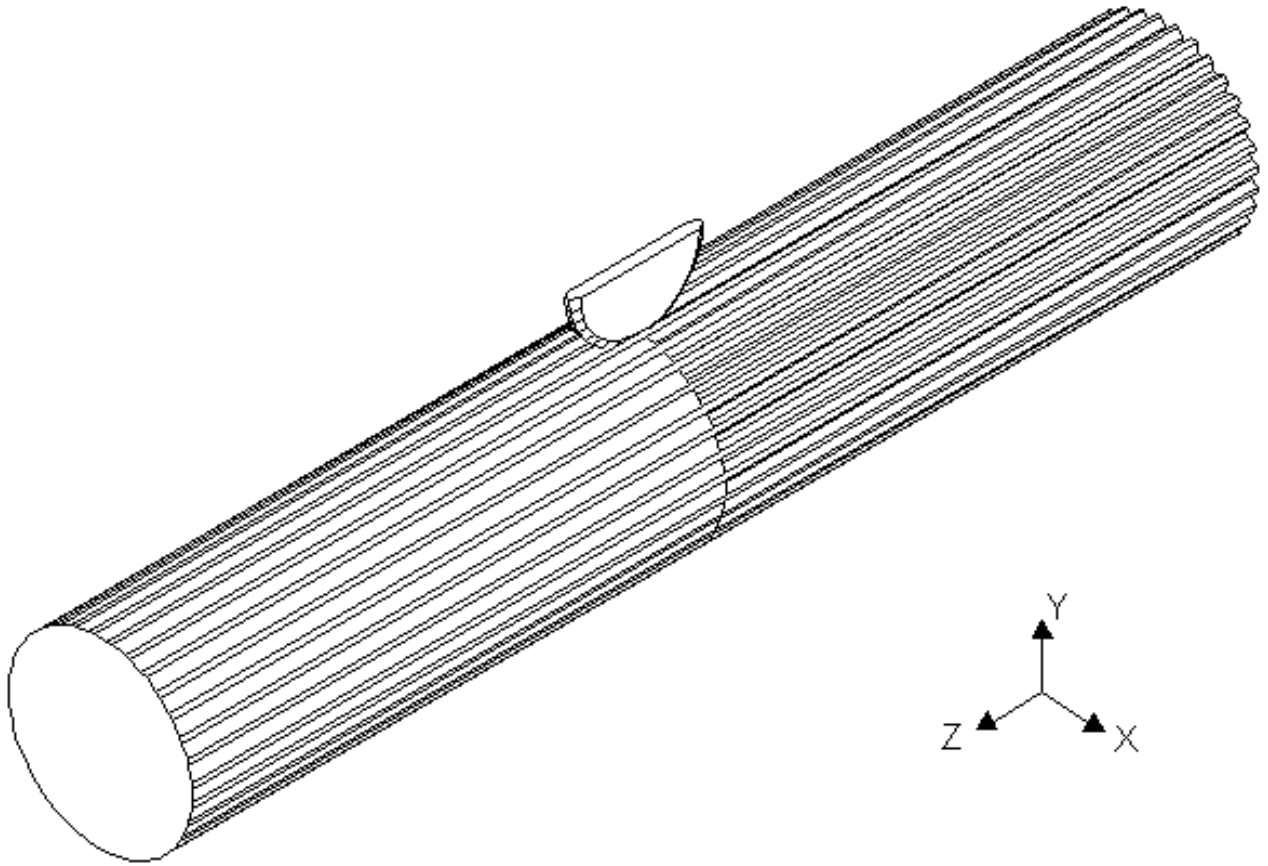

Figure 28. Isometric rendering of partially splined shaft before the incomplete teeth are created using the hob tool

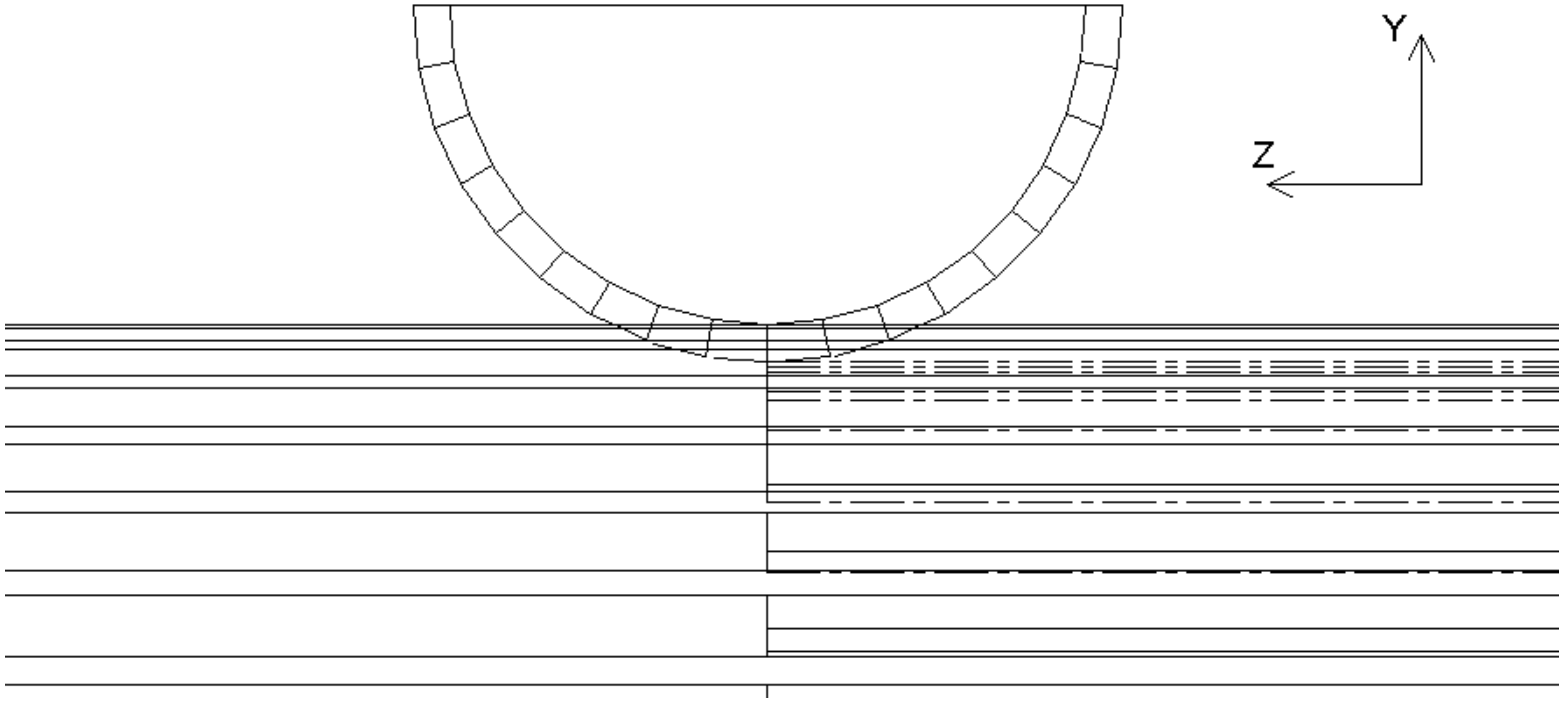

Figure 29. **A hidden line detail of the half-hob tool is also shown to illustrate how the hob creates the incomplete teeth. The other half-hob tool models are not shown here for clarity.**

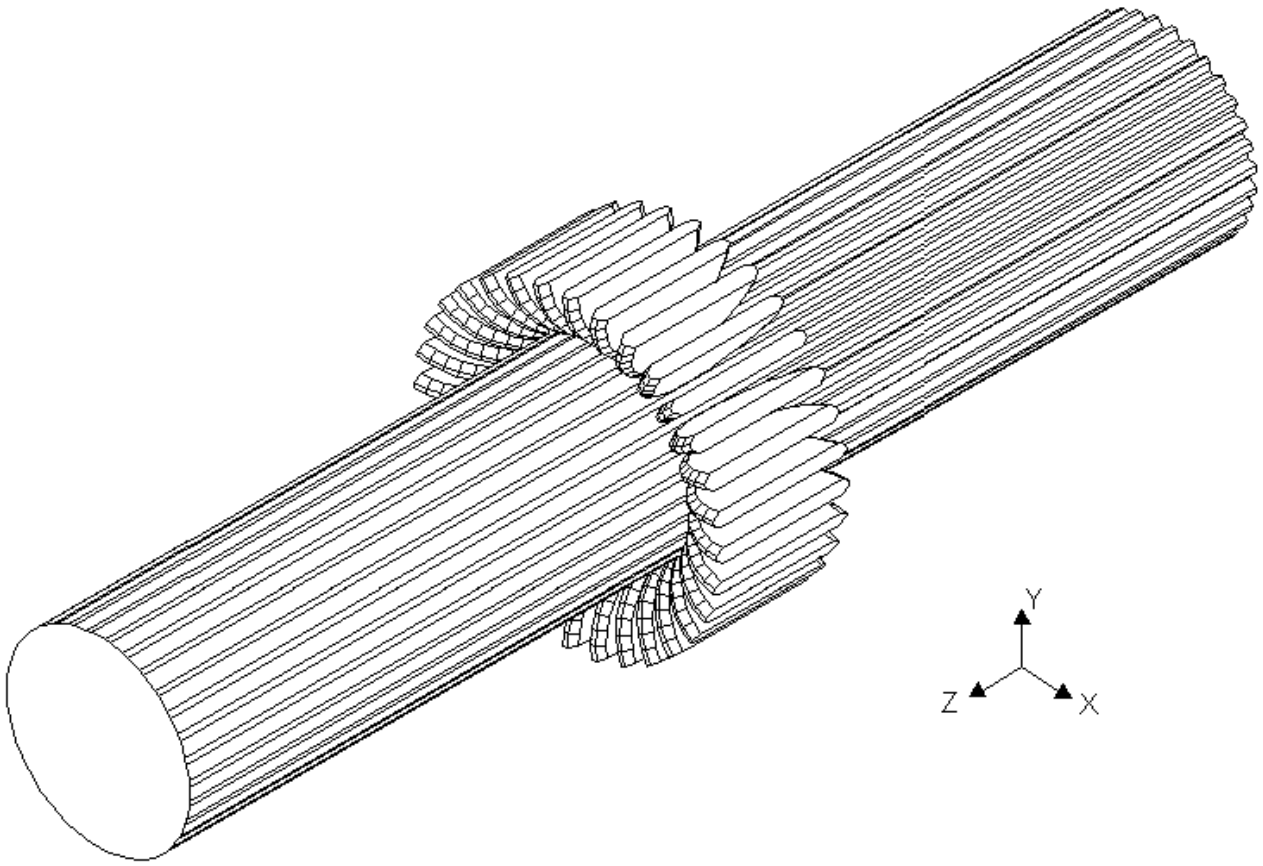

Figure 30. Solid rendering of partially splined shaft with additional half-hob tools copied on to the shaft surface.

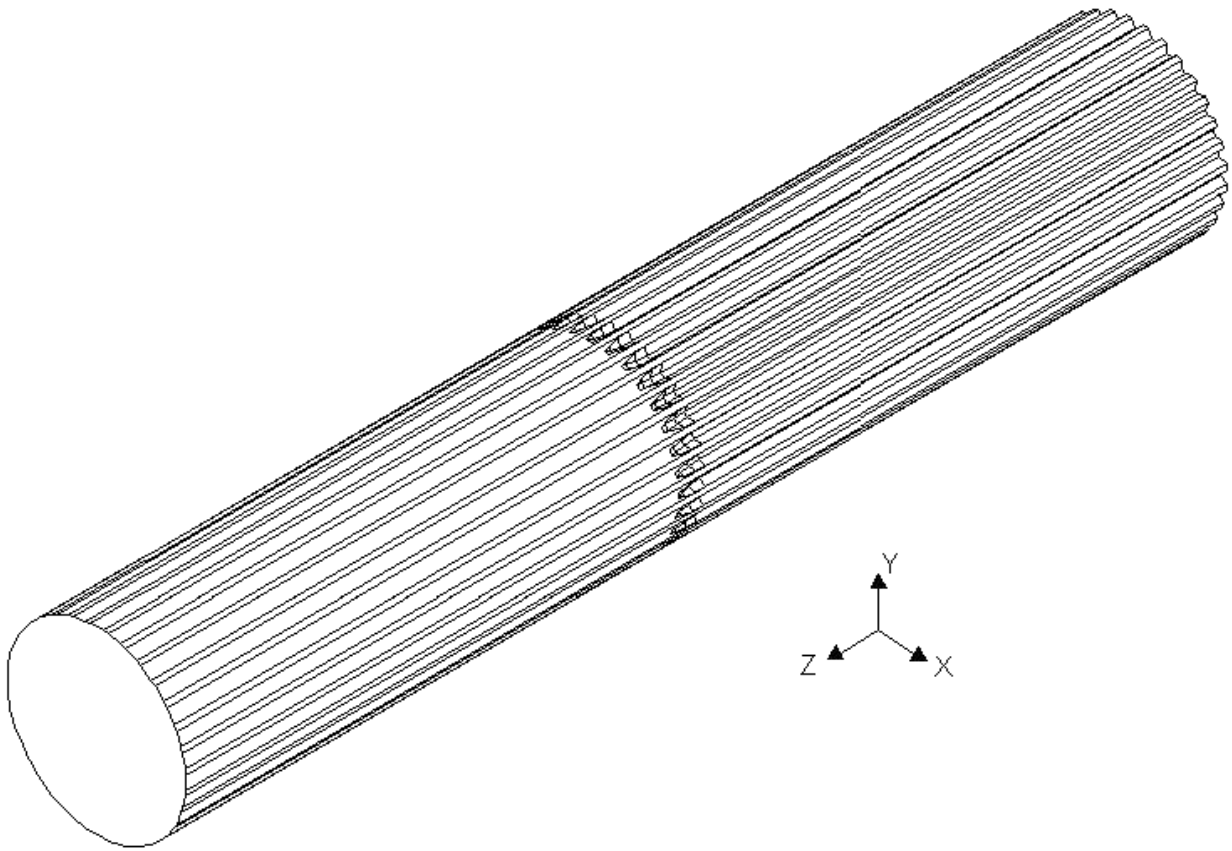

Figure 31. Isometric rendering of partially splined shaft after Boolean subtraction of hob tools.

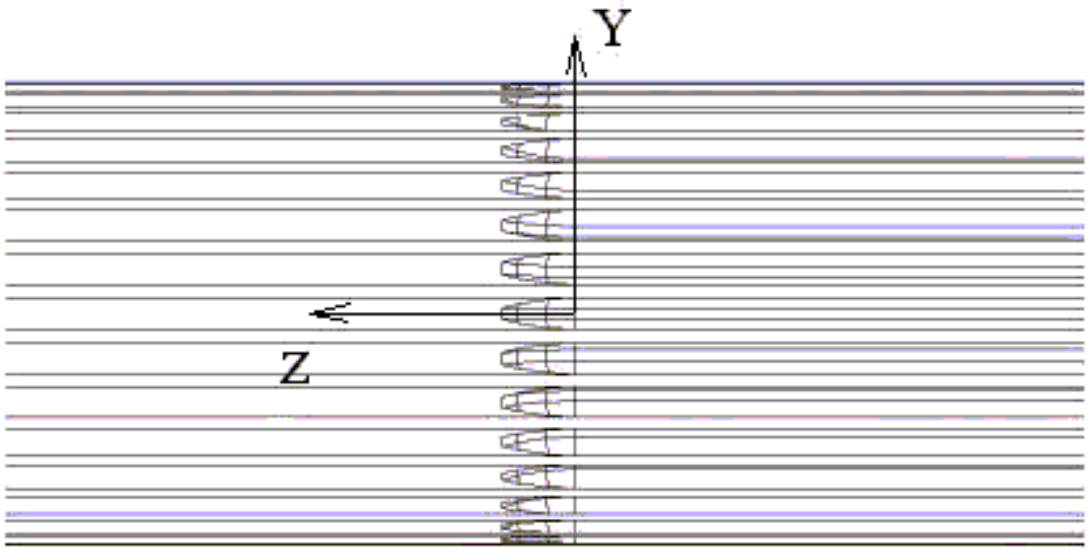

Figure 32. Plan elevation rendering showing a detail view of partial splines.

3.4 Finite Element Modeling

3.4.1. Modeling Preparation

The solid models created in Cadkey97 were converted into trimmed surface IGES files and exported to Algor. Using Algor's HOUDINI conversion software, the imported IGES surface models were converted into finite element models. Algor has the ability to generate a solid brick mesh from a well-conditioned surface mesh. The first model exported to Algor was that of the stepped shaft. The Cadkey97 computer file contained a digital, geometric representation of the stepped shaft. This file was first converted from a Cadkey97 *.prt file, to an IGES trimmed surface format using CK Solids. Once the model was exported, the Algor based tool HOUDINI was used to prepare the IGES model for meshing. HOUDINI is a "modeling environment where engineers can access Algor's surface and solid mesh enhancement/generation tools while exchanging files with popular CAD and FEA software programs" [6].

HOUDINI analyzes the IGES model to ensure that each edge of its adjacent sub-surfaces shares only two edges. HOUDINI checks for errors in the surface such as overlapping surfaces and duplicate lines. Based on the overall surface geometry, HOUDINI counts all the elements that make up the surface and presents the finished geometry to the user graphically to ensure that it is prepared for surface meshing. The user then has the option to refine the mesh manually or automatically within Algor. The user also has the choice of repairing the geometry of the raw IGES file itself if problems exist.

Once it was determined that the imported model was suitable for meshing, the Algor sub-program TSMesh was used to generate a quadrilateral mesh on its surface. TSMesh generates a default mesh based on the longest length of an element that should be used to adequately mesh the surface. Algor then gives the user the option of changing the mesh size. Percentage differences with theoretical values for the straight portion of the stepped shaft showed increasing error with any mesh size below 0.165797"(0.0042m), or about 1% of the total shaft length of 16"(0.4064m).

The Algor surface meshing software (TSMesh) divided the model surface into discrete quadrilateral elements, based on the element size prescribed. The user is provided with a visual representation of the meshed surface to show the quality and shape of the elements. Once the surface mesh was completed, it was visually examined in the Superdraw III CAD environment and checked for errors. The finished surface was also displayed using Algor's Superview visualization software. The watertight check option was invoked in Superview. The watertight check ensures that the surface model forms a closed volume and that it contains no holes or slits which could cause difficulty in generating the solid mesh. The stepped shaft model showed no mesh quality problems and appeared to fully enclose a volume. The model was now ready to be partitioned into solid finite elements. This was accomplished using Algor's automatic solid meshing software called Hexagen. Another meshing kit called Hypergen was also included with Algor. Hypergen however, generates only tetrahedral elements.

According to Docutech [6], tetrahedral elements in their 4 node, linear form are not sufficiently accurate to warrant their use for obtaining final results. The 10 node

parabolic elements are very accurate but they take large number of elements for sufficient convergence, and more than 10 times the computational time than four-node tetrahedrons.

By using brick elements, both of these dilemmas were avoided. Hexagen uses the surface mesh to generate 8 node bricks on the outermost layer of the model, and then constructs hybrid brick elements (5, 6, and 7 node brick elements) to fill in towards the interior of the model. These hybrid elements allow for more interpolation points on each element than four-node tetrahedrons and they are not as stiff. The standard meshing engine Hexagen generates such hybrid brick meshes. After several attempts at using both the hybrid and 100% 8-node brick meshing, Hexagen meshing was found to be the most efficient solid meshing mode for Algor. Thus, Hexagen was used to mesh all models for this research.

Convergence using lower order elements was achieved by decreasing the mesh size, but this was only effective down to an element size of about 0.166". Subsequent convergence was obtained by increasing the order of integration of the elements. This allowed convergence without actually decreasing the mesh size beyond 0.166". Convergence issues will be discussed in greater detail in Chapter IV.

3.4.2. Boundary Conditions

Upon completion of the solid mesh generation, a geometric representation of the nodes and elements comprising the model was displayed in Superdraw III. The boundary conditions and loads were then applied to the model. The finished solid FE model was displayed in Superdraw III. Spatial restraints were then applied to the model in order to prevent rigid body motion when the force conditions were applied. Such movement would generate a singular stiffness matrix, invalidating the model solution. The shaft model was restrained in all directions at one end, and allowed total freedom of movement at the other end. This resulted in a cantilevered shaft configuration. The restraints were placed at the end of the splined portion of the shaft, as shown in Figure 33 and Figure 34.

One of the assumptions made when modeling the shaft is that the loads on it could be accurately applied without modeling the mating "female" member of the coupling. To make up for this, the boundary conditions were applied only to the outer face of the teeth, as shown in Figure 35. Thus, the load would be transmitted primarily by the spline teeth, and not by the body of the shaft. Shifting the load to the teeth simulated the loading that would be experienced it the load were actually applied by an external, "female" spline member. All degrees of freedom were restrained at the shaft end, preventing any possibility of rigid body motion. All modeling was done using the Cartesian coordinate system, so x, y, and z translational and rotational d.o.f.'s were all restrained.

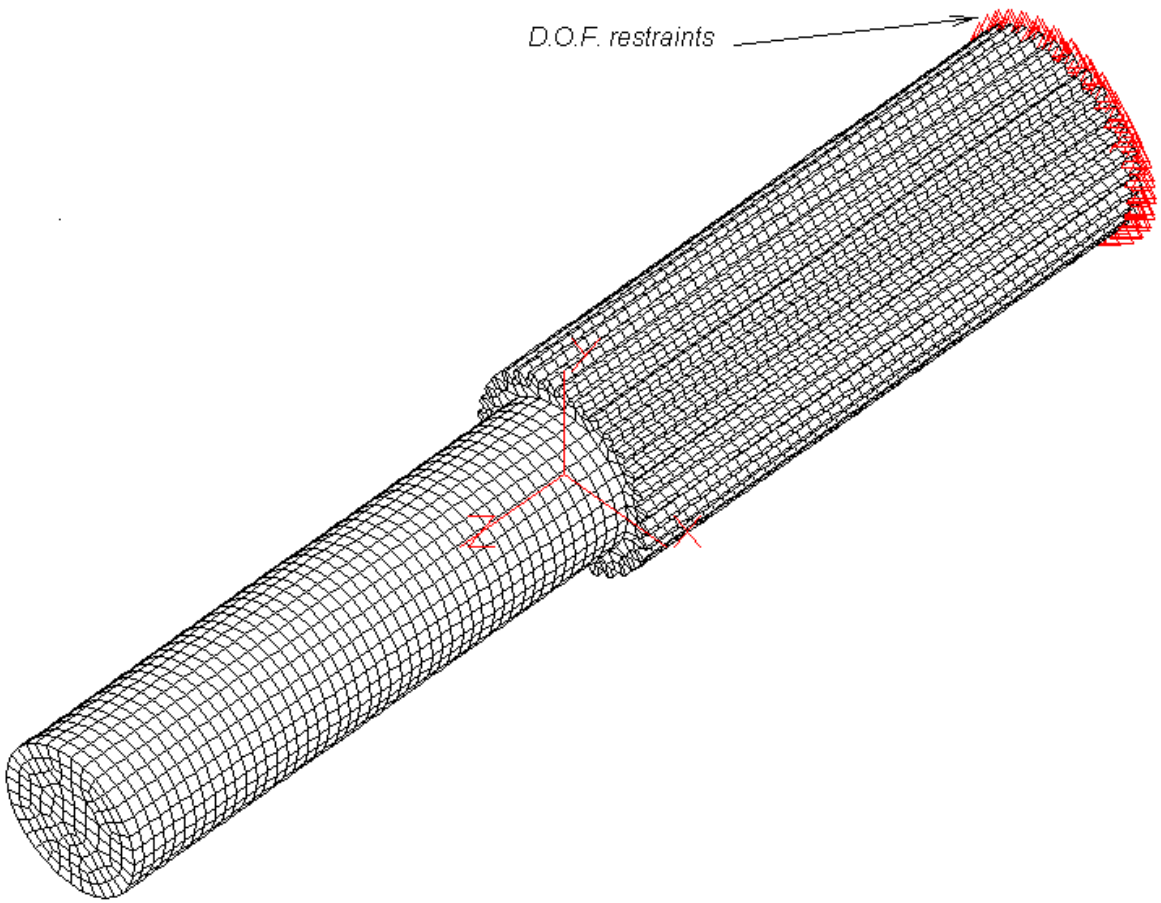

Figure 33. **Stepped splined shaft with finite element mesh and restraints applied. The triangles indicate the locations where restraints were applied**

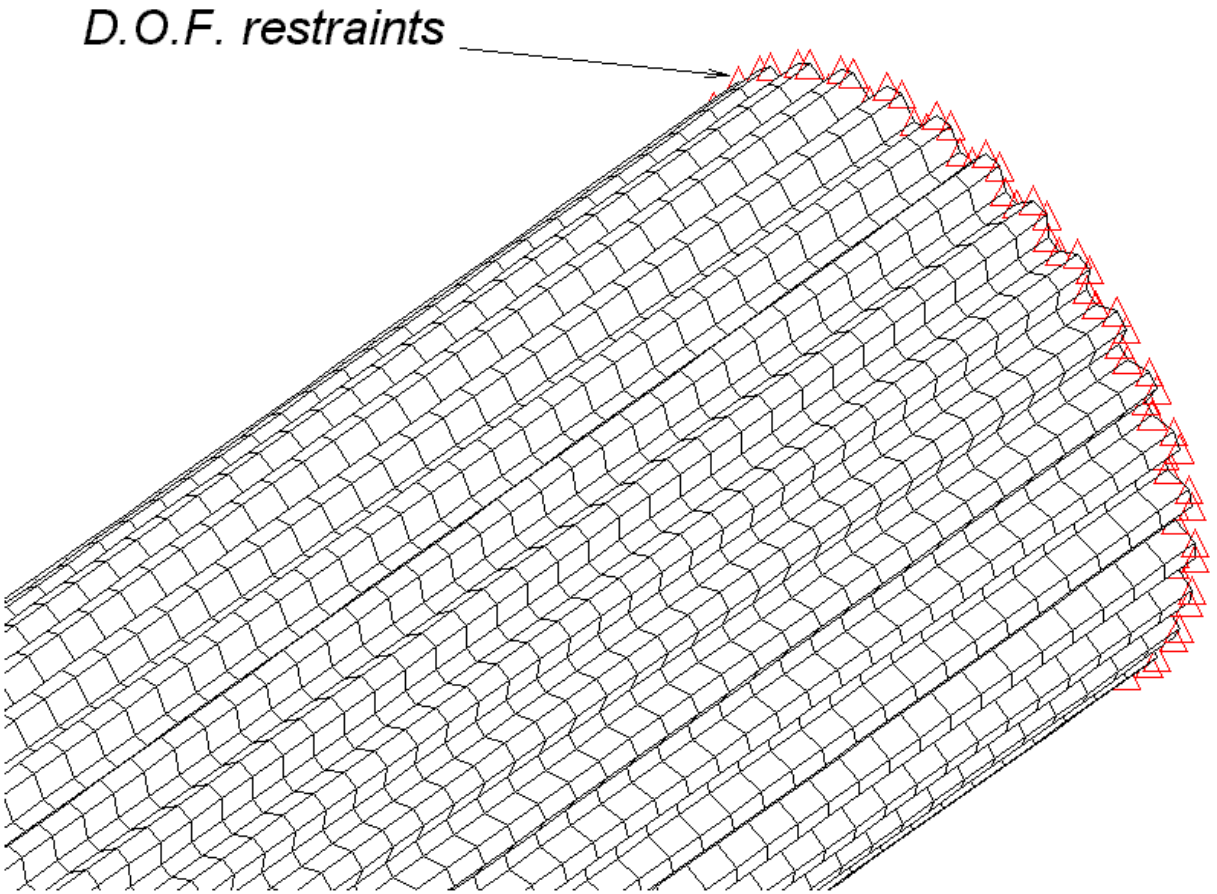

Figure 34. Detail view of the boundary restraints. (d/D = 0.75 shaft shown).

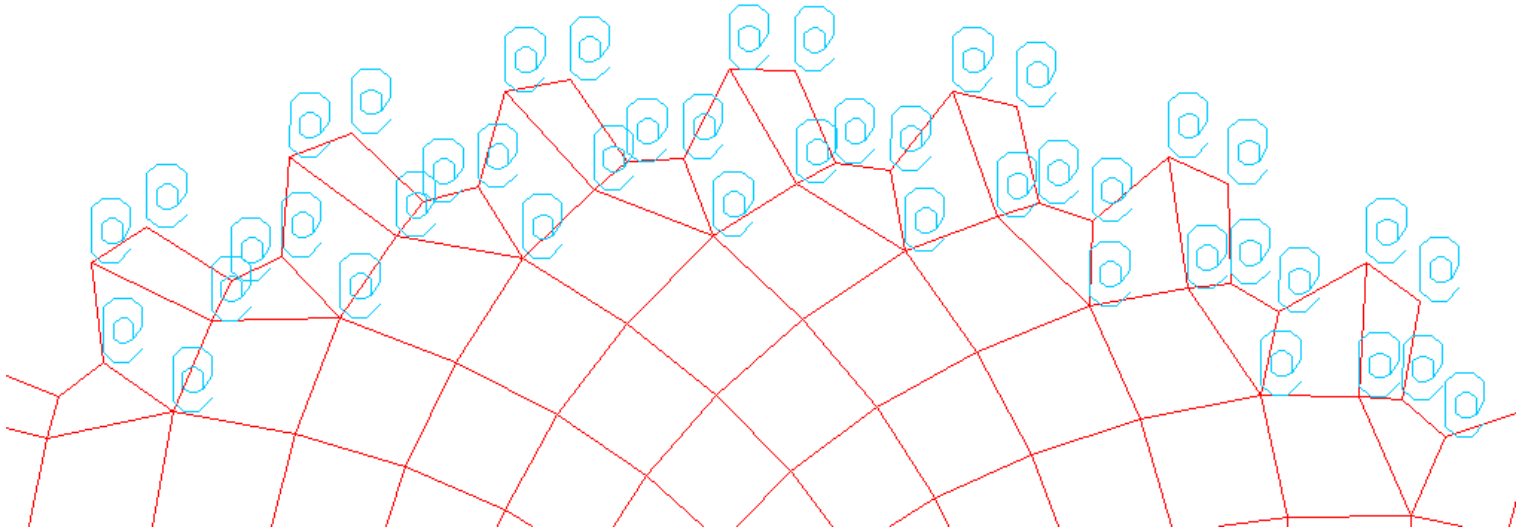

Figure 35. Illustration of spline profile with teeth restrained only. The "@" symbols represent restraints on all six degrees of freedom at each node.

Point forces were applied to the free end of the shaft to simulate the applied loading. As with the boundary conditions, the outermost surface of the free end of the shaft was changed to a different color in order to make it easier to mask the appropriate elements during selection.

Figure 36 and Figure 37 illustrate how the torsional and bending force couples were applied to both the stepped shaft and the partially splined shaft, respectively. Two types of loads were applied to the model to create the desired conditions. The bending load consisted of a force couple. Each force of the couple was equal in magnitude, but exactly opposite in direction. The forces were applied at nodes that were located on diametrically opposite sides of the shaft. The forces were applied parallel to the axis of the shaft, perpendicular to its free end face. This created a constant bending moment throughout the length of the shaft. Torsion was the other type of loading applied to the model. The torsion force couple was applied perpendicular to the axis of the shaft and parallel to the face of the free end of the shaft.

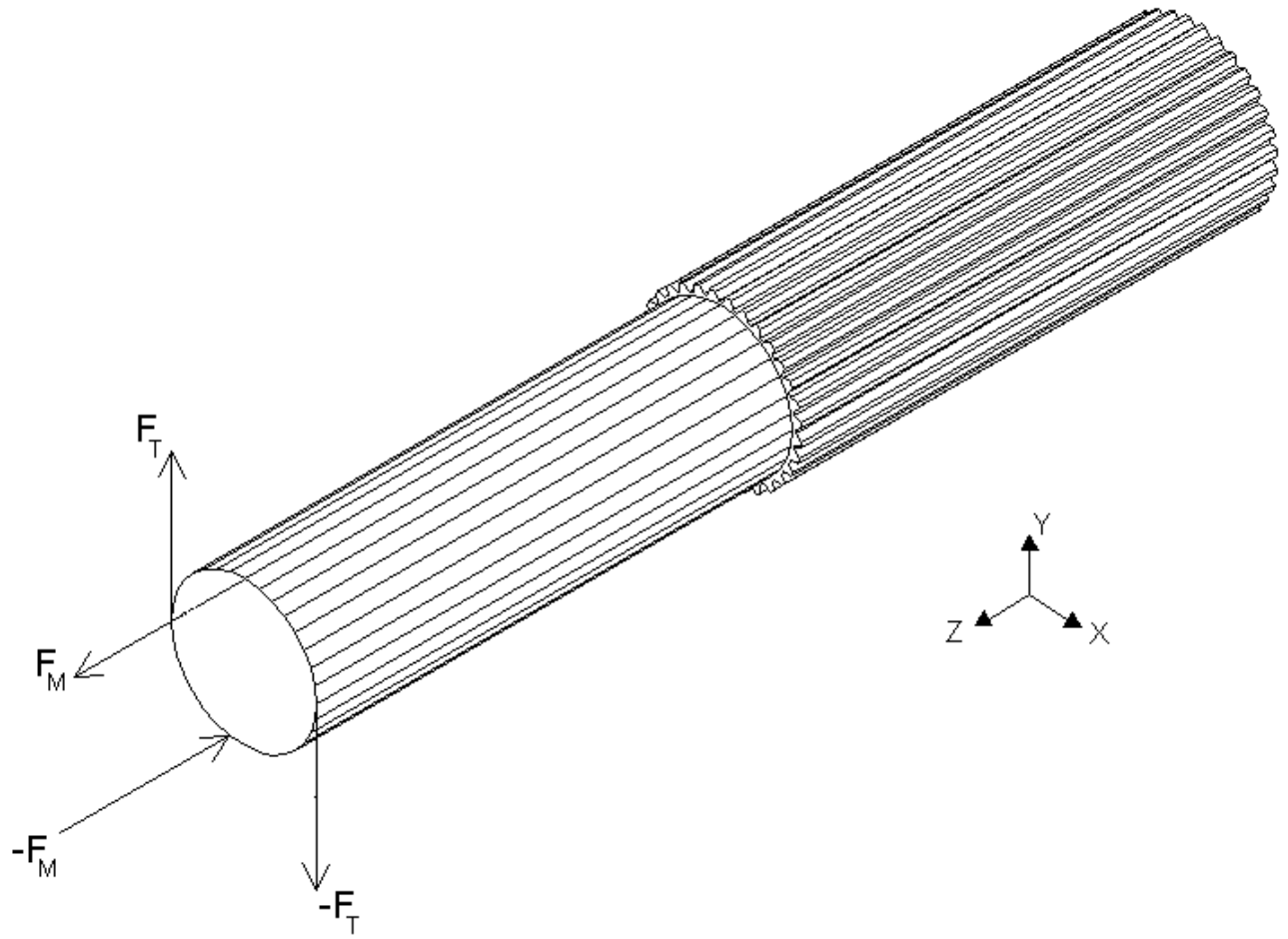

Figure 36. A rendering of the d/D=0.886 stepped shaft with bending and torsion force couples applied at the non-splined end.

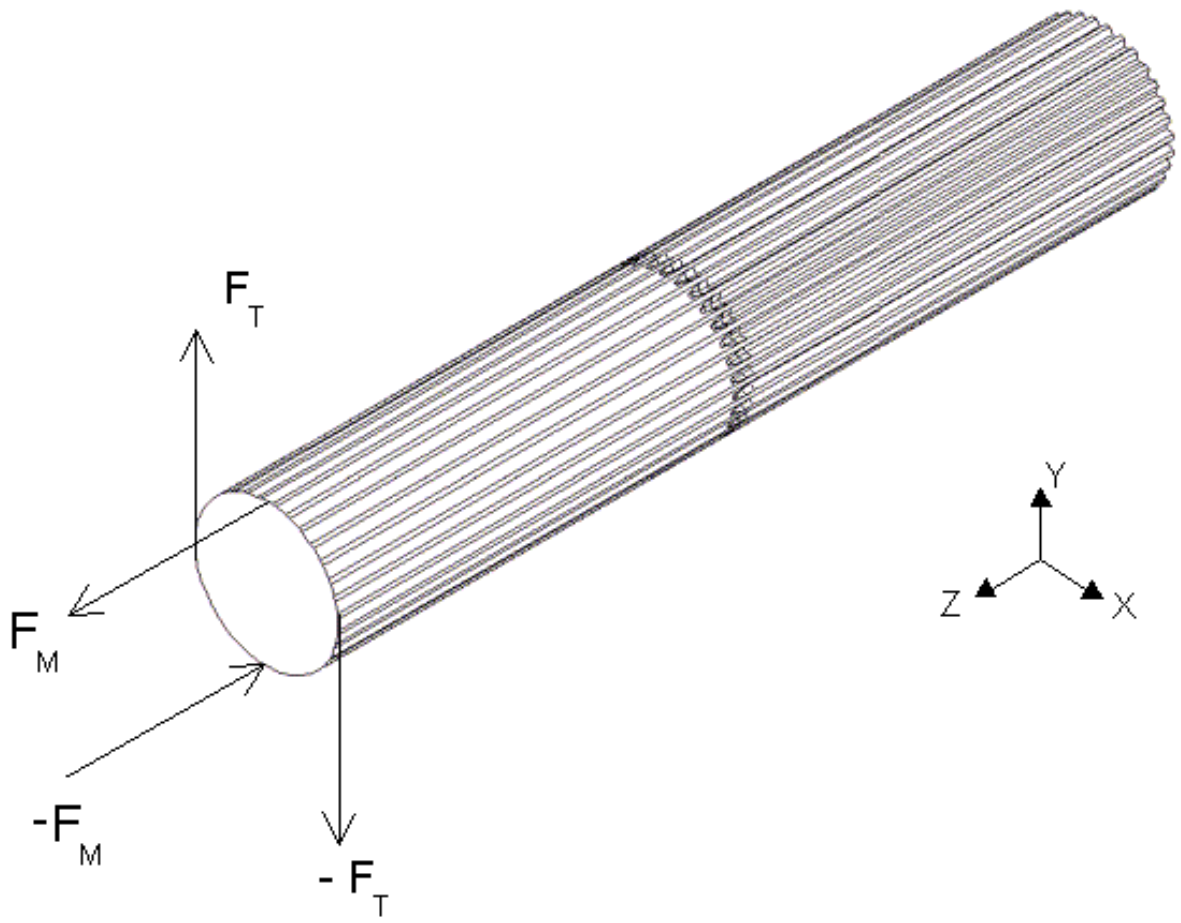

Figure 37. A rendering of the R=1.5 partially splined shaft with bending and torsion force couples applied at non-splined end.

Eleven load cases were applied to each model. Each load case contained a combination of bending and torsion force couples. The load cases were applied to each model according to Tables 2-5. Note that the characteristics of the particular load cases are captured in the "F_M/F_T" number, or the ratio of the bending force couple magnitude to the torsion couple force magnitude. The top number (F_M) gives the magnitude of the force couple creating the bending moment, while the bottom number (F_T) is the magnitude of the force couple generating torque on the shaft.

Recall that d is the diameter of the non-splined section of the stepped splined shaft, and that D is the major diameter of the splined section of the stepped shaft. The separation distance between the forces, and hence the bending moment and torque are determined by the geometry of the shaft, since the loads were applied at the end of the non-splined section. The non-splined section diameter d is varied relative to the major diameter D to give the various d/D ratios (0.5, 0.75, and 0.886).

The major diameter D is also used to indicate the size of the non-splined section in the partially splined shaft. The ratios between the diameters of the splined and non-splined sections of the partially splined shafts never change. Therefore, only one table is required to show what bending moment and torque are applied to the partially splined shaft. The "R" seen in Table 5 indicates the size hob tool used to create the incomplete tooth section of the partial splines.

Table 2. Load cases for the d/D=0.500 stepped shaft. The diameter of the non-splined section is d, and D is the major diameter of the splined section. Table 3a-US units, Table 3b-SI units.

D=2.75"		Bending			Torsion		
Load Case#		Fm(lbf)	d(in)	Moment (lbs-in)	Ft(lbf)	d(in)	Moment (lbf-in)
(Pure Bending)	1	1000	1.38	1375.0	0	1.38	0.0
	2	900	1.38	1237.5	100	1.38	137.5
	3	800	1.38	1100.0	200	1.38	275.0
	4	700	1.38	962.5	300	1.38	412.5
	5	600	1.38	825.0	400	1.38	550.0
	6	500	1.38	687.5	500	1.38	687.5
	7	400	1.38	550.0	600	1.38	825.0
	8	300	1.38	412.5	700	1.38	962.5
	9	200	1.38	275.0	800	1.38	1100.0
	10	100	1.38	137.5	900	1.38	1237.5
(Pure Torsion)	11	0	1.38	0.0	1000	1.38	1375.0

(a)

D=2.75"		Bending			Torsion		
Load Case#		Fm(N)	d(m)	Moment (N*m)	Ft(N)	d(m)	Moment (N*m)
(Pure Bending)	1	224.8	0.035	7.85	0	0.035	0.00
	2	202.32	0.035	7.07	22.48	0.035	0.79
	3	179.84	0.035	6.28	44.96	0.035	1.57
	4	157.36	0.035	5.50	67.44	0.035	2.36
	5	134.88	0.035	4.71	89.92	0.035	3.14
	6	112.4	0.035	3.93	112.4	0.035	3.93
	7	89.92	0.035	3.14	134.88	0.035	4.71
	8	67.44	0.035	2.36	157.36	0.035	5.50
	9	44.96	0.035	1.57	179.84	0.035	6.28
	10	22.48	0.035	0.79	202.32	0.035	7.07
(Pure Torsion)	11	0	0.035	0.00	224.8	0.035	7.85

(b)

Table 3. Load cases for the d/D=0.750 stepped shaft. The diameter of the non-splined section is d, and D is the major diameter of the splined section. Table 3a-US units, Table 3b-SI units.

D=2.75"	Bending			Torsion		
Load Case#	Fm(lbf)	d(in)	Moment(lbs-in)	Ft(lbf)	d(in)	Moment (lbf-in)
(Pure Bending) 1	1000	2.06	2062.5	0	2.06	0.0
2	900	2.06	1856.3	100	2.06	206.3
3	800	2.06	1650.0	200	2.06	412.5
4	700	2.06	1443.8	300	2.06	618.8
5	600	2.06	1237.5	400	2.06	825.0
6	500	2.06	1031.3	500	2.06	1031.3
7	400	2.06	825.0	600	2.06	1237.5
8	300	2.06	618.8	700	2.06	1443.8
9	200	2.06	412.5	800	2.06	1650.0
10	100	2.06	206.3	900	2.06	1856.3
(Pure Torsion) 11	0	2.06	0.0	1000	2.06	2062.5

(a)

D=2.75"	Bending			Torsion		
Load Case#	Fm(N)	d(m)	Moment(N*m)	Ft(N)	d(m)	Moment (N*m)
(Pure Bending) 1	224.8	0.052	11.78	0	0.052	0.00
2	202.32	0.052	10.60	22.48	0.052	1.18
3	179.84	0.052	9.42	44.96	0.052	2.36
4	157.36	0.052	8.24	67.44	0.052	3.53
5	134.88	0.052	7.07	89.92	0.052	4.71
6	112.4	0.052	5.89	112.4	0.052	5.89
7	89.92	0.052	4.71	134.88	0.052	7.07
8	67.44	0.052	3.53	157.36	0.052	8.24
9	44.96	0.052	2.36	179.84	0.052	9.42
10	22.48	0.052	1.18	202.32	0.052	10.60
(Pure Torsion) 11	0	0.052	0.00	224.8	0.052	11.78

(b)

Table 4. Load cases for the d/D=0.886 stepped shaft. The diameter of the non-splined section is d, and D is the major diameter of the splined section. Table 4a-English units, Table 4b-SI units.

D=2.75"	Bending			Torsion		
Load Case#	Fm(lbf)	d(in)	Moment (lbs-in)	Ft(lbf)	d(in)	Moment (lbf-in)
(Pure Bending) 1	1000	2.44	2437.5	0	2.44	0.0
2	900	2.44	2193.8	100	2.44	243.8
3	800	2.44	1950.0	200	2.44	487.5
4	700	2.44	1706.3	300	2.44	731.3
5	600	2.44	1462.5	400	2.44	975.0
6	500	2.44	1218.8	500	2.44	1218.8
7	400	2.44	975.0	600	2.44	1462.5
8	300	2.44	731.3	700	2.44	1706.3
9	200	2.44	487.5	800	2.44	1950.0
10	100	2.44	243.8	900	2.44	2193.8
(Pure Torsion) 11	0	2.44	0.0	1000	2.44	2437.5

(a)

D=2.75"	Bending			Torsion		
Load Case#	Fm(N)	d(m)	Moment (N*m)	Ft(N)	d(m)	Moment (N*m)
(Pure Bending) 1	224.8	0.062	13.92	0	0.062	0.00
2	202.32	0.062	12.53	22.48	0.062	1.39
3	179.84	0.062	11.13	44.96	0.062	2.78
4	157.36	0.062	9.74	67.44	0.062	4.18
5	134.88	0.062	8.35	89.92	0.062	5.57
6	112.4	0.062	6.96	112.4	0.062	6.96
7	89.92	0.062	5.57	134.88	0.062	8.35
8	67.44	0.062	4.18	157.36	0.062	9.74
9	44.96	0.062	2.78	179.84	0.062	11.13
10	22.48	0.062	1.39	202.32	0.062	12.53
(Pure Torsion) 11	0	0.062	0.00	224.8	0.062	13.92

(b)

Table 5. Load cases for all partially splined shafts (R=1"(0.0254m), R=1.5"(0.0381m), R=2.0"(0.0508m)). R is the radius of the hob tool used to create the incomplete teeth in each partially splined shaft model. Table 5a-English units, Table 5b-SI units.

D=2.75"	Bending			Torsion		
Load Case#	Fm(lbf)	d(in)	Moment (lbs-in)	Ft(lbf)	d(in)	Moment(lbf-in)
(Pure Bending) 1	1000	2.75	2750.0	0	2.75	0.0
2	900	2.75	2475.0	100	2.75	275.0
3	800	2.75	2200.0	200	2.75	550.0
4	700	2.75	1925.0	300	2.75	825.0
5	600	2.75	1650.0	400	2.75	1100.0
6	500	2.75	1375.0	500	2.75	1375.0
7	400	2.75	1100.0	600	2.75	1650.0
8	300	2.75	825.0	700	2.75	1925.0
9	200	2.75	550.0	800	2.75	2200.0
10	100	2.75	275.0	900	2.75	2475.0
(Pure Torsion) 11	0	2.75	0.0	1000	2.75	2750.0

(a)

D=2.75"	Bending			Torsion		
Load Case#	Fm(N)	d(m)	Moment (N*m)	Ft(N)	d(m)	Moment (N*m)
(Pure Bending) 1	202.32	0.070	14.13	22.48	0.070	1.57
2	179.84	0.070	12.56	44.96	0.070	3.14
3	157.36	0.070	10.99	67.44	0.070	4.71
4	134.88	0.070	9.42	89.92	0.070	6.28
5	112.4	0.070	7.85	112.4	0.070	7.85
6	89.92	0.070	6.28	134.88	0.070	9.42
7	67.44	0.070	4.71	157.36	0.070	10.99
8	44.96	0.070	3.14	179.84	0.070	12.56
9	22.48	0.070	1.57	202.32	0.070	14.13
10	0	0.070	0.00	224.8	0.070	15.70
(Pure Torsion) 11	0	0.000	0.00	0	0.000	0.00

(b)

3.4.3. Model Solution

Once the loads and restraints were applied to the model, Algor converted the user-supplied data into a set of elastic equations that were later solved for displacements and hence, stress. This conversion process was accomplished using the Algor sub-program called Stress Decoder (Decods). In the Stress Decoder, the user enters data about the finite element model such as element type, desired element formulation order, temperature, material density, Possion's Ratio, and elastic modulus, and nodal locations. The program uses this information to create a master database of information about the model that is then used directly by the Algor solver to calculate stresses. The stepped shaft model was successfully decoded and sent to the solver for analysis. The preceding modeling procedure was also followed for the analysis of the partially splined shaft. For the sake of dimensional simplicity, the F_M/F_T ratio number is expressed in terms of percentages. For example, the expressions F_M/F_T=1000/0 and F_M/F_T=100/0 are used interchangeably throughout the thesis to denote the pure bending load case.

IV. RESULTS

4.1 Convergence

To ensure the accuracy of the stresses generated in ALGOR, it was necessary to obtain the convergence of those stresses to reasonable values. Convergence is demonstrated for only two of the 11 possible load cases: pure bending and torsion. Henceforth, the characteristic shaft length is defined as L_o, and is equal to 10" (0.254m). To simplify further analysis of the stress data, locations along the shafts' axes will be normalized. That is, the dimensionless location on the shaft axis Z^* is defined by the ratio between the actual position on the Z-axis of the shaft Z, relative to the origin and the characteristic length of the shaft L_o. Thus, shaft position is defined as Z/L_o.

The stresses in each model were converged using an h-refinement scheme. An h-refinement changes the element size without changing the element type [11]. Again, to simplify the analysis of the convergence data, the element size h was also non-dimensionalized. The element size will henceforth be defined as the ratio between the actual element size and the initial element size h_o; or h/h_o.

4.1.1 Convergence of Stepped Shaft Stresses

Convergence was sought at the step in each stepped shaft model. This location was of greatest interest since the peak stresses were expected to be located near the step Figure 38 shows the location on the stepped shaft where the stress values were converged.

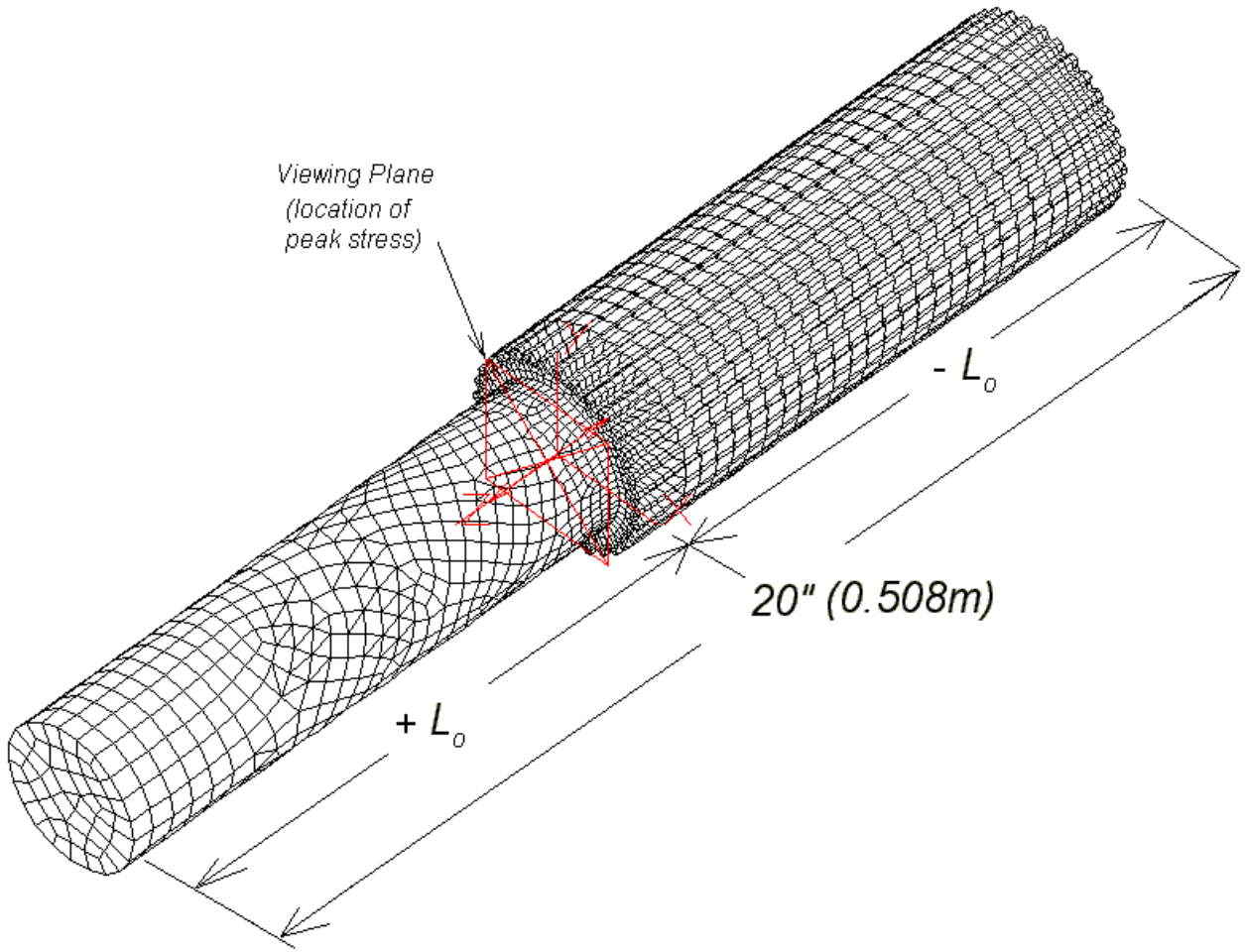

Figure 38. Stepped shaft model with FE mesh applied. The maximum von Mises were converged using values at location Z*=+0.0167. In Algor, the viewing plane was used to view the cross-section of the model and extract the maximum stress at that location.

The initial mesh size for the stepped shaft was 0.3316". (0.0084 m). The h-refinement convergence of the von Mises stress is shown in Figure 39. Only the convergence of the d/D_o = 0.75 stepped shaft model is shown, since the other models showed similar, quasi-monotonic convergence behavior. Convergence was obtained by generating several finite element models from the same solid geometry model. Each model contained successively smaller brick elements near the step, thereby yielding more accurate stresses in the region of interest.

The stresses obtained from Algor for the convergence study were also made dimensionless. For the stepped shaft, a nominal stress σ'_o was defined. The nominal stress is the value of stress outside of the transition zone, which remains relatively constant along the length of the shaft. Since convergence was obtained only for the load cases of pure bending, and pure torsion, a different value of nominal stress (σ'_o) was used to calculate the stress ratio for each load case. The nominal stress for pure bending in the d/D_o = 0.75 stepped shaft was 2413 psi (17 MPa). The nominal stress for the pure torsion case was 2106 psi (15 MPa). Table 6 is provided to show that the stresses converged to a value within the criterion tolerance band of 2%.

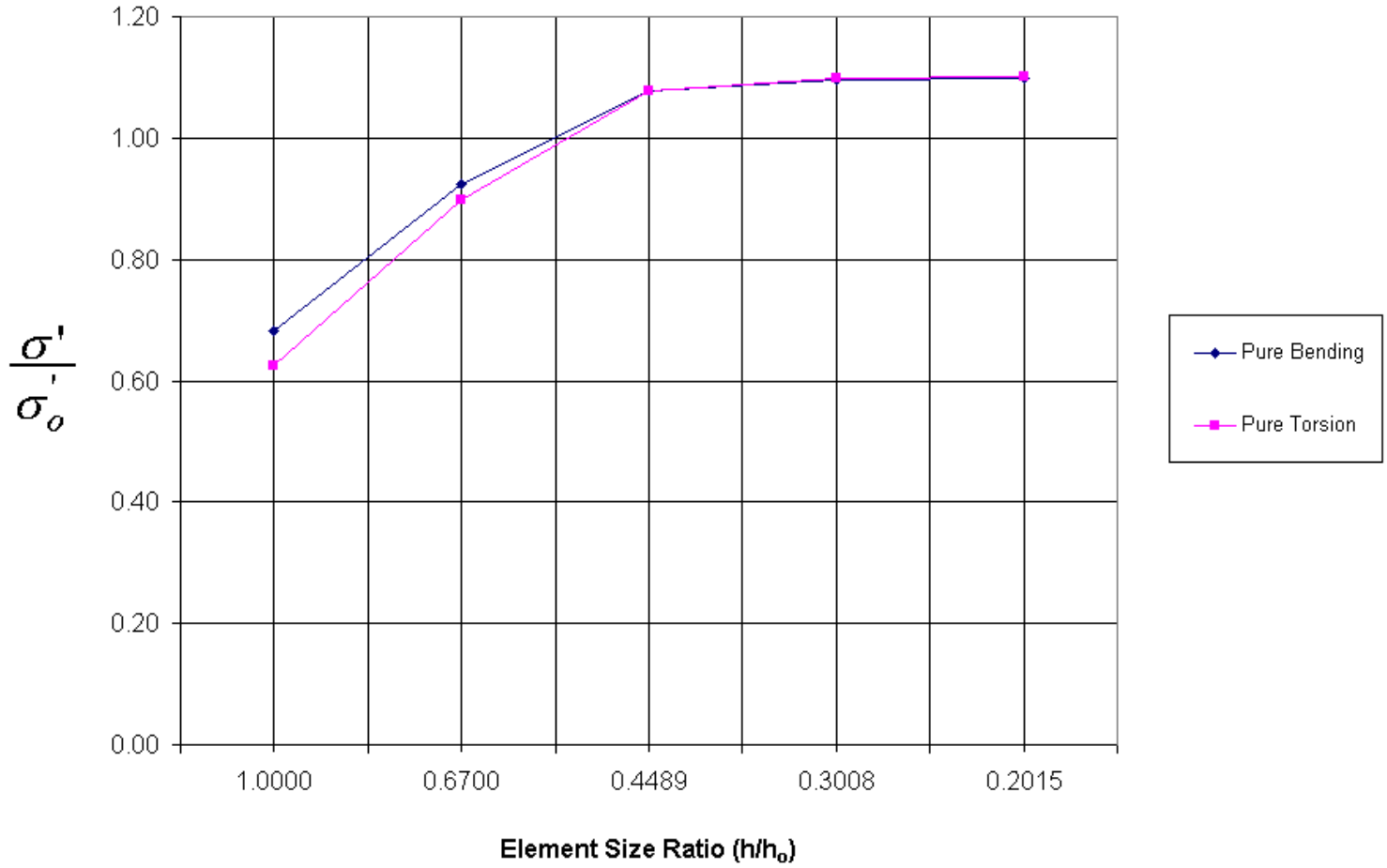

Figure 39. Convergence of ALGOR generated maximum von Mises stress using h-refinement for the d/D=0.75 stepped shaft model. Results for both the pure bending and pure torsion load cases F_M/F_T=100/0 (pure bending) and F_M/F_T=0/100 (pure torsion) are shown.

Table 6. H-refinement convergence of ALGOR generated von Mises stresses in the stepped shaft model. The convergence tolerance is also shown in the "% difference" column. Stresses taken at the Z^*=+0.0167 location on the shaft. Results are for the d/D=0.75 model.

Iteration #	Element Size Ratio (h/ho)	Pure Bending	% difference	Pure Torsion	% difference
1	1.00	0.681	--	0.625	--
2	0.67	0.924	35.70%	0.898	43.61%
3	0.45	1.078	16.67%	1.077	19.87%
4	0.30	1.097	1.75%	1.099	2.06%
5	0.20	1.097	0.04%	1.100	0.10%

An example of the von Mises stress contours over the shaft cross section is shown in Figure 40. The cross-section shown corresponds to a location within the splined section, but outside the transition zone. The stress contours shown in Figure 40 represent well-developed stresses for the pure bending case. The peak stresses were not located near the shaft step. Rather, they were located at the Z^{*}=-0.5 location in every case. The results shown were extracted from Algor.

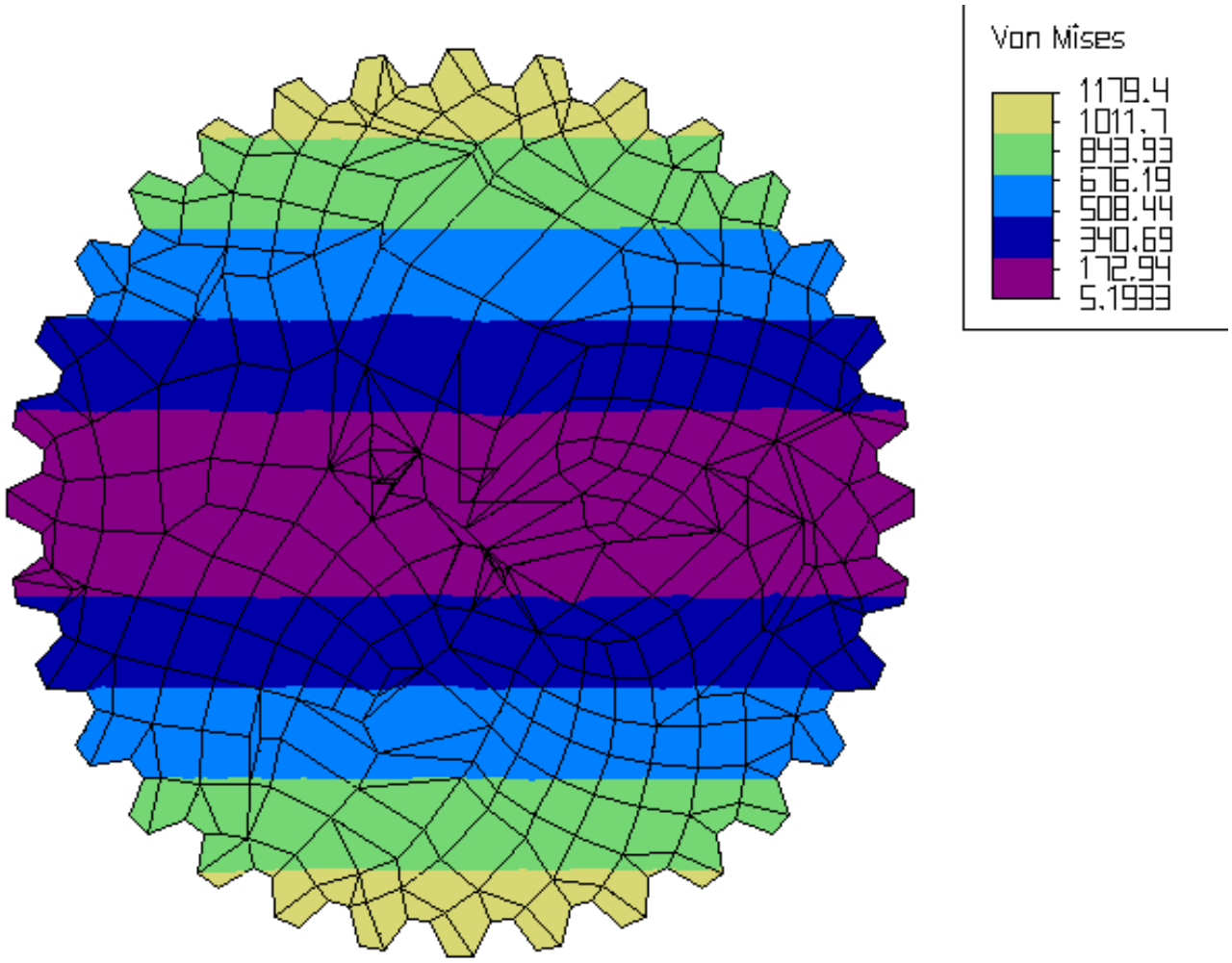

Figure 40. Stress contours on the cross-section of the d/D_o=0.75 shaft at the Z^*=0.50 location. The pure bending load case is shown.

4.1.1.1 Verification of Stepped Shaft Stresses

No theoretical model is proposed for predicting the stresses at the shaft step. Solutions have been developed for round, shouldered shafts with finite fillet radii. However, nothing in the literature suggests an analytical solution for predicting the stress in a stepped splined shaft with a zero-radius fillet at the step.

Theoretical predictions of the stresses in the non-splined and splined sections of the stepped shaft were made. These calculated stresses were calculated at locations in the shaft where the stresses are well developed (locations Z^*=+0.500 and Z^*=-0.500). The calculated stresses were then compared to the Algor generated stresses at the same location on the shaft. The percentage difference between the theoretical stresses and the Algor stresses was calculated and displayed in Figure 41 through Figure 46.

The calculated and Algor stresses in the non-splined section of the stepped shafts differ by between 0% and 2.3%. However, the difference between the calculated and Algor generated stresses becomes much larger in the splined section. The two stresses are close only when pure bending loads is applied to the shaft. As the load on the shaft becomes increasingly torsional, the difference between the Algor stresses and calculated stresses becomes more pronounced. This indicates that the analytical model used does not adequately predict the response to torque loading of the solid splined shaft as modeled in this thesis. This is because the theoretical model used is strictly valid only for circular cross sections.

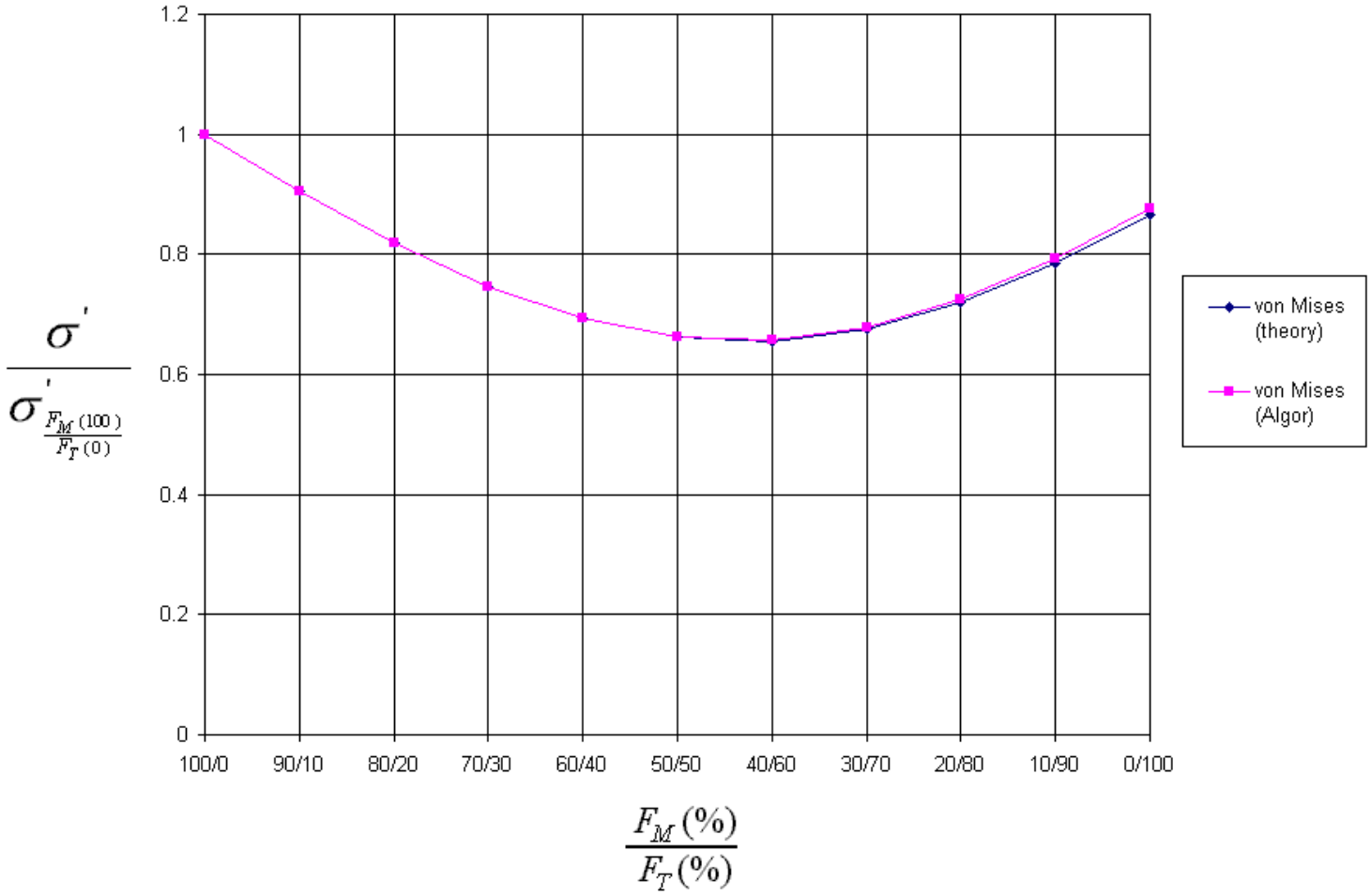

Figure 41. Percent difference between Algor and calculated stresses, stepped shaft d/D=0.500, non-splined section

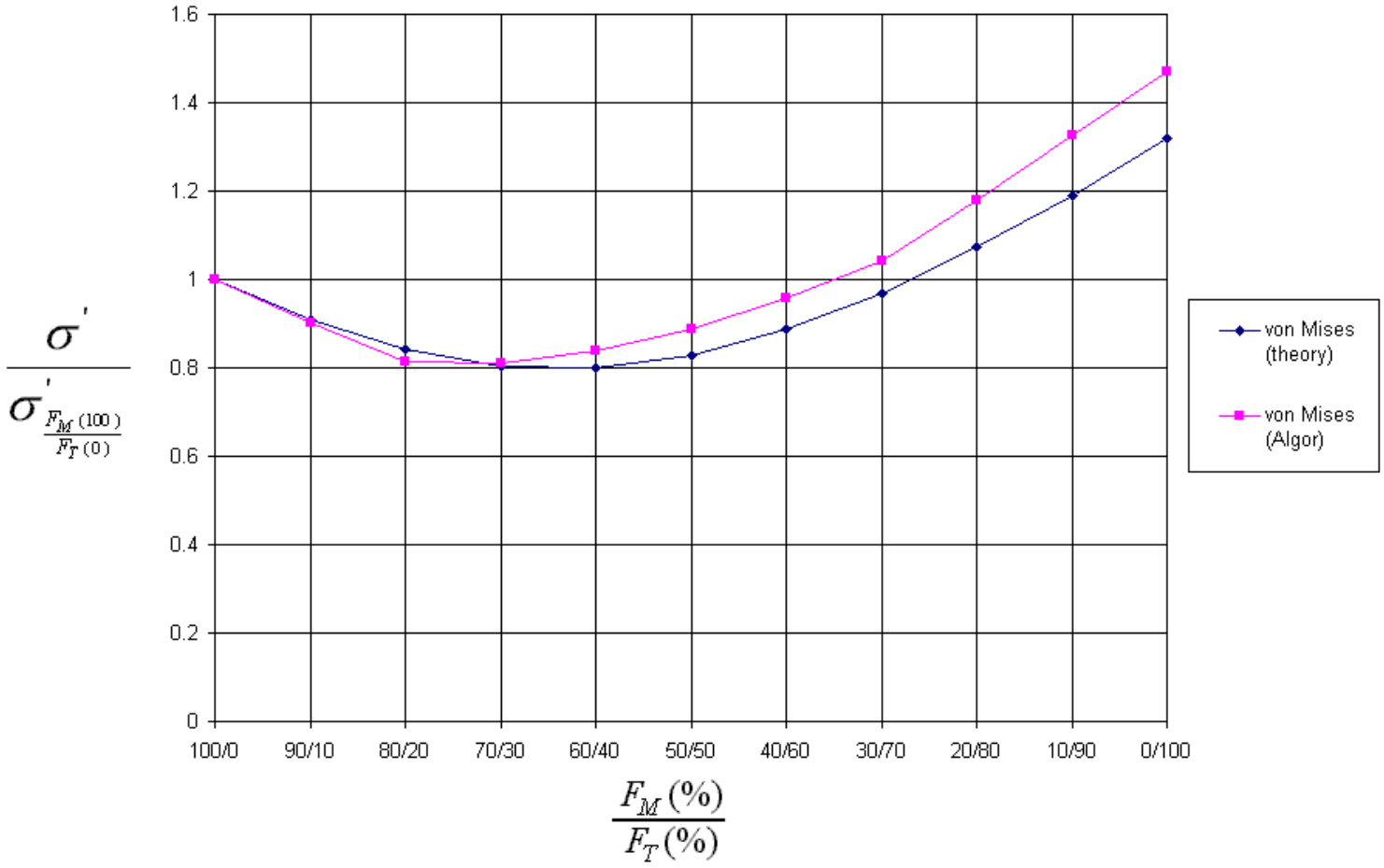

Figure 42. Percent difference between Algor and calculated stresses, stepped shaft d/D=0.500, splined section.

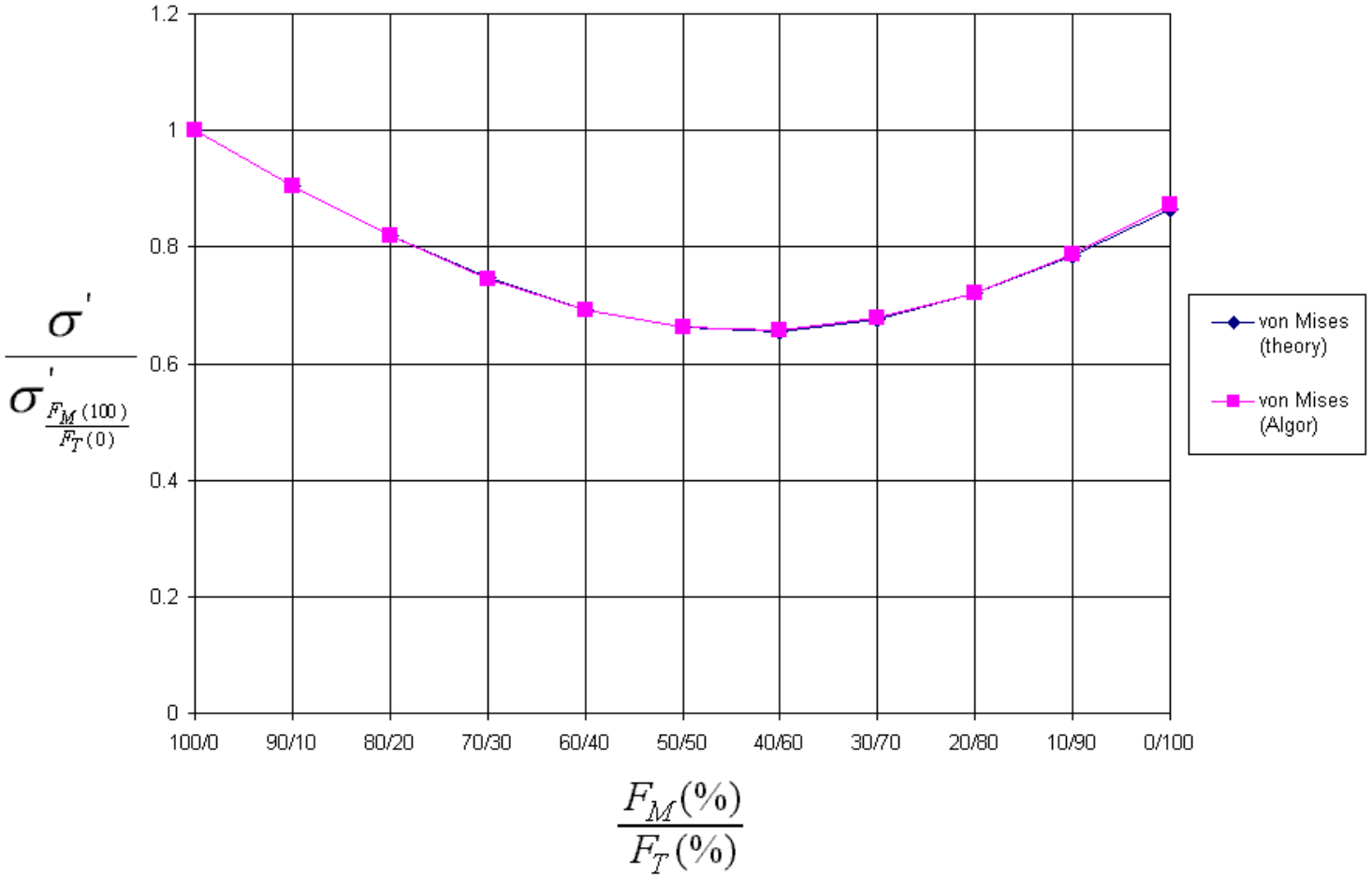

Figure 43. Percent difference between Algor and calculated stresses, stepped shaft d/D=0.750, non-splined section.

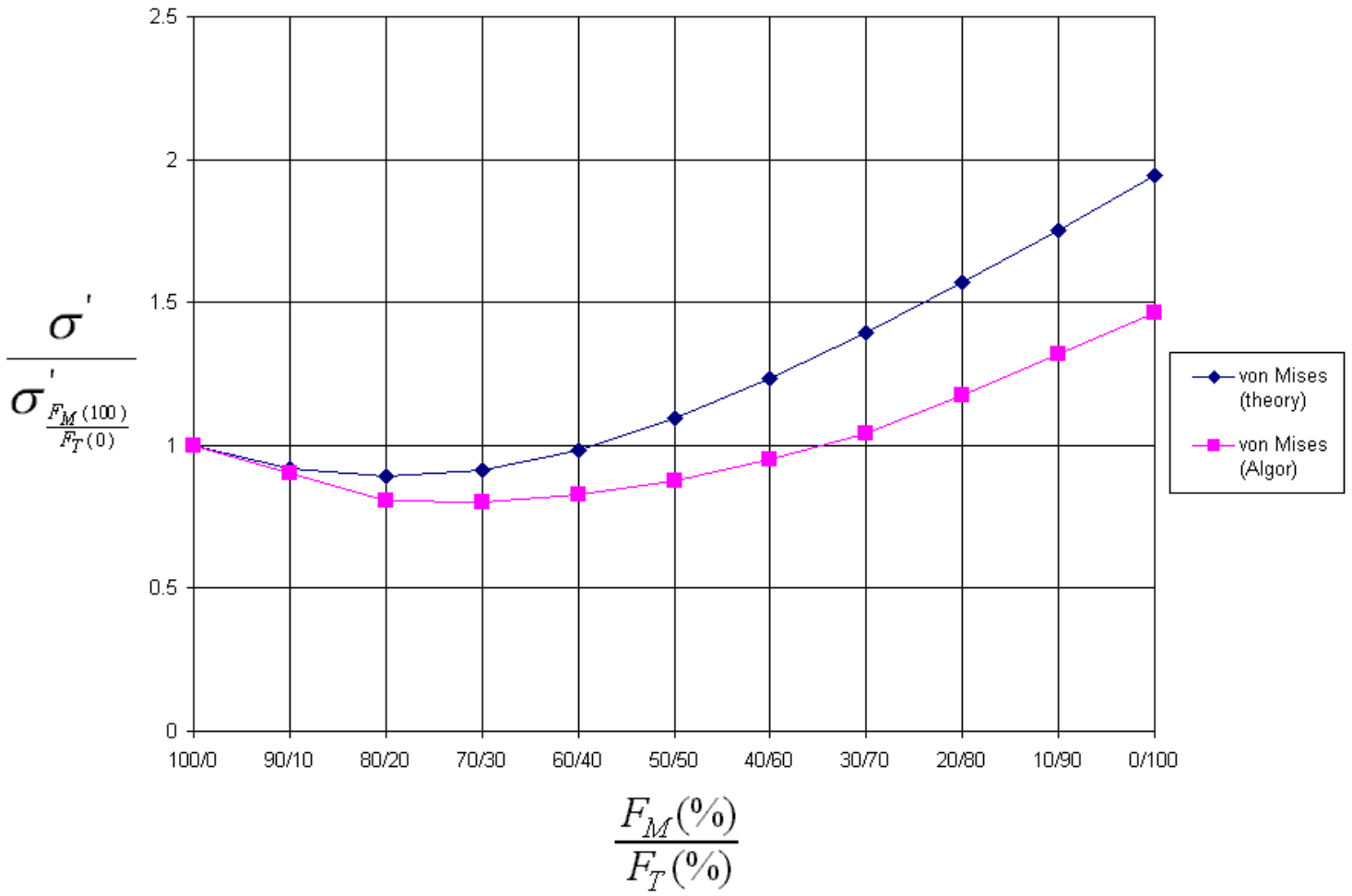

Figure 44. Percent difference between Algor and calculated stresses, stepped shaft d/D=0.750, splined section.

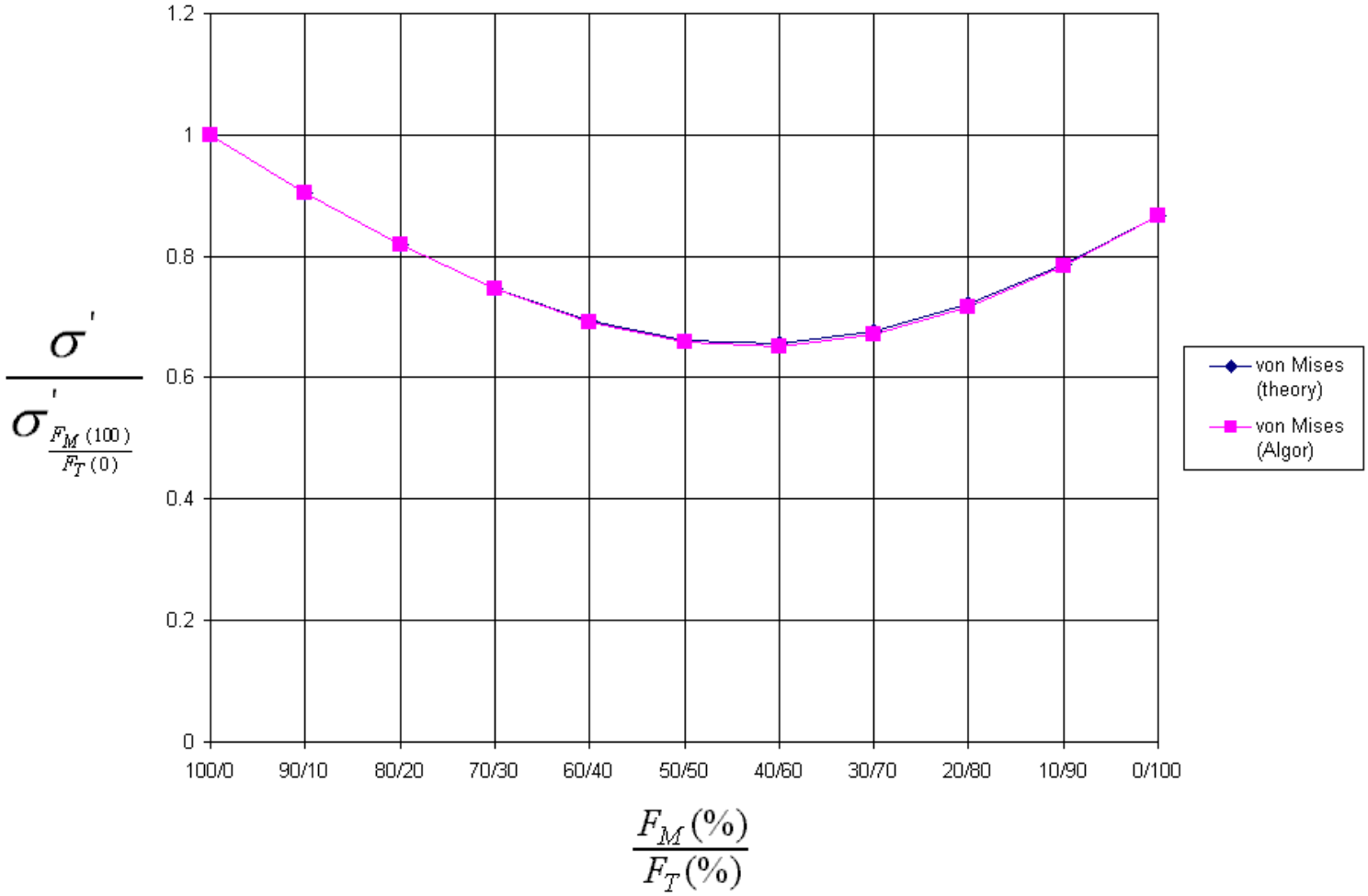

Figure 45. Percent difference between Algor and calculated stresses, stepped shaft d/D=0.886, non-splined section.

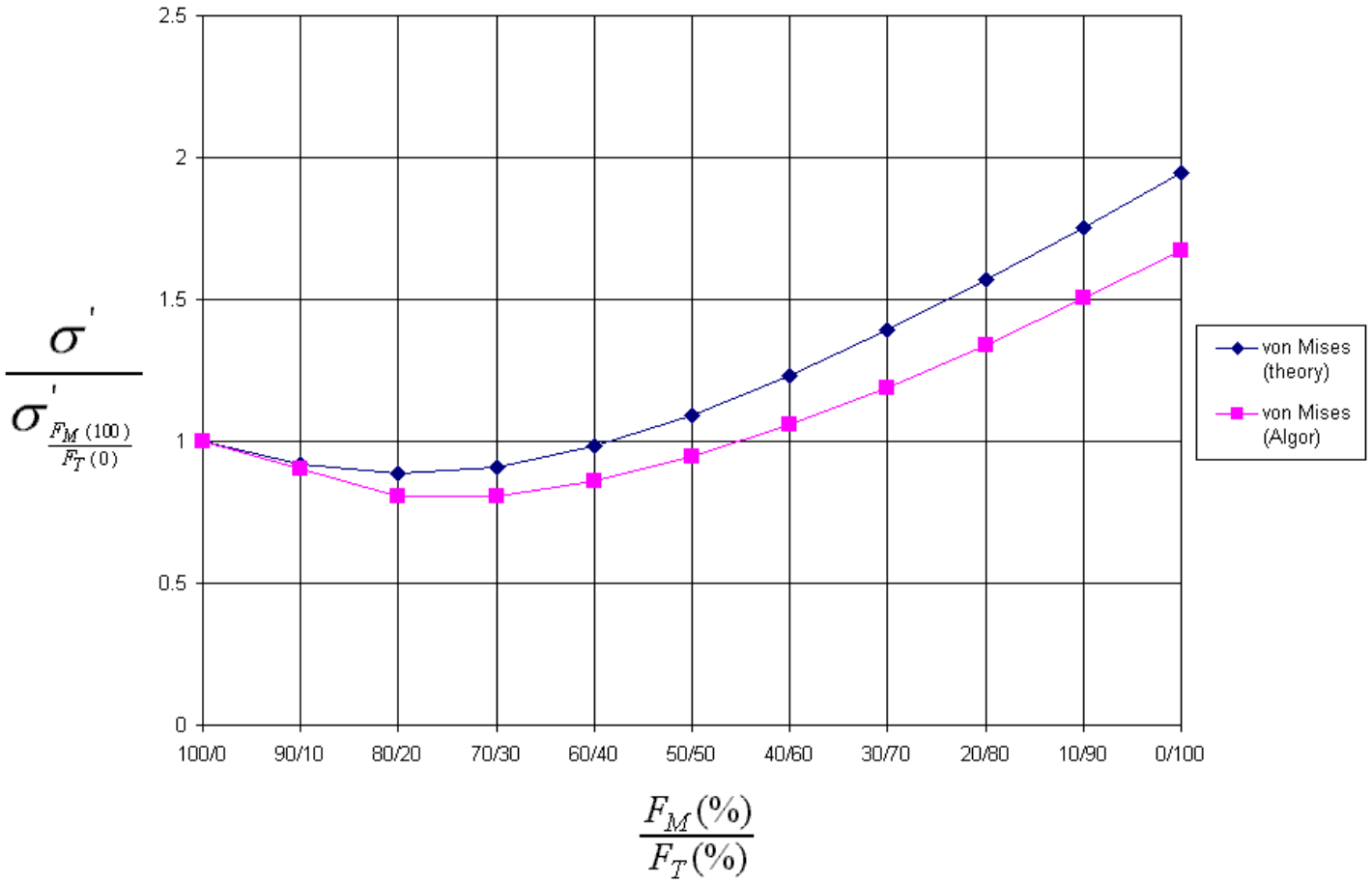

Figure 46. Percent difference between Algor and calculated stresses, stepped shaft d/D=0.886, splined section.

4.1.2 Convergence of Partially Splined Shaft Stresses

A similar convergence process was used for the partially splined shaft. Figure 47 shows the location at which stresses in the partially splined shaft were converged. The stress values reported in Figure 47 were for both the pure bending and the pure torsion cases. Only the convergence of the R=1.5”(0.0381m) stepped shaft model is shown, since the other models showed similar, quasi-monotonic convergence behavior.

An h-refinement scheme was also used to converge the stress values in the partially splined shaft. The convergence study focused on the region near Z^{*}=-0.0167 since the peak stresses were found to exist there. The initial mesh size for the stepped shaft was 0.3392” (0.0086 m). Convergence was obtained by generating several finite element models from the same solid geometry model. Each model contained successively smaller brick elements near the incomplete teeth, thereby yielding stresses that are more accurate.

The von Mises stress contours on the cross-section of the R=1.5" shaft is shown in Figure 48. Figure 48 shows the pure bending stresses at the Z^{*}=0.0 location in the partially splined shaft. The results shown were extracted from Algor.

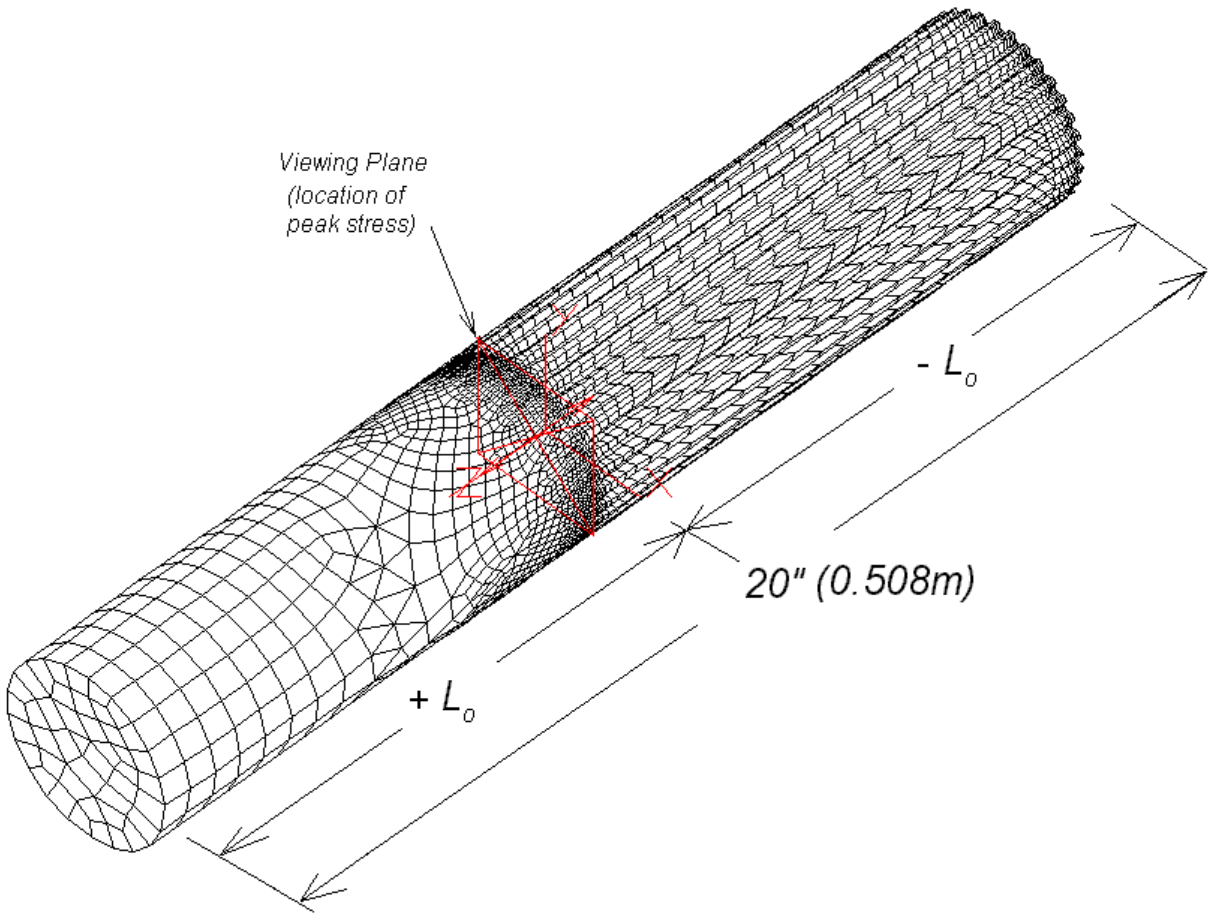

Figure 47. Partially splined shaft model with FE mesh applied. The maximum von Mises stress was converged using values at location Z^*=-0.0167. In Algor, the viewing plane was used to view the cross-section of the model and extract the maximum stress at that location.

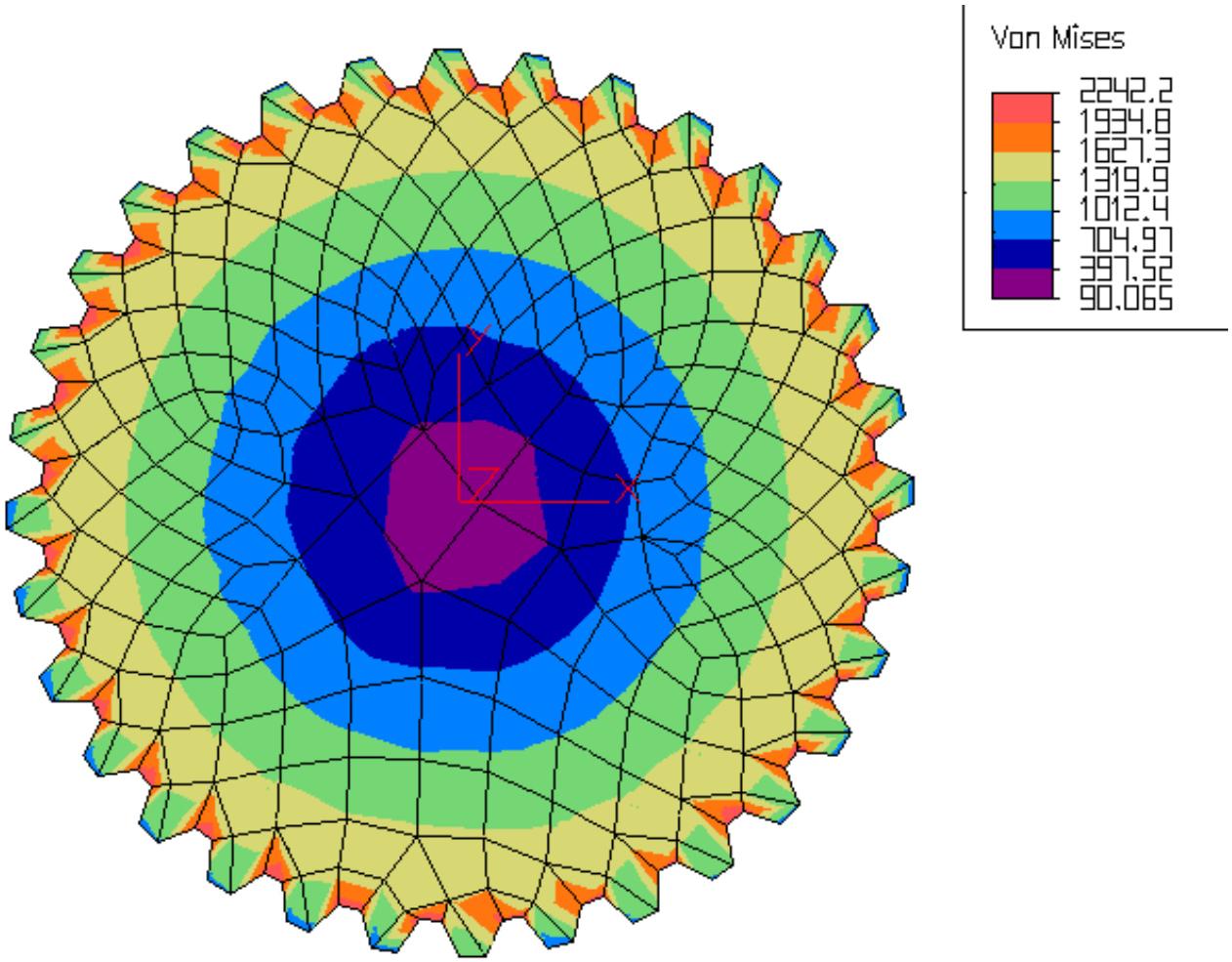

Figure 48. Stress contours on the cross-section of the R=1.5" partially splined shaft. Pure torsion load case shown.

The stresses obtained from Algor for the convergence study, shown in Figure 49, were also made dimensionless. For the partially splined shaft, a nominal stress σ'_o was also defined. The nominal stress, which remains constant throughout the shaft, is the value of stress outside of the transition zone. A different value of nominal stress σ'_o was used to calculate the stress ratio for each of the two load cases. The nominal stress for pure bending in the R=1.5" (0.0381 m) stepped shaft was 1567 psi (10.8 MPa). The nominal stress for the pure torsion case was 2236 psi (15.4 MPa).

Table 7 shows that the stresses converged to a value within the criterion tolerance band of 2%. Because the values from the fourth iteration step were within the convergence tolerance band, those values were used for all subsequent analysis. Generating a finer mesh was unnecessary.

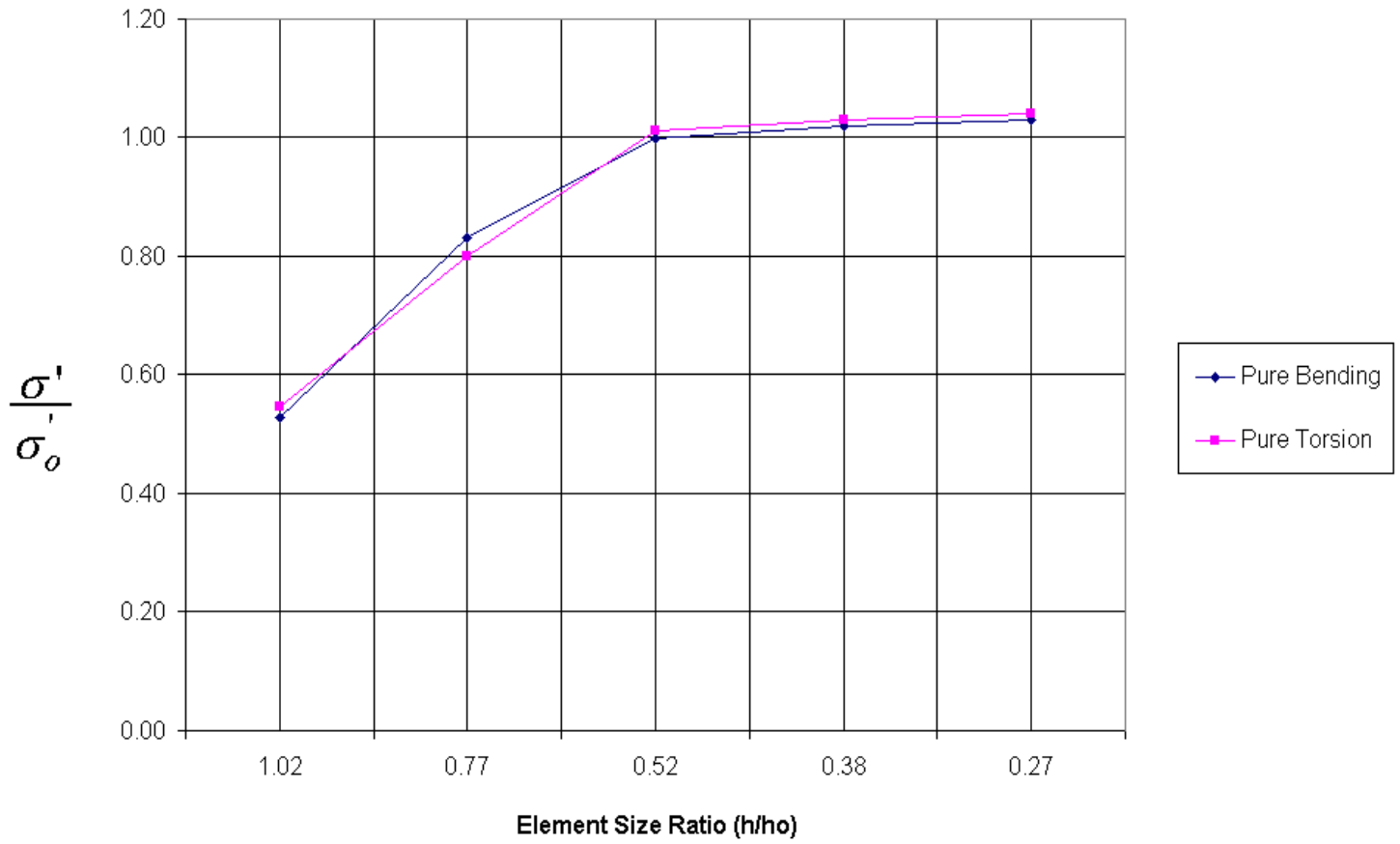

Figure 49. Convergence of ALGOR generated maximum von Mises stress using h-refinement for the R=1.5"(0.0381 m) partially splined shaft model. Load cases F_M/F_T=100/0 (pure bending) and F_M/F_T=0/100 (pure torsion) are shown.

Table 7. H-refinement convergence of ALGOR generated maximum von Mises stresses in the stepped shaft model. The convergence tolerance is also shown in the "% difference" column. Stresses taken at the Z^{*}=-0.0167 location on the shaft. Results are for the R=1.5"(0.0381 m) model.

Iteration #	Element Size Ratio (h/ho)	Pure Bending	% difference	Pure Torsion	% difference
1	1.02	0.528	--	0.545	--
2	0.77	0.832	57.36%	0.801	46.83%
3	0.52	0.999	20.19%	1.012	26.46%
4	0.38	1.020	2.06%	1.031	1.86%
5	0.27	1.030	1.01%	1.042	0.99%

4.1.2.1 Verification of Partially Splined Shaft Stresses

In Figure 50 through Figure 55, the Algor generated finite element stresses are compared with the stresses calculated from Equations 2.6 for the partially splined shafts. Algor stress results for all load cases in the non-splined portion of the shaft closely match those determined using the calculated values. The Algor results for the splined sections of the shafts were comparable to the analytical model only for load cases that were very near pure bending (F_M/F_T = 100/0). No closed form analytical solution exists for accurately predicting even the well-developed stresses at the spline tooth roots in the particular types of splined shafts studied here. The analytical models used here are very simplified compared to algorithms used to calculate stresses in Algor. Where the analytical models use only one shear stress and one bending stress, Algor considers all three normal and shear stresses in its calculation. No closed form solution was developed for predicting the peak stresses that occur at the step in stepped splined shaft, or the incomplete teeth in the partially splined shaft.

Within the non-splined portion of the shaft, the Algor stresses are very close to the calculated stresses. In the splined section of the partially splined shafts, the Algor and calculated stresses are close only for low F_M/F_T ratios, or when bending loads are much greater then torsional loads. Therefore, as the F_M/F_T ratio decreases the divergence between the Algor and calculated stresses increases.

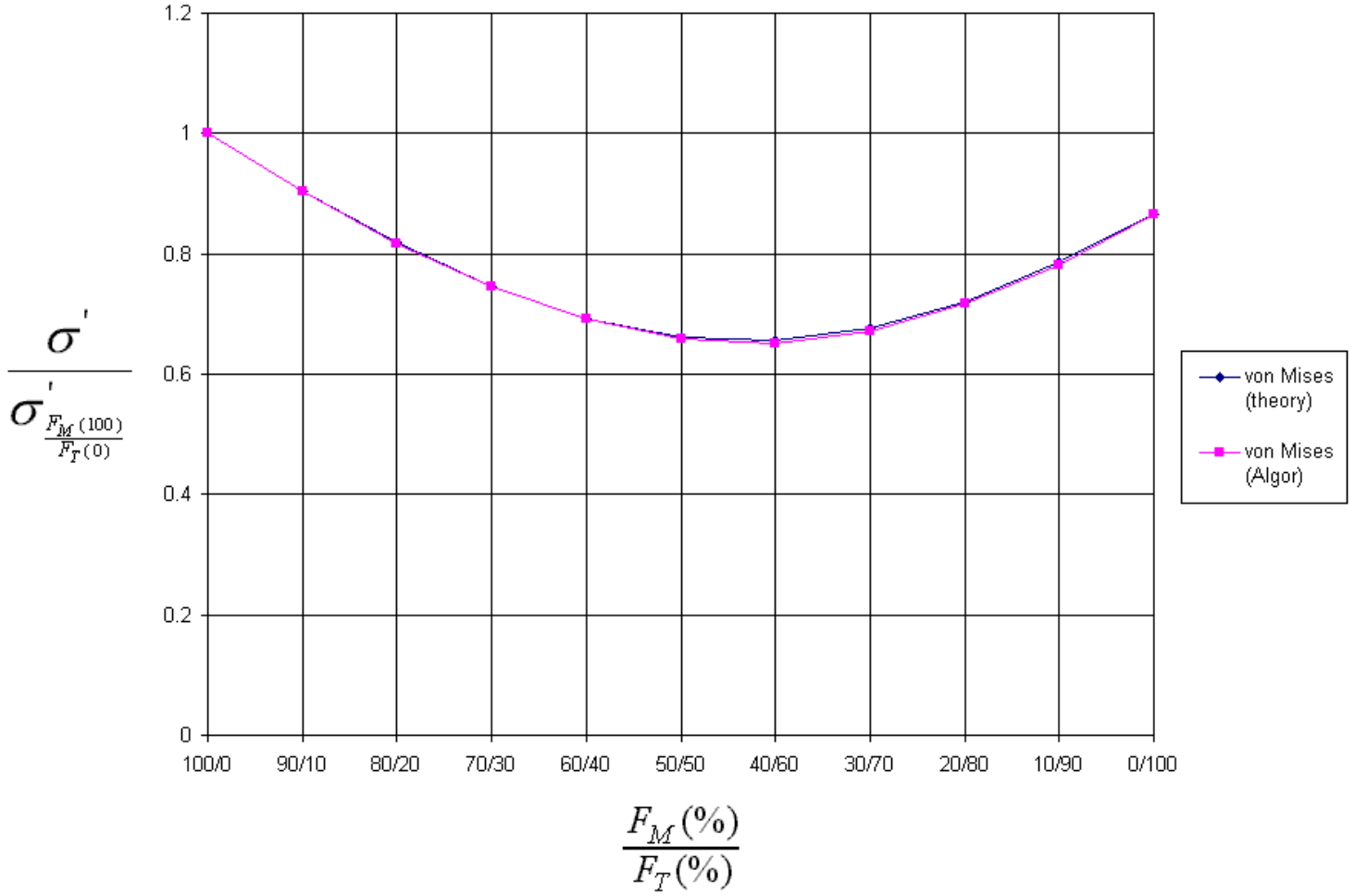

Figure 50. Percent difference between Algor and calculated stresses, partially splined shaft R=1.000"(0.0254m), non-splined section

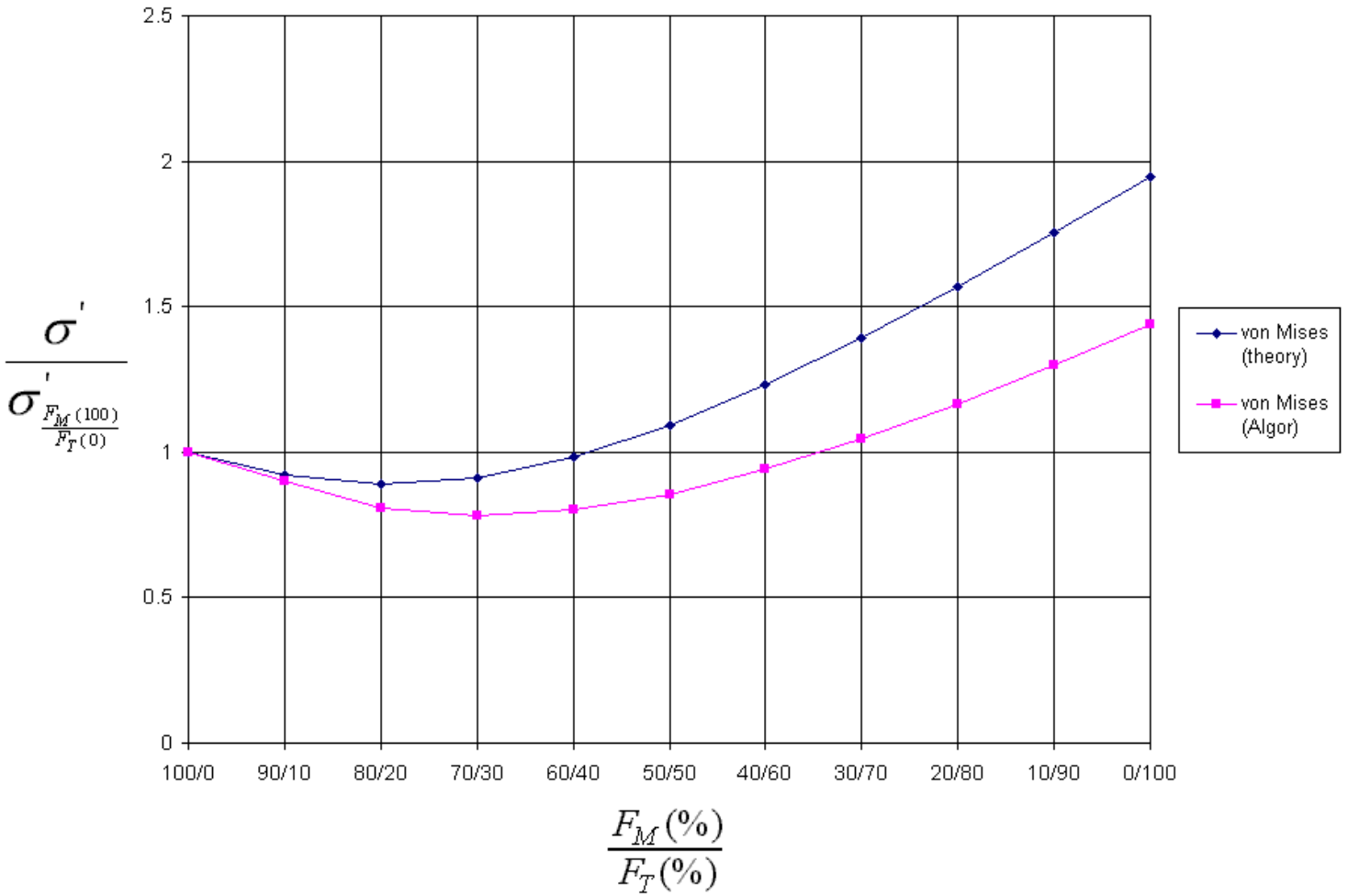

Figure 51. Percent difference between Algor and calculated stresses, partially splined shaft R=1.000"(0.0254m), splined section

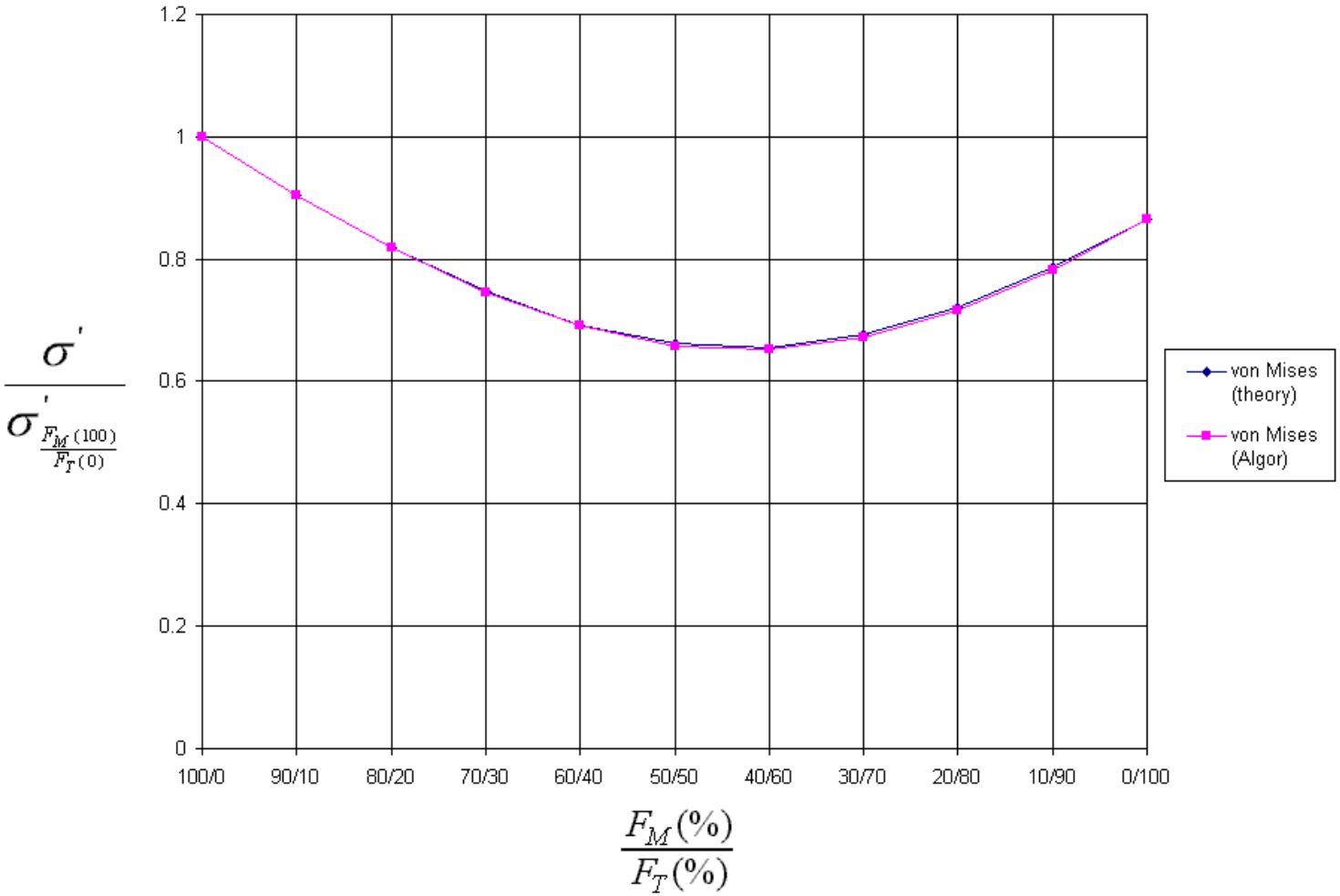

Figure 52. Percent difference between Algor and calculated stresses, partially splined shaft R=1.500"(0.0381m), non-splined section.

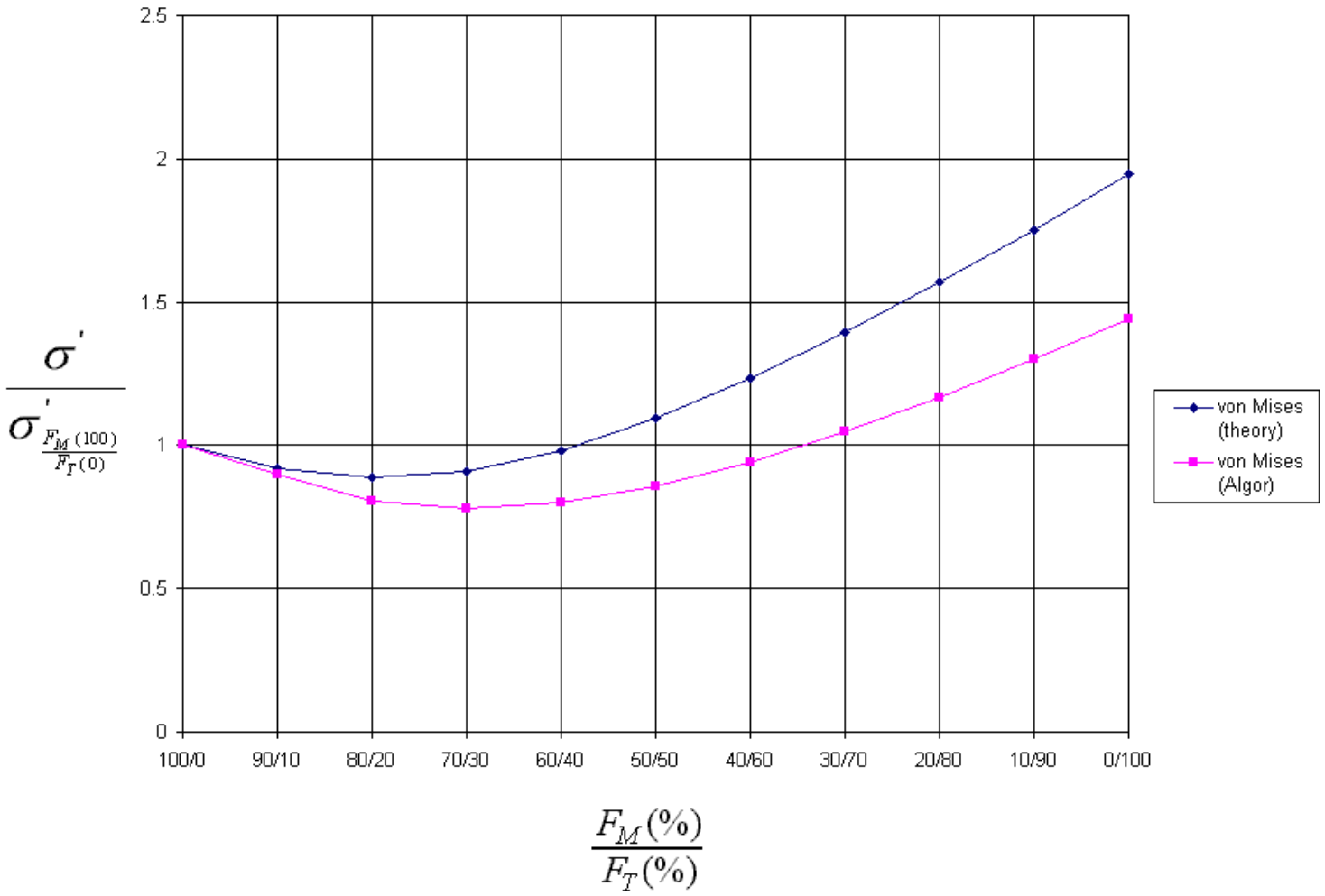

Figure 53. Percent difference between Algor and calculated stresses, partially splined shaft R=1.500"(0.0381m), splined section

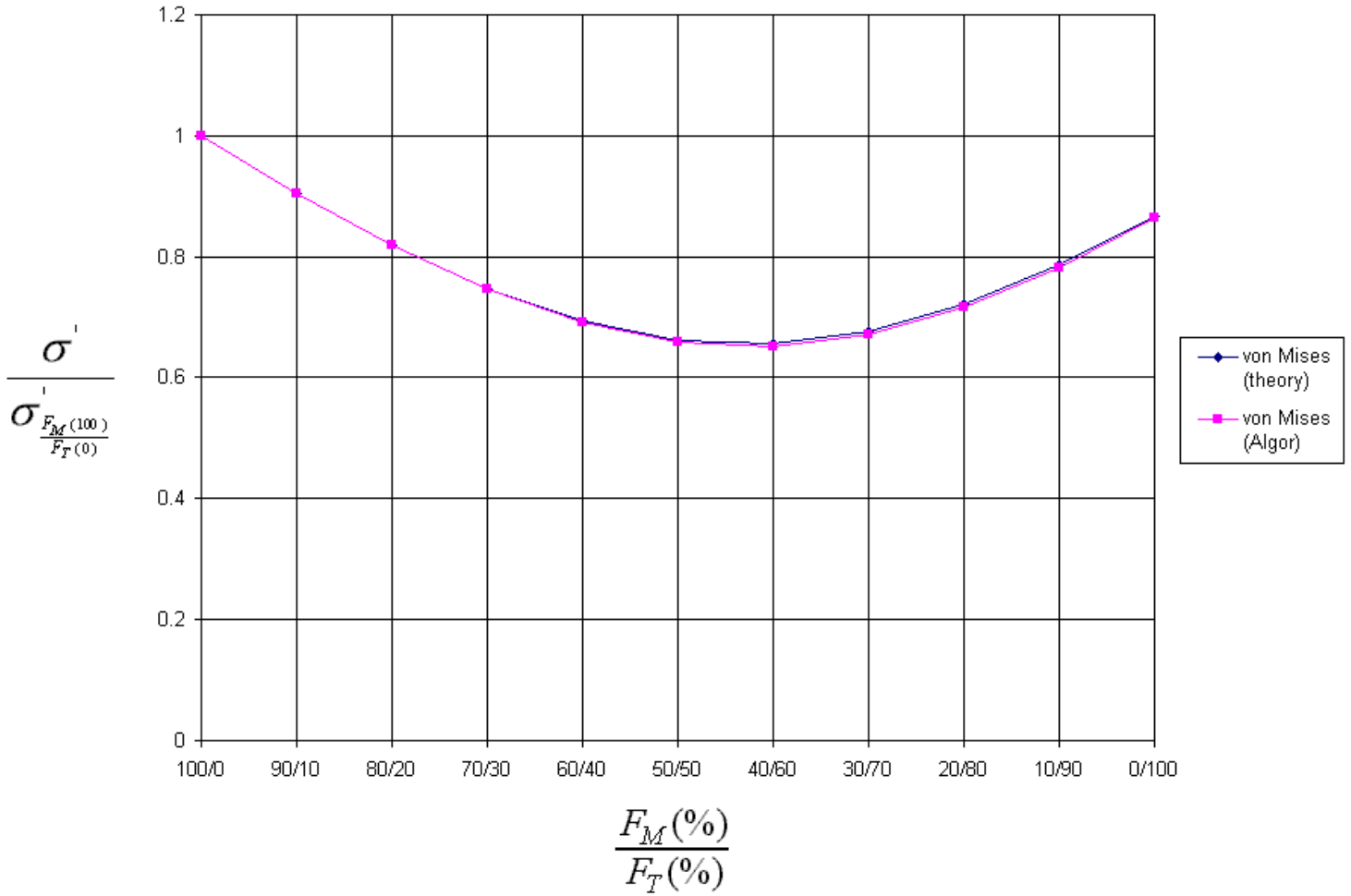

Figure 54. Percent difference between Algor and calculated stresses, partially splined shaft R=2.000"(0.0508m), non-splined section.

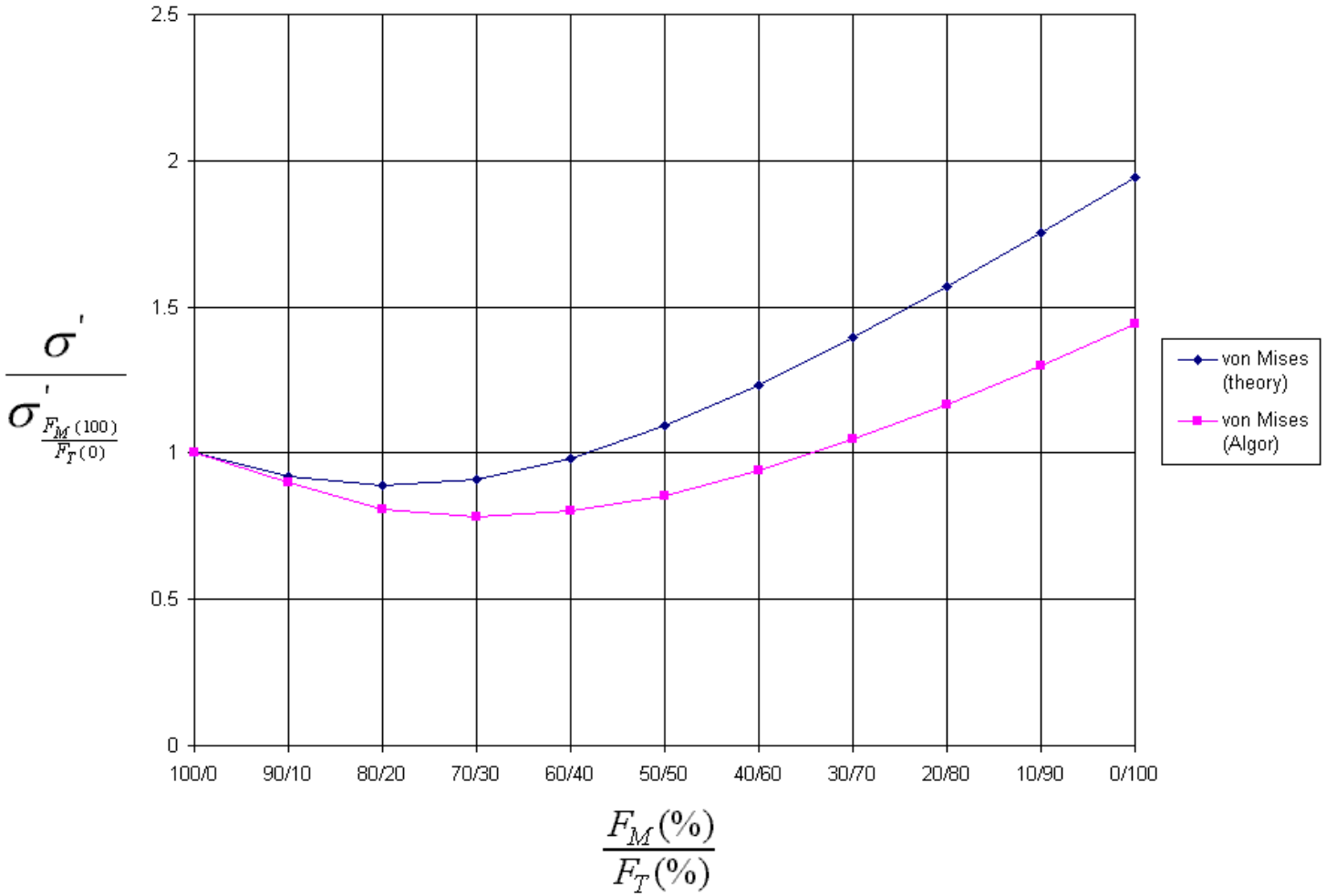

Figure 55. Percent difference between Algor and calculated stresses, partially splined shaft R=2.000"(0.0508m), splined section.

4.2 Stresses-Stepped Shaft Models

Three finite element models of a stepped splined shaft were constructed using step ratios (d/D_o) of 0.500, 0.750, and 0.886. Each model was subjected to applied loads ranging from pure bending to pure torsion including several combinations of bending and torsion. Figure 56 -Figure 58 illustrate the relationships between the von Mises and the step ratio (d/D) of each stepped shaft, for 11 combinations of bending and torsion loads.

Figure 56 describes the stresses generated in the d/D_o=0.500 shaft model. The behavior of the von Mises stresses is very similar at all locations along the shafts. There is a 70% difference between the stress levels before and after the step. The reason for this difference in stress level is the change in cross sectional area of the shaft between the splined and non-splined sections. The non-splined section of the shaft has a smaller diameter than that of the splined section, yet the same load is transmitted to both. The section with the least cross-sectional area (and hence, the least overall stiffness) will experience the higher stress while bearing the same load.

The peak stresses occur between the Z^*=+0.0125 and +0.0167 locations in the non-splined section of the shaft. This is consistent with the location of the cracks in the Fairchild shafts. The peak von Mises stress occurs at load case (F_M/F_T=100/0) and is 88% greater than the well-developed stresses in the larger diameter, splined section. The peak von Mises stress is 16% greater than the well-developed stresses in the smaller diameter, non-splined section.

The peak stress decrease across the shaft step, finally reaching a local minimum at the Z^*=-0.100 location in the splined section of the shaft. Stresses in the shaft become well developed and reach a nominal value beyond the Z^*=-0.200 location in the splined section of the shaft.

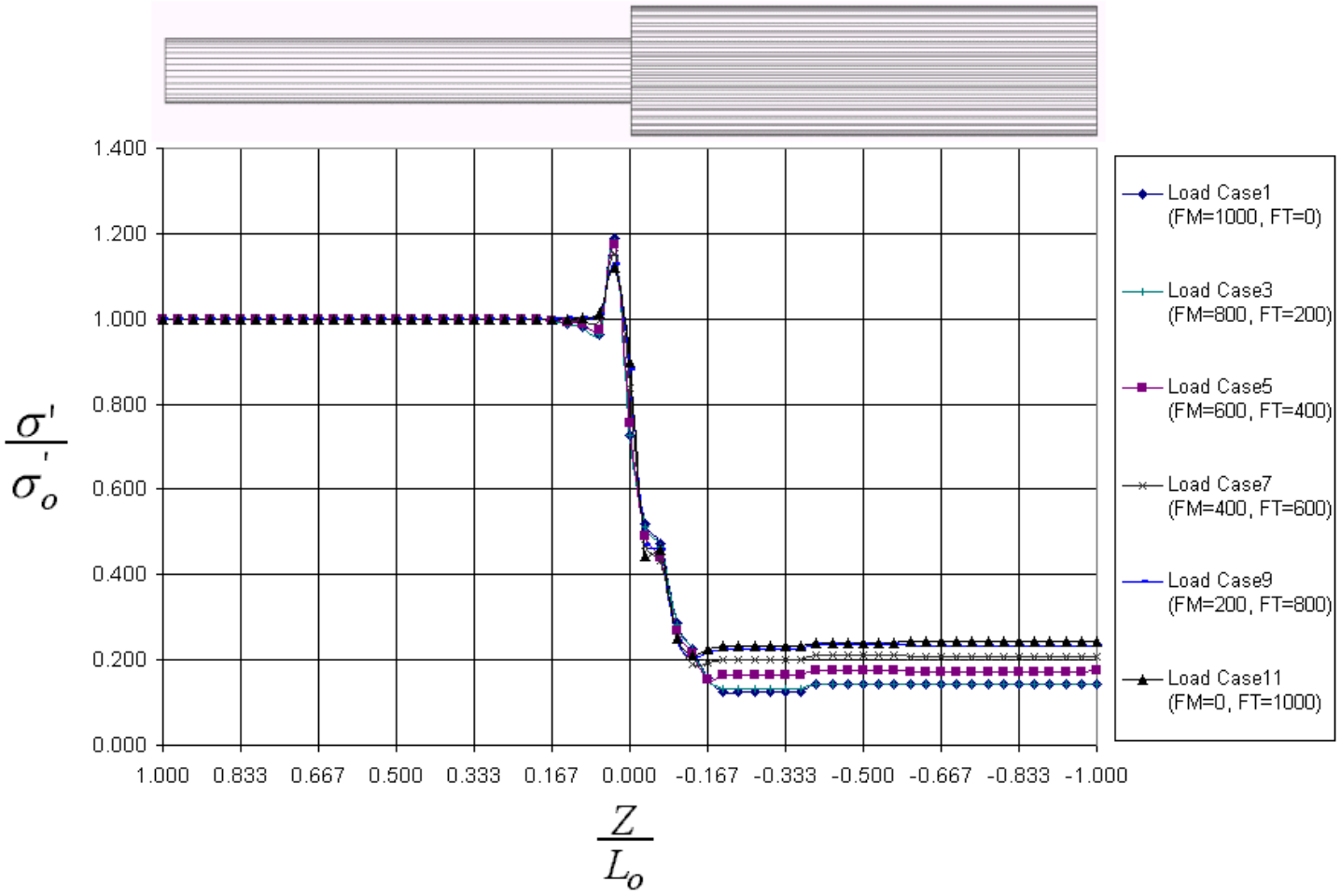

Figure 56. Variation of von Mises stress with ratio of bending to torsion for stepped splined shaft (d/D=0.500)

Figure 57 shows the stresses generated in the d/D=0.750 shaft model. There is a 60% difference between the stress levels before and after the step because of the change in cross-sectional area of the shaft.

The peak stresses occur about the Z^*=+0.0125 location of the non-splined section of the shaft. This is consistent with the location of the cracks seen in the Fairchild shafts. The peak von Mises occurs at load case 1 (F_M/F_T=100/0).

The peak von Mises stress is about 55% greater than the well-developed stresses in the larger diameter, splined section. The peak von Mises stress is about 9% greater than the nominal stresses in the smaller diameter, non-splined section.

The peak stress, decreases across the step, reaching a minimum level between the Z^*=0.00 and Z^*=-0.0750 locations in the splined portion of the shaft. The stress levels for each load case begin to increase again after the Z^*=-0.0750 position within the splined section. The stress levels then reach a plateau after the Z^*=-0.1000 location in the splined section.

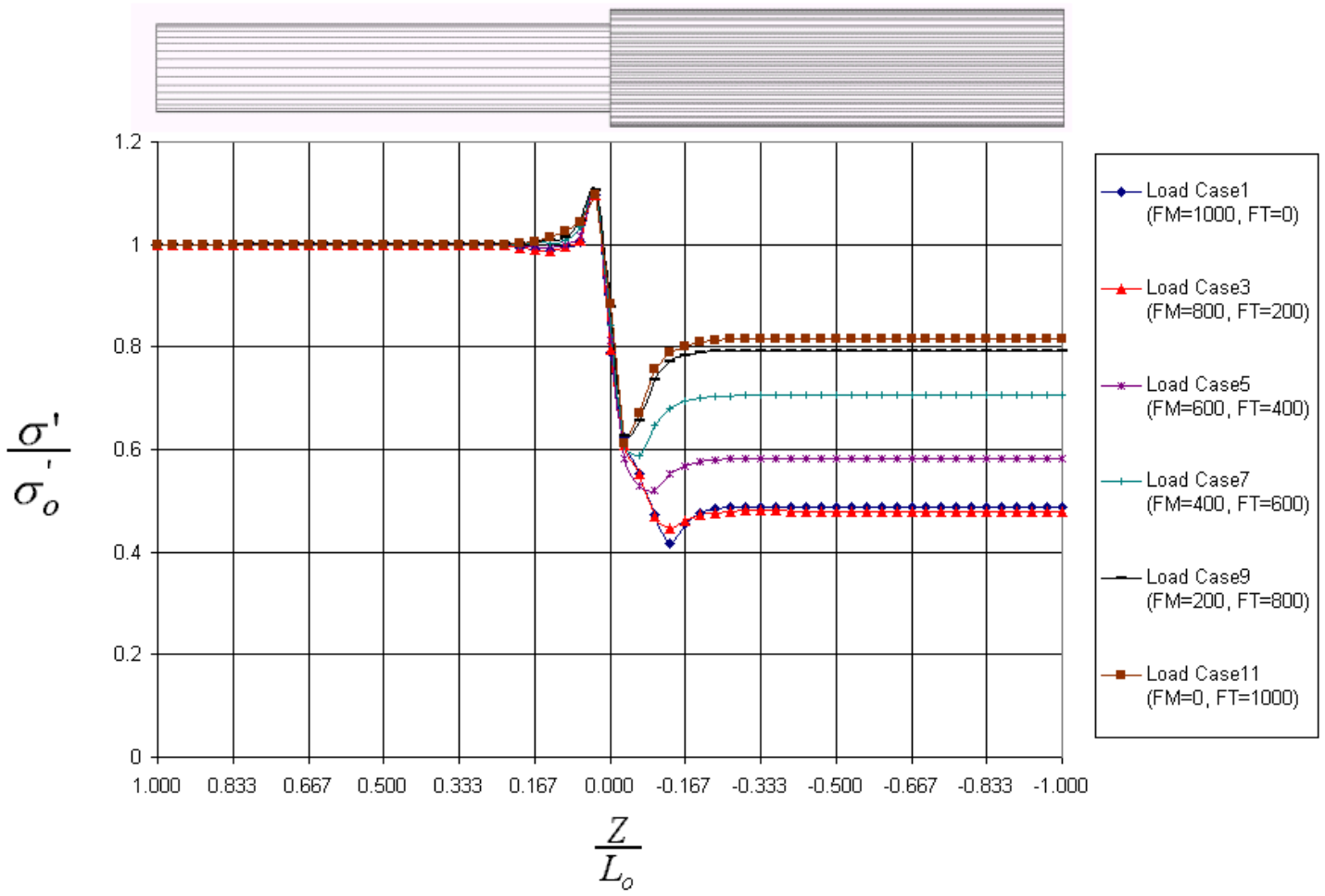

Figure 57. Variation of von Mises stress with ratio of bending to torsion for stepped splined shaft (d/D=0.750)

For the d/D=0.886 shaft, there is a departure from the expected behavior in the von Mises stress, as shown in Figure 58. The von Mises stress exhibits a local peak stress near the step at the Z^*=+0.0125" location in the non-splined section of the shaft for load cases 1 (F_M/F_T =100/0) to 5 (F_M/F_T =60/40). The highest of these peaks, occurring at load case 1 (F_M/F_T =100/0), is 16% greater than the nominal stresses in the non-splined section, and 33% higher than the nominal stresses in the splined section.

However, in subsequent load cases, as torsion loading becomes proportionally greater than bending, the von Mises peaks become smaller. For pure torsion, or load case 11 (F_M/F_T =0/100), no peaks exists at all on the non-splined side of the step. As the twisting force F_T becomes greater than the bending force F_M, the resulting stresses in the vicinity of the step become smaller than those generated in the splined section at the root of the spline teeth. In fact, at load case 11 (F_M/F_T =0/100) the von Mises stresses in the splined section exceeds the peaks generated in the non-splined section of the shaft by 11%. This translates to approximately 50% greater than the largest nominal stress in the non-splined section. There were no greater stresses in the splined section.

The location of the peak stresses in the d/D=0.886 shaft is consistent with the location of the cracks seen in the Fairchild shafts, with the exception of the stresses at the higher load cases. From the peak level, the stresses decrease across the step, reaching a minimum level for each load case between the Z^*=0.00 and Z^*=-0.075 locations on the shaft. The stresses for each load case begin to increase again after the Z^*=-0.075 position. The stress then reaches a nominal value after the Z^*=-0.100 location.

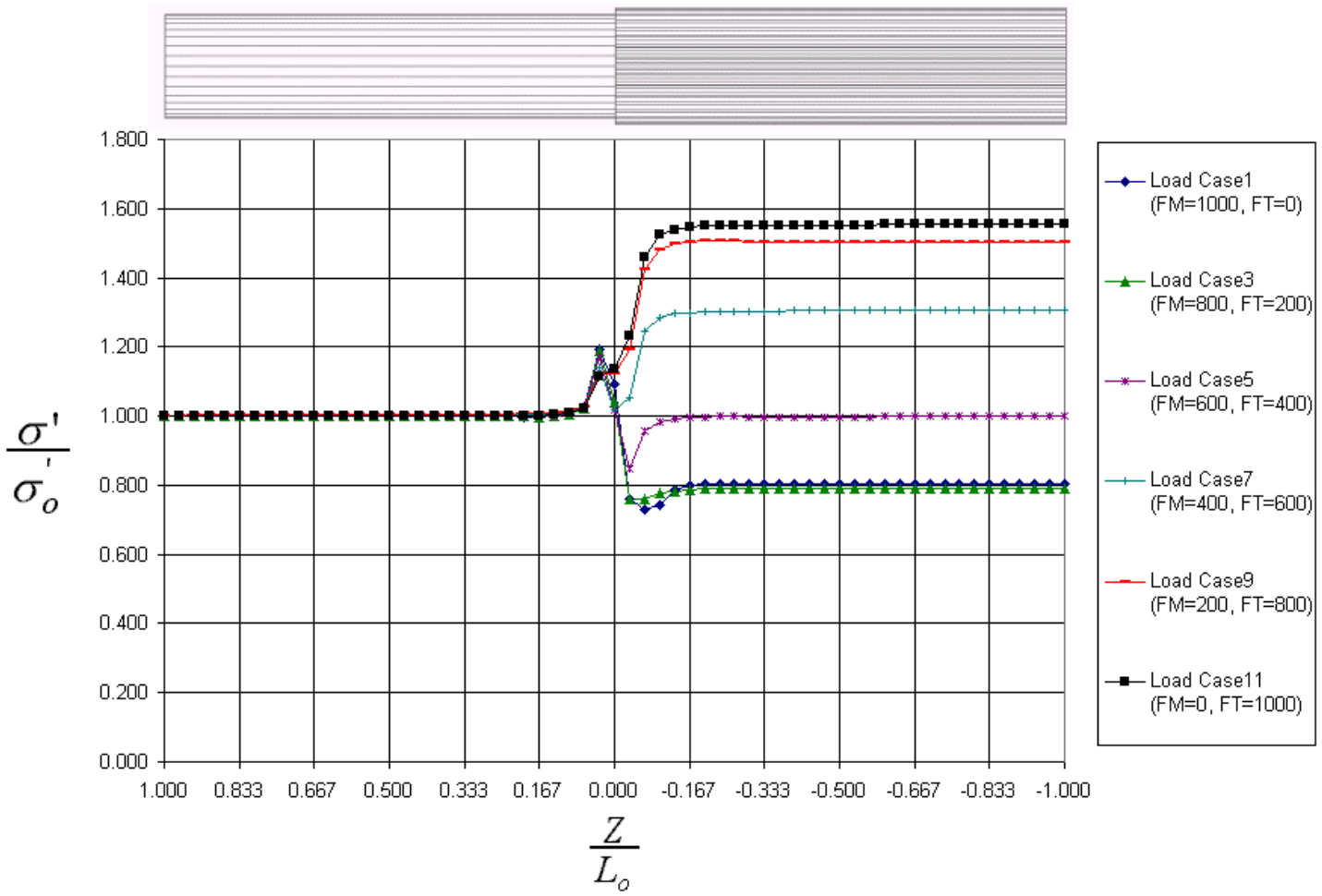

Figure 58. Variation of von Mises stress with ratio of bending to torsion for stepped splined shaft (d/D=0.886)

The behavior of the peak stresses for each load case in the stepped shafts is depicted in Figure 59. The peak values occur at various locations within the zone of transition of each shaft, or within the Z^*=0.00 to Z^*=+0.0125 range along the shaft axis.

In the case of the stepped shaft, the magnitude of the peak stresses decreases with increasing shaft step ratio (d/D_o). Figure 59 shows that the smallest step ratio, d/D_o=0.500, yields the highest stresses of all three models. The higher stresses in each model tend to occur when bending forces are in greater proportion to torsion forces. The d/D_o=0.886 shaft presents the exception to this as torsion becomes more prominent.

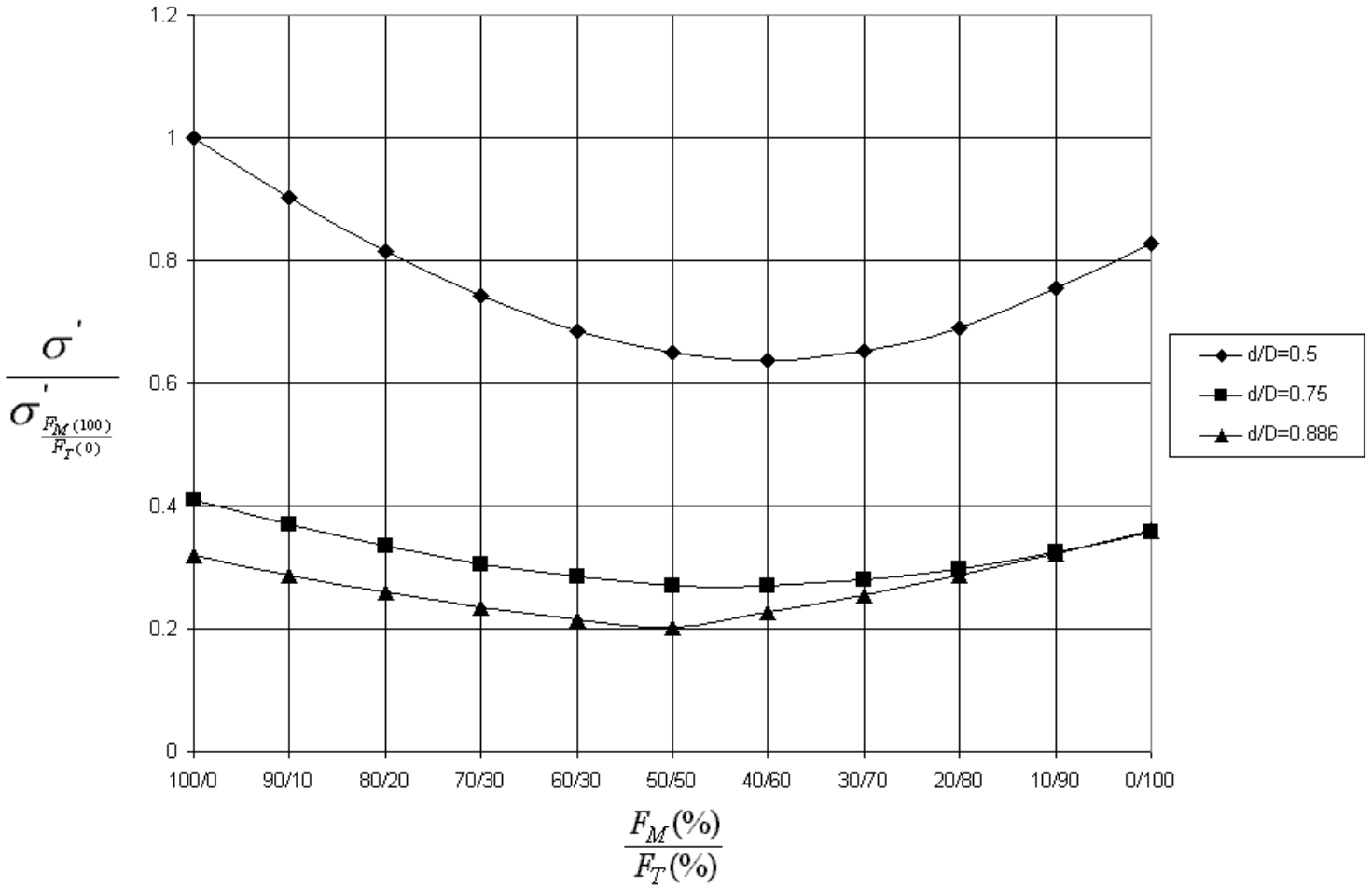

Figure 59. Peak von Mises stresses for stepped shafts

4.3 Stresses-Partially Splined Shaft Models

Three finite element models of the partially splined shaft were constructed with hob radii of R= 1.000"(0.0254m), 1.500"(0.0381m), and 2.000"(0.0508m). Each model was subjected to applied loads ranging from pure bending to pure torsion and several combinations of bending and torsion. The following graphs illustrate the relationships between the von Mises stress and the hob radius (R) of each partially splined shaft.

The behavior of the von Mises stress in the R=1.000"(0.0254m) partially splined shaft is shown in Figure 60. For the first 9 load cases (F_M/F_T= 100/0 to F_M/F_T= 20/80), the von Mises stress takes on a nominal value until about the Z^*=+0.0500 location in the non-splined section of the shaft. The stress then begins to sharply increase to a peak value at the Z^*=-0.0250 location in the splined section of the shaft. However, at load cases 10 and 11 (F_M/F_T= 10/90 and F_M/F_T= 0/100), where the influence of torsion is greater than that of bending, the increase becomes much more pronounced. The peak stress occurs at the load case 11 (F_M/F_T= 0/100), or when torsion loads are proportionally greater than bending loads. This indicates that the incomplete tooth geometry has a much more profound effect on stress when the shaft is subjected to torsion loads.

The peak von Mises stress is 41% above the nominal non-splined section stress, and 3% greater than nominal splined section stress. This greatest stress level occurs at Z^*=-0.0125 in the splined section, at load case 11. The von Mises stress reaches a nominal value beyond the Z^*=-0.0500 location, outside the influence of the incomplete teeth geometry.

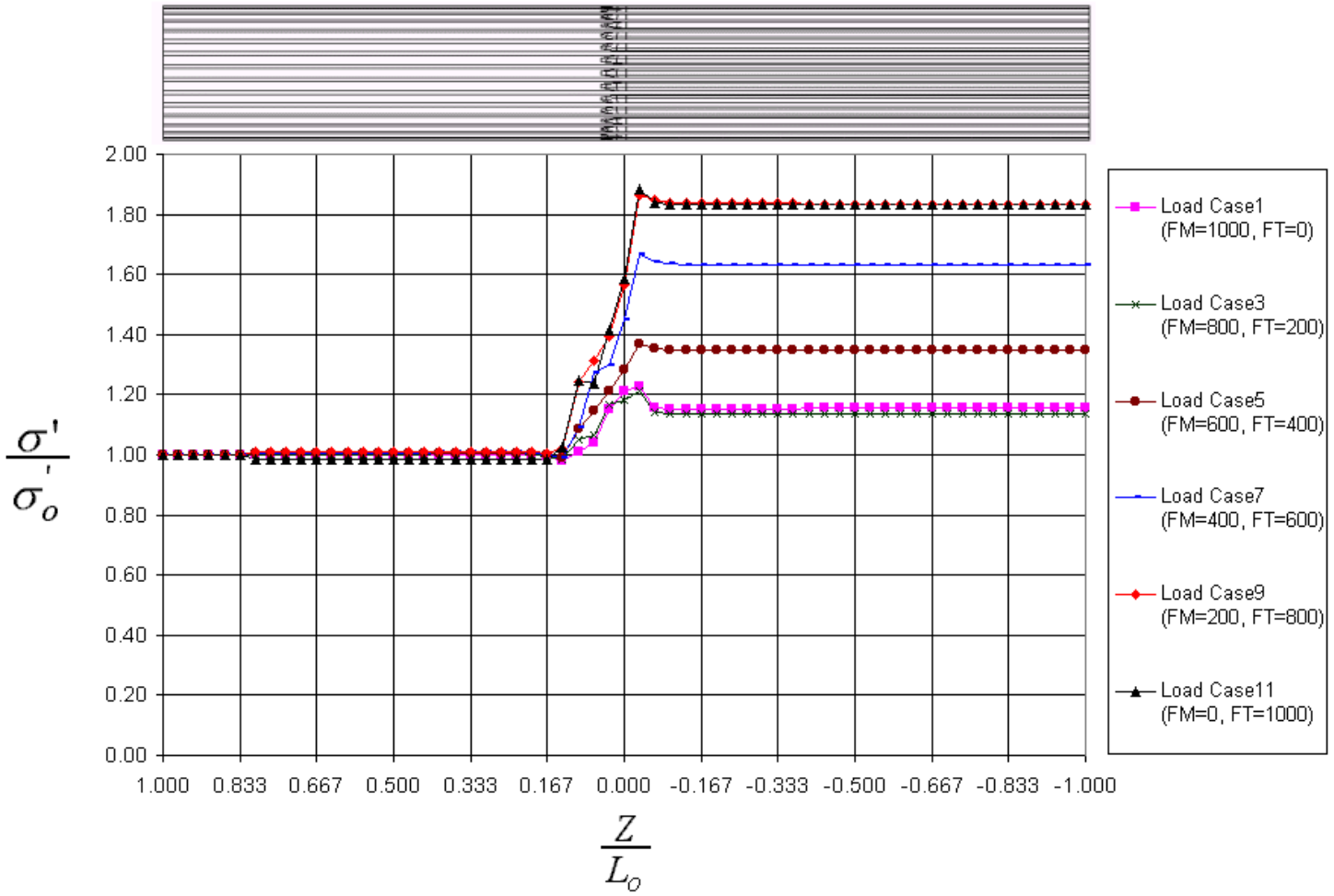

Figure 60. Variation of von Mises stress with ratio of bending to torsion for partially splined shaft (R=1.00"(0.0254m))

Similar behavior is shown in Figure 61 for the R=1.500" (0.0381 m) partially splined shaft model. In Figure 61, the peaks are larger and more pronounced. The peak von Mises stress is 41% greater than the nominal stress in the non-splined section, and 3% greater than the nominal stress in the splined section. Also, there are two noticeable peaks that occur, the smallest near the Z^*=+0.0250 location in the non-splined section, and the larger peak at the Z^*=-0.0166 location in the splined section.

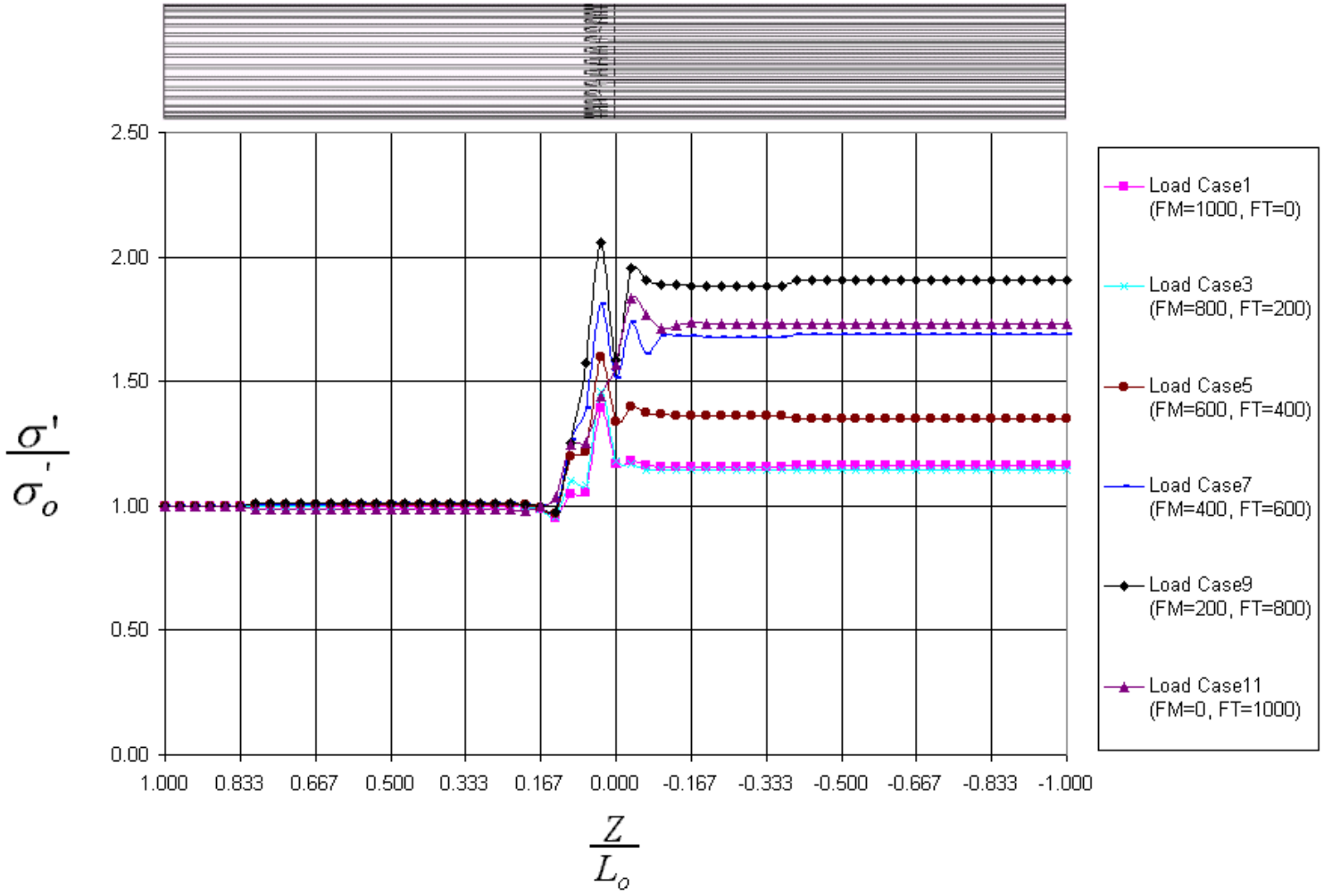

Figure 61. Variation of von Mises stress with ratio of bending to torsion for stepped splined shaft (R=1.5"(0.0381m))

In Figure 62, the double peak phenomenon, which occurred in the previous models, occurs in the R=2.000"(0.0508m) model as well. The von Mises stress reaches a smaller, local peak near the Z^*=+0.0500 location before the larger peak which occurs near the Z^*=-0.0125 location in the splined section of the shaft. From Figure 62 it is evident that the peak von Mises stress in the R=2.000"(0.0508m) shaft occurs at load case 11 (F_M/F_T= 0/100) near the Z^*=-0.125”(-0.003175m) location in the non-splined portion of the shaft. This peak is also 42% higher than the nominal stress in the non-splined section of the shaft, and about 3.5% higher than the nominal stress in the splined section of the shaft.

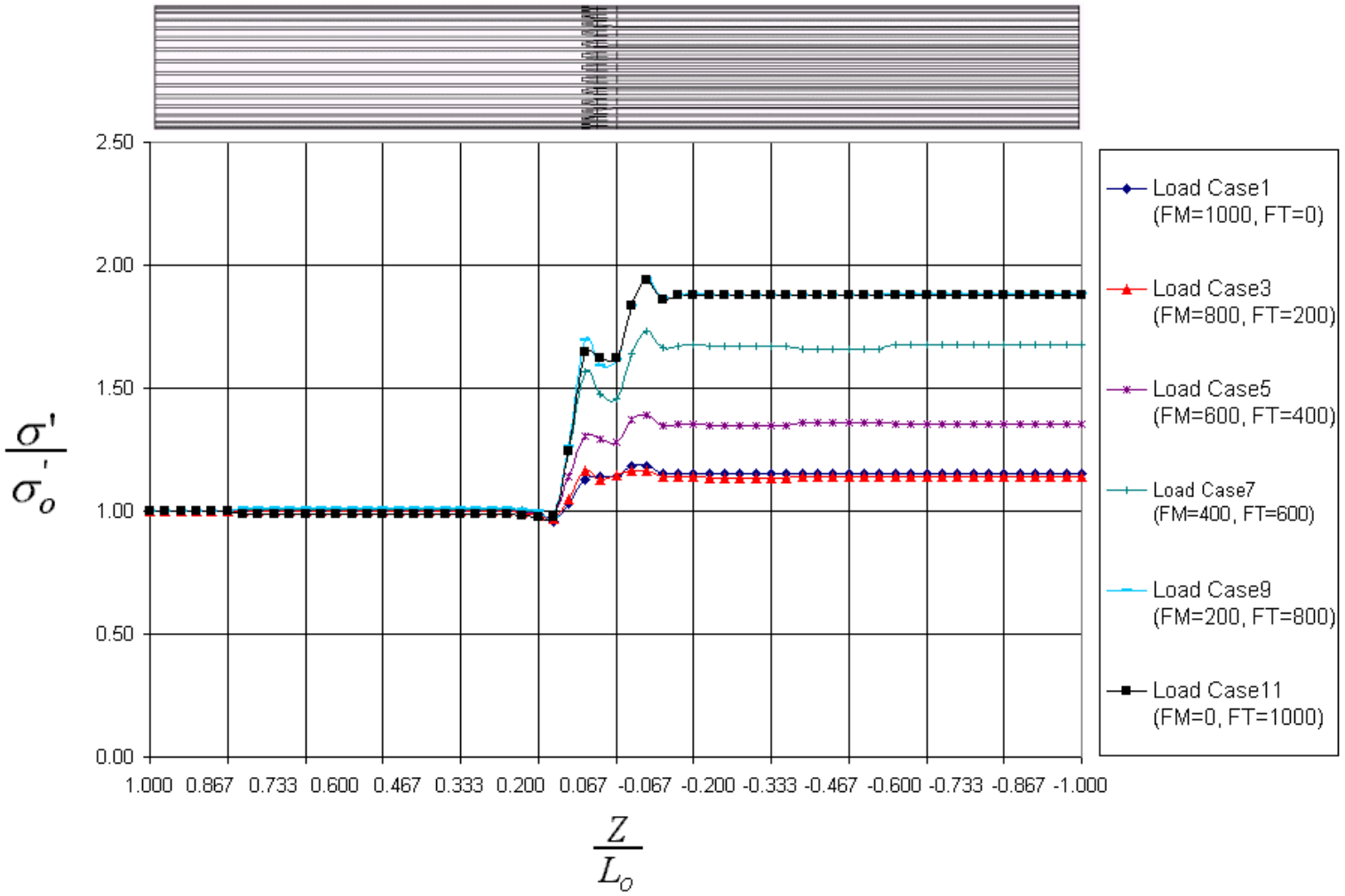

Figure 62. Variation of von Mises stress with ratio of bending to torsion for stepped splined shaft (R=2.000"(0.0508m))

The behavior of the peak stresses in the partially splined shaft is more clearly depicted in Figure 63. The peak values occur at locations within the previously discussed zone of transition (within the Z^*=+0.200 to Z^*=-0.200 range along the shaft axis). In the case of the partially splined shafts, the stress magnitude does not seem to be a function of the size of the incomplete teeth or the size of the hob radius. The greater von Mises stresses occur at load cases in which the applied torque is in greater proportion than applied bending moment.

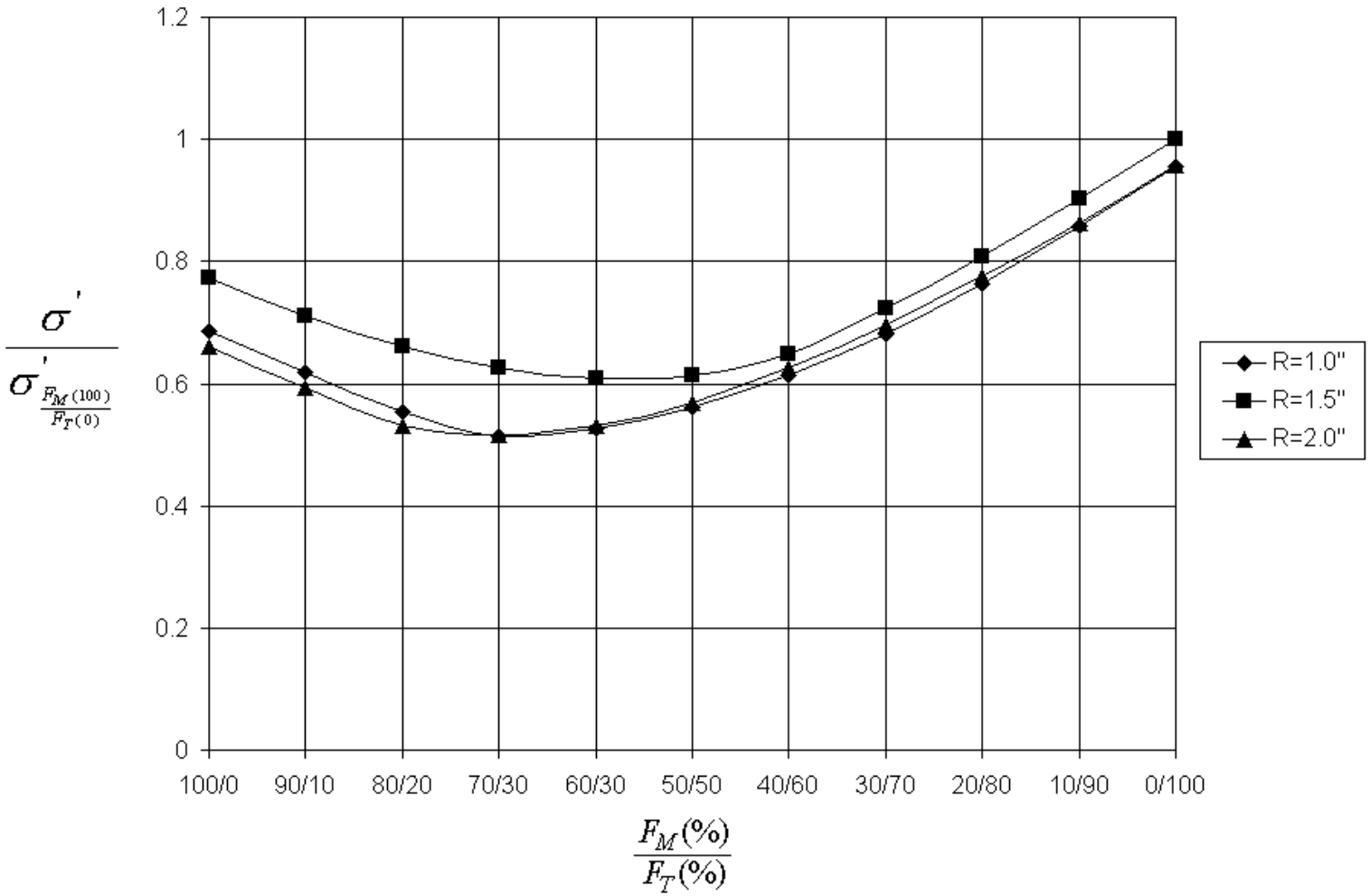

Figure 63. Peak von Mises stresses for partially splined shafts

V. CONCLUSIONS

For stepped splined shafts with step ratios of d/D=0.500 and d/D=0.75, the peak von Mises stress occurs in the non-splined section of the shaft at +0.125" (+0.0032 m) from the step. In the d/D=0.500 shaft, peak von Mises stress was 16% greater than the nominal stress in the non-splined section. The peak von Mises stress was 88% greater than the nominal stresses in the splined section and occurred at load case 1 (F_M/F_T=100/0).

The peak von Mises stress in the d/D=0.750 shaft was 9% greater than the nominal stresses in the non-splined section. This peak stress occurred at load case 1 (F_M/F_T=100/0), and was 55% greater than the nominal stresses in the splined section.

For the shaft with a step ratio of d/D=0.886, a slightly different pattern of variation of the von Mises stress was evident as the applied load on the shaft changed from mostly bending to mostly torsion. As the load becomes more influenced by torsion, stresses at the root of the spline teeth are *greater* than the local peak stresses near the step in the non-splined section. The greatest von Mises stress in the d/D=0.886 shaft is located approximately 0.5" (0.0127m) into the splined section as opposed to 0.125" (0.0032m) in the non-splined section in the other stepped shafts.

The local von Mises stress peaks are easily recognizable between load cases 1 (F_M/F_T= 100/0) and load case 5 (F_M/F_T= 60/40). After load case 5 (F_M/F_T= 60/40), the well-developed nominal stresses in the splined section of the shaft becomes greater than the nominal stresses in the non-splined section. For load cases 1-5 (F_M/F_T= 100/0 to

F_M/F_T= 60/40), the local peak von Mises stresses are about 16% higher than the nominal stresses in the non-splined section. For the load cases greater than load case 5 (F_M/F_T= 60/40), the peak von Mises stresses are the well-developed stresses in the splined section. These largest of these von Mises stresses occurs at load case 11 (F_M/F_T= 0/100), and is 11% greater than the highest of the local peaks in the non-splined section (at load case 1 (F_M/F_T= 100/0)).

Finite element results from the partially splined shaft showed little or no correlation between the hob radius and the magnitude of the peak stress. In the partially splined shafts, two peaks are evident for each load case, compared to only one in the stepped shafts. The first, smaller peak is located about 0.166" inside the non-splined section of the shaft, while the second, greater peak is located 0.250" inside the splined section. However, a strong correlation exists between the severity of the peaks and the proportion of bending to torsion.

The largest peak von Mises stress for the partially splined shafts occurs when the pure torsion is applied to the shaft. This peak stress, which is the larger of the two peaks, is about 7% greater than the nominal stress in the non-splined section of the shaft, and up to 42% greater than the nominal stress in the splined section.

In the stepped splined shafts, peak stresses occur when bending loads are more prevalent. The stresses near the step are up to 88% greater than nominal stresses in the non-splined section of the stepped shafts and up to 50% greater than nominal stresses in the splined section of the stepped shafts. With the magnitude of the forces being equal

for all the stepped shaft models, the d/D_o=0.500 model resulted in the highest peak stress near the shaft step, at the pure bending load case (F_M/F_T=100/0).

Finite element results in the partially splined shaft showed little or no correlation between the size of the hob radius and the magnitude of the peak stress. However, it was shown that the peak stress in each model increased with the proportion of torsion to bending load. Further, the peaks occurred within 0.125"(0.0032m) of the incomplete teeth region of the shaft. Stresses in the partially splined shafts were up to 42% greater than the largest nominal stress in the non-splined section and up to 7% greater than the well-developed, nominal stress in the splined section of the shaft.

There is a limited amount of information currently available in technical literature concerning splines and splined shafts. Future study of the mechanics of splined shafts is therefore warranted. Future studies of stepped and partially splined shaft should include a variation of the number of spline teeth and the tooth pitch. In addition, it is recommended that fillets of varying sizes replace the single step. A fillet with some finite area should also be introduced at the roots of the spline teeth. The variation of these parameters would give additional insight into ways that the stress distribution within the splined shafts can be influenced. It is recommended that future studies of this type include the use of gap elements to model the contact stresses developed between mating spline teeth. Such a study would serve to show how forces are transmitted between the internal and external components of a spline connection through the spline teeth.

VI. References

1. Volfson, B.P., "Stress Sources and Critical Stress Combinations for Splined Shaft". Journal of Mechanical Design. Vol. 104, No. 551, (1983): 65-72.

2. ANSI B92.1-1970. "Inviolate Splines and Inspection". The American National Standards Institute, 1970.

3. Peterson, R.E., Stress Concentration Factors, John Wiley & Sons, 1974.

4. Beer, Ferdinand P., E. Russell Johnston, Jr., Mechanics of Materials, McGraw-Hill Company, 1981.

5. Cook, Robert D., Warren C. Young. Advanced Mechanics of Materials. Macmillan, 1985.

6. Algor, Technical Documentation Access and Search (Docutech), v.2.16 WIN, 1997 (CD-ROM).

7. Cedoz, R.W., M.R. Chaplin. Design Guide for Involute Splines. Society of Automotive Engineers, 1994.

8. Oberg, E., F.D. Jones, H.L. Horton, H.H. Ryffel, Machinery's Handbook: 24th Edition. Industrial Press Incorporated, 1992.

9. Hayashi, Iwao, Teru Hayashi. "Miniaturization of Involute Splined Couplings-Discussion from Torsional Stiffness and Yield Torque". Bulletin of the Japan Society of Mechanical Engineers. Vol. 28, No. 236, (1985): 259-266

10. Shigley, Joseph E., Charles R. Mischke. Mechanical Engineering Design: 5th Edition. McGraw Hill Book Co., 1989.

11. Cook, Robert D., Finite Element Modeling for Stress Analysis. John Wiley and Sons, 1995.

VII. Vita

Donald Alexander Baker was born March 30, 1970 in Baltimore, Maryland. After graduation from Baltimore City College High School in 1988, he enrolled at University of Maryland-Eastern Shore. During the summers of 1989 and 1991, he worked as an intern at both NASA and Delmarva Power, respectively. In 1991, he transferred to the University of Maryland-Baltimore County to complete his degree requirements. In the summer of 1992, he interned again for Delmarva Power. He graduated in May 1993 with a Bachelor of Science in Engineering degree, majoring in Mechanical Engineering. After graduation, he was hired full time as an engineer by Delmarva Power in Newark, Delaware. In 1996, he enrolled at Virginia Polytechnic Institute and State University to pursue a Master's Degree in Mechanical Engineering.